THE UNIVERSITY OF CHICAGO

COORDINATED RESPIRATORY AND BRAIN RHYTHMS DURING SPATIAL NAVIGATION AND LEARNING

A DISSERTATION SUBMITTED TO

THE FACULTY OF THE DIVISION OF THE SOCIAL SCIENCES

IN CANDIDACY FOR THE DEGREE OF

DOCTOR OF PHILOSOPHY

DEPARTMENT OF PSYCHOLOGY

BY

ANDREW ALEXANDER SHERIFF

CHICAGO, ILLINOIS

AUGUST 2021

TABLE OF CONTENTS

List of Figures

Acknowledgments

Thank you to my mother, father, and sister, for lifelong support in pursuing my interests. Your genuine love and kindness has always kept me grounded in what matters most.

Thank you to the Institute for Mind and Biology, Department of Psychology, and the neuroscience cluster. The neuroscience softball team, and countless departmental social events have really accented my experiences nicely throughout graduate school.

Thank you to my wonderful lab members; Dr. Boleslaw Osinski for getting me started on computer programming and signal processing along with performing beautiful music, Dr. Shane Peace for support through surgeries and generating ideas, Vivian Nguyen for trusty animal care and surgery assistance, and Jenna Pandolfi for extensive video coding efforts, Rui He for always being there when I needed something and a pleasure to work with, and Yu Ji for being a good friend.

Thank you to my committee members, Dr. Howard Nusbaum and Dr. Alfredo Garcia, for providing instrumental ideas along the formation of my dissertation and thought-provoking discussion that helped me along the way.

A special thank you to my academic advisor, Dr. Leslie Kay, for all the time and energy put into training me as a student and independent scientist, for being a walking encyclopedia of neural anatomy and physiology, and personal support along the way.

A thank you to our lovely Hyde Park Cats, Amber and Oliver, who are as old as this dissertation project.

Finally, a huge thank you to my number one person, my partner, Gina Giase, for infinite amounts of love and support, and for coming with me to Chicago as a first step towards the rest of our life together.

Abstract

Rhythms are ubiquitous in nature. Brain rhythms coordinate large populations of neurons within and between different brain regions. The respiratory rhythm is an ongoing process controlled by brainstem networks. Olfaction depends on respiration at a fundamental level, as do the robust neural oscillations generated by the olfactory system that are important for perception and learning. More centrally, hippocampal circuits, which receive input from all sensory modalities and most directly from the olfactory system, are a major generator of brain rhythms important for spatial navigation and learning. Recent studies in rodents and humans have shown neural oscillations in prefrontal, limbic, primary sensory and motor areas phase-locked simultaneously to both the respiratory and hippocampal theta rhythms. Rodents breathe faster than humans at a frequency (~2-12 Hz) that overlaps with hippocampal theta oscillations (4-12 Hz). This suggests previous studies on hippocampal functioning may have overlooked, due to lack of respiratory recordings, roles of the respiratory rhythm, similar to those of hippocampal theta, in coordinating activity for spatial memory processes. Here, we characterize dynamic respiratory and theta network configurations depending on the perceptual environment during spatial navigation and learning. In the first set of experiments, local field potentials (LFPs) were recorded in olfactory areas including the olfactory bulb (OB) and piriform cortex (PC), along with CA1 and dentate gyrus of the hippocampus, and the primary visual cortex, simultaneously with nasal respiratory recordings during spatial navigation in rats. We compared interactions among these areas while rats foraged using either visual or olfactory spatial cues and found high coherence during foraging in both modalities compared to home cage activity in two frequency bands that matched slow and fast respiratory rates. Directional analysis shows stronger

interactions between primary sensory areas relevant to the sensory modality of the foraging environment. We provide the first evidence of respiratory-OB-PC-hippocampal interactions in awake freely moving rats, supporting the theory that the PC promotes widespread respiratory coherence. In the second set of experiments, half of the rats from the first experiment were used along with another set of rats in which we also recorded from primary somatosensory (S1), secondary motor (M2), medial parietal association (mPtA), and entorhinal (EC) cortices. All rats were trained on a spatial learning task in which they had to navigate to a learned location using either visual or olfactory cues. We compared measures of neural interaction dependent on modality of spatial cues and naïve versus learned states. High levels of coherence were seen between limbic system and sensory cortices at a single frequency around hippocampal theta (~7-8 Hz). In the third study we applied phase amplitude coupling analyses to assess the modulation of faster oscillations, which represent more local activity, by the slower respiratory and theta rhythms. High gamma (60-100 Hz) amplitude was modulated by respiratory and theta rhythms in several areas during foraging and spatial learning. Primary sensory areas and the hippocampus show increased modulation of gamma amplitude by respiratory and theta phase during spatial learning. Our results support the hypothesis that respiration works dynamically with hippocampal theta as part of a master clock for global brain connectivity and help to characterize the role of these coordinated rhythms in cognitive behaviors.

Chapter 1: Introduction

It is a major aim of neuroscience and psychology research to understand how complex neural systems are connected anatomically and physiologically (*e.g.,* the Human Connectome Project, the BRAIN Initiative), including how interactions between neural systems give rise to cognitive processes. Dynamic interactions between distal brain regions can be detected by recordings of local field potentials (LFPs) of large populations of neurons which show different rhythms, or neural oscillations. Slower neural oscillations, occurring at lower frequencies (0.1-14 Hz), can help to link distal brain regions by coordinating activity in constrained time periods, which can be measured by various coherence metrics (Fell and Axmacher, 2011; Freeman, 2015; Fries, 2015). Modern theories suggest coordinated pre- and post-synaptic firing that facilitates memory is enabled in part by coherence of large neuronal populations (Fries, 2015; Igarashi, 2015). Some of the first empirical evidence of neurophysiological mechanisms underlying cognitive processes via coherence between neural systems during perceptual and motor learning were shown during visual (Bressler et al., 1993) and olfactory (Boeijinga and Lopes da Silva, 1989; Kay and Freeman, 1998) behaviors. Neural oscillations appear to be the best candidate mechanisms for coordination between brain regions (Buzsáki and Freeman, 2015). Several recent studies show phase-locked activity between neural oscillations and another slow physiological rhythm, the ongoing respiratory rhythm, in some cases associated with cognitive performance (reviewed in Tort et al., 2018a; Heck et al., 2019). This suggests the intrinsic rhythm of breathing may help coordinate interactions between diverse neural systems similarly to other global brain rhythms.

Respiration

Movements for breathing are generated by rhythmic activities in the pontine-medullary brainstem network that coordinate activity of spinal and cranial motoneurons (Cohen, 1979; Smith et al., 2007). A region of the ventral medulla of the mammalian brainstem, the pre-Bötzinger Complex (preBötC), was initially discovered to be necessary (Smith et al., 1991), and later to be sufficient (Tan et al., 2008), for generating inspiration (Figure 2). This finding was confirmed in cats (Connelly et al., 1992) and the excitatory neuronal projections were identified anatomically in rats (Ellenberger and Feldman, 1994). The preBötC generates respiration along with nearby ventral medullary nuclei making up the ventral respiratory group (VRG) which are the primary population controlling phrenic motoneurons (Dobbins and Feldman, 1994). The VRG contains a specialized set of cells with intrinsic oscillatory properties that work as pacemakers for mammalian breathing, similar to other central pattern generators that produce rhythmic movements in invertebrates and lower vertebrates (Marder and Calabrese, 1996; Grillner, 2006; Selverston and Ayers, 2006; Smith et al., 2007). Recently, an area anterior to the preBötC was discovered to generate post-inspiratory excitatory activity in mice, and was termed the post-inspiratory complex, or PiCo (Anderson et al., 2016). Combined with previous findings of a different excitatory network associated with active expiration which is recruited during high metabolic demand (Pagliardini et al., 2011; Huckstepp et al., 2015), this led to the proposal that each of the three phases of breathing (pre-inspiration, post-inspiration, and exhalation) is generated by a distinct excitatory network (Anderson et al., 2016).

Links to olfactory behavior and physiology

It has long been known that respiratory activity phase-locks with brain activity, from pioneering research by Lord Adrian with olfactory bulb (OB) recordings in hedgehogs (Adrian, 1942) and other mammals including rabbits and cats (Adrian, 1950). This was extended into the discovery of mechanoreceptor responses in the nasal epithelium that could be detected in OB electrophysiological recordings (Walsh, 1956; Mozell, 1958; Ueki and Domino, 1961). Later studies on cats (Boudreau and Freeman, 1963), hamsters and mice (Macrides and Chorover, 1972), rabbits (Freeman and Schneider, 1982; Barrie et al., 1996) and rats (Kay et al., 1996) also showed that olfactory system LFPs are coherent with respiration. A large number of OB mitral and tufted cells are activated with each breath during nasal respiration from mechanical and odor stimulation of olfactory sensory neurons (Grosmaitre et al., 2007). Electrical stimulation of the OB is sufficient to trigger sniffing (Monod et al., 1989), which emphasizes reciprocal roles between olfaction and respiration (Buonviso et al., 2006). More recently, OB LFPs were shown to be coherent directly with the respiratory muscle, the diaphragm, over the whole range of rat respiratory frequency (2-12 Hz) (Rojas-Líbano et al., 2014).

Rodents increase their respiratory frequency to around 6 to 12 Hz during active sniffing while exploring or performing odor discrimination tasks (Welker, 1964; Kay and Laurent, 1999; Kepecs et al., 2007; Wesson et al., 2009; Wachowiak, 2011; Rojas-Líbano et al., 2014; Lefèvre et al., 2016). Odor discrimination above chance can be supported by a single rapid sniff (Uchida and Mainen, 2003; Wesson et al., 2008; Frederick et al., 2017) which suggests each sniff may act as a unit of odor coding (Kepecs et al., 2006). Indeed, spontaneous activity of mitral and tufted cells synchronize to breathing in anesthetized (Walsh, 1956; Macrides and Chorover, 1972; Onoda and Mori, 1980) and awake preparations (Chaput and Holley, 1979; Pager, 1985). Mitral

cells track slower respiration (4-6 Hz) and lose respiratory patterning during faster sniffing (6-12 Hz) with odor onset (Bhalla and Bower, 1997; Kay and Laurent, 1999). During faster sniffing for odor discrimination, most mitral cells changed responses in respect to stimulus contingency over odor specificity, suggesting top-down input from piriform cortex and hippocampal areas (de Olmos et al., 1978; Shipley and Adamek, 1984; Van Groen and Wyss, 1990) may modulate activity at the first central synapse of olfactory perception (Kay and Laurent, 1999).

Gamma oscillations (~40-100 Hz) of the local field potential represent coordinated and precise timing (on the order of 3-4 msec) of large numbers of mitral cells (Eeckman and Freeman, 1990) (Eeckman and Freeman, 1990). Gamma bursts lasting 60-100 msec are locked to the OB respiratory rhythm (Figure 1), appearing at the end of inspiration and continuing into exhalation (Freeman and Skarda, 1985; Rojas-Líbano and Kay, 2008; Kay et al., 2009). Larger gamma oscillations represent more precisely coordinated firing of the neurons (Gray and Skinner, 1988). Fine odor discrimination, in which rats discriminate very similar odorants, leads to enhanced gamma OB activity (Beshel et al., 2007; Frederick et al., 2016a). This does not occur during discrimination of odorants that are very different from each other (coarse discrimination). Furthermore, artificially enhancing gamma oscillations in the mouse olfactory bulb leads to enhanced fine discrimination, and ablating odor-evoked fast oscillations in the analogous honeybee antennal lobe leads to impairments in fine odor discrimination (Stopfer et al., 1997; Nusser et al., 2001). During both olfactory two-alternative choice and go/no-go tasks fast gamma oscillations (80-110 Hz) dominate OB LFPs early in odor sampling and slow gamma oscillations (62-80 Hz) are maintained later in odor sampling when beta oscillations (15-35 Hz) dominate (Frederick et al., 2016b). Beta power has been shown to increase with olfactory discrimination learning (Martin et al., 2004, 2007), though this was not replicated in a later study

but appeared to be associated with general expertise in the odor discrimination task rather than the specific odors to be discriminated (Frederick et al., 2016b).

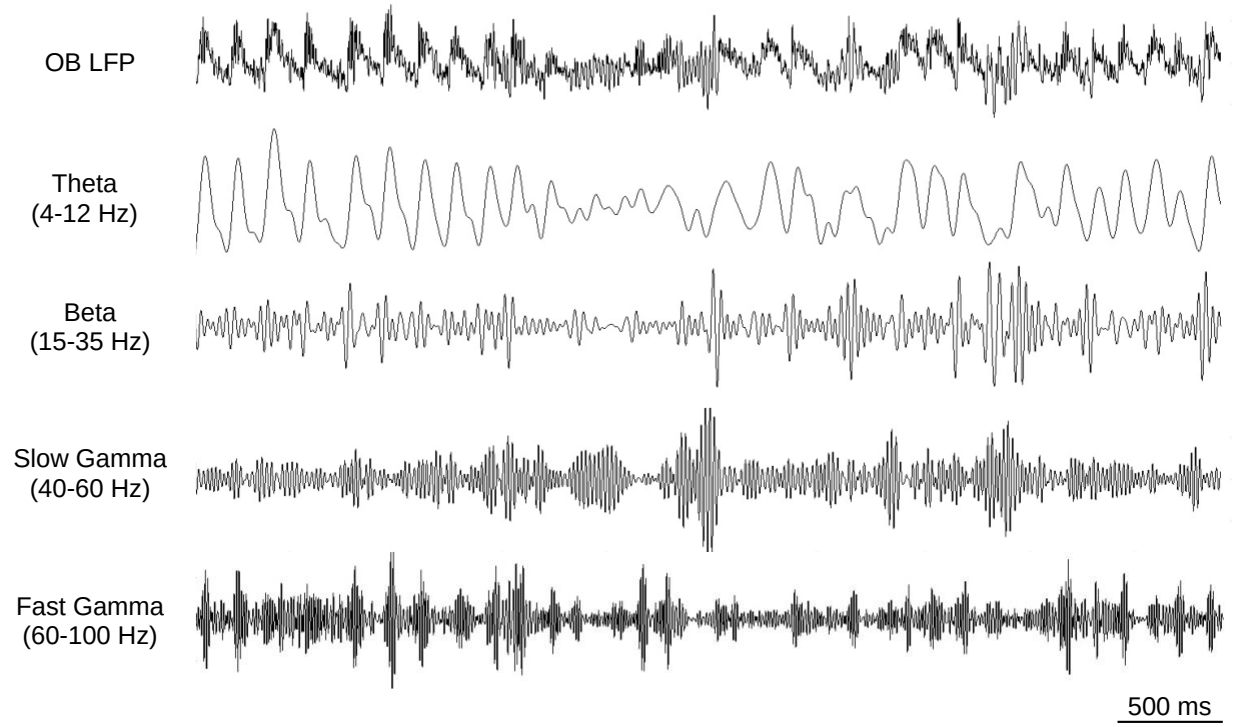

Figure 1. Olfactory bulb (OB) local field potential and its filtered subcomponents at frequencies labeled on the left. This example is from one rat with a reversal across the dipole of the OB cortical layer during home cage activity.

Respiration and sensorimotor integration

Respiration has largely been studied separately within olfactory and brainstem circuits, although respiration is fundamental to olfaction, and olfaction influences respiration. Early support for centrifugal inputs from central areas synchronizing OB activity around respiration came from studies of OBs isolated from centrifugal inputs which reduced respiratory coordination of OB neuronal firing in hamsters (Potter and Chorover, 1976) and rabbits (Chaput, 1983). Further, respiratory patterns were still observed in more than one-third of cells in the absence of nasal airflow after rats were tracheotomized, suggesting a more central role of

respiratory patterning (Ravel et al., 1987; Ravel and Pager, 1990). Volitional breathing (including sniffing) has been associated with primary motor cortex activity (Gandevia and Plassman, 1988; Maskill et al., 1991), and voluntary breathing can inactivate brainstem respiratory centers by a different mechanism than inactivation during normal metabolic breathing (Orem and Trotter, 1994), suggesting separate pathways for automatic and voluntary breathing (Masaoka et al., 2014).

Active sensing is fundamental to orofacial behaviors beyond active sniffing (Verhagen et al., 2007; Wesson et al., 2009; Wachowiak, 2011), including rhythmic licks (Travers et al., 1997) and whisking (Moore et al., 2013). Facial motor neurons that drive muscles for whisking are located anterior to the medullary respiratory nuclei and time-lock to breathing (Huangfu et al., 1993). A nucleus in the ventral medulla, termed the vibrissa zone of the intermediate band of the reticular formation (Figure 2), was shown to be necessary and sufficient for the generation of whisking, and during active sniffing was reset with each inspiration by the neighboring preBötC (Moore et al., 2013). Rats trained to whisk in search of a food reward displayed whisking frequencies from 5-15 Hz, referred to as exploratory whisking, that were under active muscular control even after loss of sensory feedback, suggesting a central pattern generator similar to that mentioned above for respiration (Berg and Kleinfeld, 2003). Sniffing and whisking show strong coherence from 4-12 Hz during open field foraging behavior (Ranade et al., 2013).

Coordinating respiratory and hippocampal rhythms

An increasing number of studies show phase-locked activity between neural oscillations and the ongoing respiratory rhythm. Respiratory coherence with oscillations in hippocampal and/or neocortical areas, including mouse whisking cortex (Ito et al., 2014), has been reported in

anesthetized (Yanovsky et al., 2014; Lockmann et al., 2016), awake head-fixed (Ito et al., 2014; Nguyen Chi et al., 2016; Liu et al., 2017), and freely moving rodents (Rojas-Líbano et al., 2018; Tort et al., 2018b). Although human respiratory rates (~0.2 Hz) are much slower than rodents (2-12 Hz) (Rojas-Líbano et al., 2014; Zelano et al., 2016), respiration was shown in a preprint report to modulate power of gamma oscillations in human frontal, parietal, and temporal cortices (Heck et al., 2016). Furthermore, respiratory modulation of the power of human delta (0.5-4 Hz), theta (4-8 Hz), beta (13-30 Hz) oscillations in the piriform cortex, amygdala, and hippocampus hippocampal theta (4-8 Hz) have been reported (Zelano et al., 2016). Respiratory coupling appears to be driven by the OB, since tracheotomy (Yanovsky et al., 2014; Lockmann et al., 2016), bulbectomy (Ito et al., 2014), and pharmacological silencing of the OB (Liu et al., 2017) ablate respiratory coupling with other cortical oscillations. Furthermore, multiple studies in humans report that nasal, and not oral, respiration is implicated in cognitive processes, including olfactory (Arshamian et al., 2018), episodic, and fear memory (Zelano et al., 2016). However, both nasal and oral respiratory oscillations in neocortical areas were correlated with visuospatial performance in another study (Perl et al., 2019). Thus, it is an open question how brainstem and olfactory-driven pathways work to propagate respiration as a global brain rhythm (Tort et al., 2018a). The medial septum is potentially a principal mediator of OB respiratory and hippocampal theta LFPs. In rats foraging in an open field arena coupling in the fast sniffing frequency around 9-12 Hz was seen between the CA1 of the hippocampus and the nasal respiratory rhythm, which was reduced to 6-8 Hz following muscimol blockade in medial septum (Tsanov et al., 2014). Indeed, the OB receives strong centrifugal feedback connections from the horizontal limb of the diagonal band of Broca where the medial septum is located (Shipley and Adamek, 1984), and the medial septum is a generator of theta oscillations with strong projections

to the EC and CA1 (Buzsáki, 2002; Pan and McNaughton, 2004). Earlier studies also proposed the medial septum as a key mediator of OB respiratory and hippocampal theta rhythms coupling during olfactory sensorimotor tasks (Macrides et al., 1982; Forbes and Macrides, 1984).

Positioned anatomically between the OB and hippocampus is the piriform cortex (PC; Figure 2). PC also couples with the respiratory rhythm in some frequencies under different levels of anesthesia in rodents at the levels of single cell firing patterns (Wilson, 1998; Bouret and Sara, 2002; Litaudon et al., 2003), multiunit firing patterns (Rennaker et al., 2007), and LFPs (Fontanini and Bower, 2005; Litaudon et al., 2008). Human PC theta oscillations are modulated by the respiratory rhythm, but OB recordings were unattainable in that study (Zelano et al., 2016). OB respiratory rhythm may propagate to the hippocampus input via direct projections from OB mitral cells to stellate cells in layer 2 of lateral entorhinal cortex (Santiago and Shammah-Lagnado, 2004; Figure 2). PC may also propagate the OB respiratory rhythm to downstream limbic structures through anatomical projections to the hippocampus via the entorhinal cortex (Truchet et al., 2002; Fontanini and Bower, 2006). Moreover, PC is reported to be an anatomical hub for the cerebral cortical association connectome (Bota et al., 2015). This fits with previous studies of PC showing highly distributed associational fibers across the entire length of the rodent cerebral hemisphere (Haberly and Price, 1978; Luskin and Price, 1983; Johnson et al., 2000) with bidirectional projections to the entorhinal and prefrontal cortices (Johnson et al., 2000). Altogether, this suggests the PC is a candidate to mediate theta and respiratory frequencies for linking nearby olfactory and hippocampal systems, along with more distal sensory systems like the visual cortex. This would emphasize a role for the PC in propagating the respiratory rhythm as a global temporal scaffold for connecting distal brain areas (Tort et al., 2018a). However, the PC has not been studied in the context of both hippocampal

theta and OB respiratory rhythm during exploratory behaviors. This will be investigated here along with further characterization of connectivity patterns driven by both OB respiratory and hippocampal theta rhythms.

The hippocampus and spatial cognition

The hippocampus is essential for spatial navigation and learning (O'Keefe and Dostrovsky, 1971; O'Keefe and Nadel, 1978; McNaughton et al., 1983; Morris et al., 1986; Wilson and Mcnaughton, 1993; Buzsáki and Moser, 2013) and episodic memory (Squire, 1992; Fortin et al., 2002; Squire et al., 2004). Related to these functions, the hippocampus is a major generator of neural oscillations related to learning and memory encoding during waking and consolidation during sleeping activity (Vanderwolf, 1969; Skaggs et al., 1996; Siapas and Wilson, 1998; Martin et al., 2007; Skelin et al., 2018). The hippocampus exhibits theta oscillations (4-12 Hz) during locomotor activity (Vanderwolf, 1969) which help mediate place cell firing dynamics (J.O'Keefe and Recce, 1993; Agarwal et al., 2014). There are two types of hippocampal theta in rodents, one which occupies the frequency band of 4-7 Hz and appears during behavioral immobility, and the other which occupies the frequency band of 7-12 Hz that appears during motor behaviors (Kramis et al., 1975). Hippocampal theta oscillations have long been theorized to play a role in sensorimotor integration (Vanderwolf, 1969, 1971; Bland et al., 1983; Bland, 1986; Bland and Oddie, 2001).

The dentate gyrus (DG) of the hippocampus receives input from neocortical areas of all sensory modalities via the entorhinal cortex (EC) and perforant pathway (Bliss and Gardner-Medwin, 1973), which leads through the hippocampal circuit and back out through EC to the rest of the neocortex and subcortical areas (Skelin et al., 2018; Figure 2). CA1 pyramidal cells in the

hippocampus tend to fire the same phase window relative to hippocampal theta (Skaggs et al., 1996). CA1 pyramidal cells fire about 90˚ after DG granule cells, with place cells showing a spread in phase of 90-120˚ (Skaggs et al., 1996). Theta oscillations may temporally order entorhinal grid cells similarly to how they order hippocampal place cell activity as a mechanism for integrating temporal and spatial information for spatial and episodic memory (Buzsáki and Moser, 2013). Location-specific firing in primary visual cortex (V1) actually leads place cell firing in the hippocampus during spatial navigation, and V1 and CA1 cells with overlapping place fields comodulate in respect to direction (Haggerty and Ji, 2015). Altogether, this suggests phase coding for primary sensory information, received from all senses by DG, is integrated into spatial coding by the hippocampal circuit.

While rhythmic coherence with neocortical areas gates sensory input to the hippocampus, the hippocampus also sends output back to the neocortex (Kleinfeld et al., 2016). For example, there are direct connections between the CA1 and prefrontal cortex in rats (Swanson, 1981). Hippocampal theta in rats interacts with neocortical areas such as the medial prefrontal cortex at the unit level during spatial navigation (Hyman et al., 2005; Jones and Wilson, 2005a) and spatial memory (Jones and Wilson, 2005b; Benchenane et al., 2010). Further, hippocampal theta shows coherence with the medial prefrontal cortex during spatial memory performance (Jones and Wilson, 2005b; Benchenane et al., 2010; Kaplan et al., 2014). The phase of hippocampal theta oscillations (6-12 Hz in rats and mice), along with coherent gamma oscillations (40-100 Hz), propagates along the septotemporal axis (Lubenov and Siapas, 2009; Sabolek et al., 2013).

Although most studies of navigation and hippocampal networks use visual spatial cues, navigation has been proposed to be the primary evolutionary role of olfaction, with parallel evolution of the olfactory and hippocampal systems (Jacobs, 2012). In support of this theory,

olfactory spatial cues form spatial field representations in the rodent hippocampus (Save et al., 2000; Zhang and Manahan-Vaughan, 2015) and grid-like representations in the entorhinal cortex of humans (Bao et al., 2019). Among all sensory cortices, the olfactory system is most directly connected with the hippocampus, separated only by two synapses in the most direct route (Vanderwolf, 1992). The lateral EC and dorsal hippocampus show increased beta coherence during odor sampling on an odor-place association task (Igarashi et al., 2014). While rats explored a familiar environment, fast gamma-coupling between the medial EC and dorsal CA1 of the hippocampus emerged (Colgin et al., 2009). Increased gamma coherence between OB, PC, and lateral EC emerged late in sniffing of an odor on an olfactory go/no-go task (Kay and Freeman, 1998).

The neocortex and spatial cognition

The posterior parietal cortex, including medial parietal association area (Figure 2) is also involved in spatial processing. This area exhibits coding properties relevant to routes (Nitz, 2006, 2012) and head-direction (Chen et al., 1994) in rodents, fitting with earlier findings of impairments only on local and not distal spatial processing following lesions of posterior parietal cortex (Save et al., 2000). As an associational cortical region, the posterior parietal cortex integrates sensory inputs from multiple modalities with centrifugal prefrontal and afferent

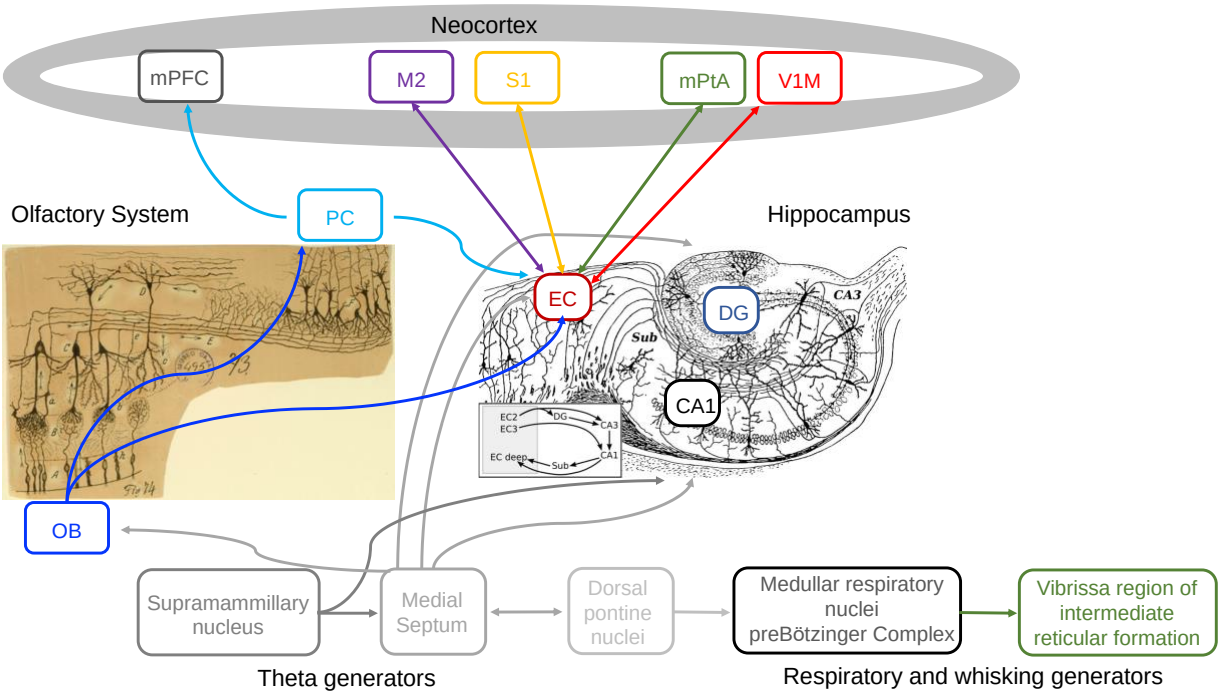

Figure 2. Diagram of relevant brain areas, both recorded and non-recorded areas shown. Recorded areas for navigation and spatial learning data were olfactory bulb (OB), piriform cortex (PC), dentate gyrus (DG) and CA1 of the hippocampus, and primary visual cortex, monocular (V1M). Additional recorded areas for the spatial learning data included entorhinal cortex (medial; EC), secondary motor cortex (M2), primary somatosensory cortex (S1), and medial parietal association cortex (mPtA). Bottom row includes non-recorded subcortical and brainstem areas relevant for theta and respiratory rhythm generation. Figure adapted from Cajal drawings (Figueres-Oñate et al., 2014) and based on anatomical connections described in (Swanson, 1981; Shipley and Adamek, 1984; Burwell et al., 1995; Truchet et al., 2002; Pan and McNaughton, 2004; Aronoff et al., 2010; Tsanov et al., 2014; Mamad et al., 2015; Kleinfeld et al., 2016)

subcortical proprioceptive and vestibular signals (Solari and Hangya, 2018). Thus, this region plays a central role in sensorimotor transformations for targeting actions to specific locations (Whitlock et al., 2012). Human visual scene processing, navigation of specific routes, and memory recall also rely on the posterior parietal cortex (Olsen et al., 2017; Silson et al., 2019). In relation to the medial entorhinal cortex which processes spatial relations, posterior parietal cortex seems more important for handling the organization of actions based on unit recordings in freely foraging rats (Whitlock et al., 2012). Further, patterns of posterior parietal cortex multi-units

showed patterns tuned to egocentric motion while rats ran on a circular platform that were reactivated during sleep and coupled to cortical delta waves and hippocampal sharp-wave ripples (Wilber et al., 2017). The parietal cortex also shows coupling with both respiratory and hippocampal theta rhythms during exploration and REM sleep (Tort et al., 2018b).

The motor system also relies on neural oscillations for learned behaviors. One study showed increased gamma power at the final sniff and high gamma coherence between posterior PC and primary motor cortex during an olfactory go/no-go task with reaching trained as a go response (Hermer-Vazquez et al., 2007). This study also showed increased beta multi-unit oscillations in PC during go trials (Hermer-Vazquez et al., 2007). Recently in nonhuman primates, beta oscillations were suggested to have a causal role for initiating movements, with quicker reaction times when stimulation was congruent with natural beta amplitude propagation direction in the motor cortex (Balasubramanian et al., 2020).

The rat somatosensory system relies on whisking which is topographically represented in the barrel cortex of primary somatosensory cortex (S1) (Simons, 1978). The hippocampus and S1 are connected via the longitudinal associational bundle from CA1 of the hippocampus (Cenquizca and Swanson, 2007) and the perirhinal and entorhinal cortices (Witter, 1993; Burwell et al., 1995). Whisking electromyogram (EMG) and S1 unit firing are phase-locked with hippocampal theta (Komisaruk, 1970; Grion et al., 2016). Whisking, sniffing, and hippocampal theta were shown to be coherent for periods of active sniffing during odor presentation in hamsters (Macrides, 1975). However, another recent study showed hippocampal theta and whisking EMG were not coherent during exploratory whisking on a runway (Berg et al., 2006). A more recent study reconciled these findings by showing that in a texture discrimination task upon touching a learned texture, there was over 40% of an increase in coherence between

whisking rhythm and hippocampal theta upon touch of a texture, and increased somatosensory cortex unit firing phase-locked to hippocampal theta during task engagement (Grion et al., 2016). Furthermore, this study showed that trials with increased theta-whisking coherence from approach to touch showed quicker and more accurate stimulus identification (Grion et al., 2016). During tactile discrimination tasks S1 neurons (Pais-Vieira et al., 2013; Kunicki et al., 2019) and LFPs show anticipatory activity, suggesting a role of top-down feedback from thalamus and cortical areas (Pais-Vieira et al., 2013; Bedwell et al., 2014). The motor and somatosensory cortices also receive projections from V1 (Miller and Vogt, 1984) and connect to the hippocampus through perirhinal and entorhinal cortices (Burwell et al., 1995).

Spatial cognition integrated through respiratory and theta oscillations

In order to understand more how respiratory, hippocampal and sensory processing collaborate in spatial cognition, I recorded neural activity from olfactory, hippocampal and visual system during foraging and expanded to include somatosensory and motor areas in a spatial learning task. I studied systemwide interactions engaging respiratory and theta rhythms in navigation and spatial learning. LFPs from the OB, PC, primary visual cortex, monocular (V1M), dentate gyrus (DG) and CA1 areas of the hippocampus, and nasal respiration were recorded simultaneously, during foraging behavior (n=7) and three of these same rats were also recorded from during spatial learning. Additionally, during spatial learning, LFPs from the OB, PC, V1M, EC, medial parietal association cortex (mPtA), secondary motor cortex (M2), and primary somatosensory cortex (S1) were recorded from three more rats. Coherence and functional connectivity between primary sensory cortices and the limbic system via theta and respiratory oscillations was compared while rats used different spatial cues (*i.e.*, visual vs.

olfactory). Findings here show broad network connectivity supported by both theta and respiratory rhythms, in which the PC appears to play a mediating role. Widespread coherence in both respiratory and theta frequencies was found in both modalities. Directionality results show effects of behavioral condition and modality. Local populations are also modulated by respiration shown by phase amplitude coupling analyses. The dynamic range of respiratory frequencies are highlighted to support treating the respiratory rhythm as an overlooked mechanism for long-range neural system connectivity (Tort et al., 2018b; Heck et al., 2019).

Chapter 2: Methods

Two behavioral electrophysiology studies were performed to allow description of neural systems involved in spatial cognition. We recorded the LFP from 5-8 different brain areas simultaneously during execution of two different types of spatial tasks. Experiment 1 tested rats in a foraging task that had few cognitive demands other than finding food in either dim light with visual cues or darkness with olfactory cues. Experiment 2 tested rats in a maze task where they were rewarded for finding a location using either visual or olfactory cues. Standard spectral analysis methods (power and coherence spectra) were supplemented with Granger causality to examine the structure of the spatial network in the two conditions. Finally, phase-amplitude coupling (PAC) permitted a deeper inquiry into how long-range connections and slow oscillatory processes (respiration and theta oscillations) can facilitate organization of neural activity in high frequency bands (beta and gamma) within and across cortical areas.

Behavioral Methods:

Experiment 1

We used seven adult male Long Evans rats (Envigo; ~400-450 g throughout Experiment 1). Rats were individually housed on a 14/10 h light/dark cycle (lights on at 0800 CST). All experiments were conducted during the light period to avoid fracturing circadian rhythms with light exposure during the dark period. Rats are known to entrain to food availability and periodic behavioral demands, and so were tested and fed at the same time every day (Travlos et al., 2001; Bedrosian et al., 2013). Rats were dieted to 85% of their *ad libitum* weight before experiments and maintained at this level for the remainder of the study. All procedures were done under veterinary supervision and oversight of the University of Chicago Institutional Animal Care and

Use Committee in accordance with Association for Assessment and Accreditation of Laboratory Animal Care standards.

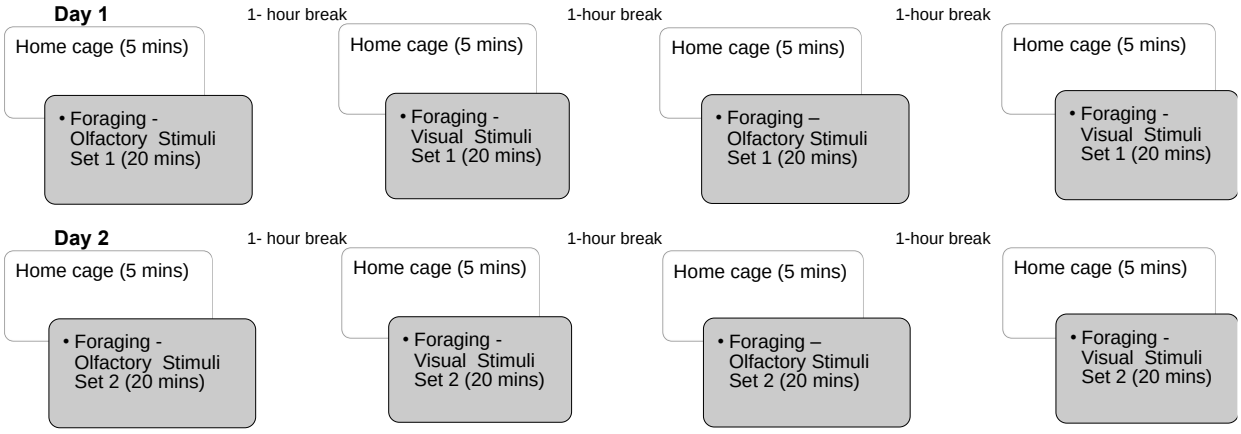

Figure 3. Within-subjects behavioral protocol for foraging. Days 1 and 2 were replicates apart from different stimulus sets used for each modality. Rats were pseudorandomly assigned to begin with either olfactory or visual condition.

Rats freely foraged in an open field environment (124 x 124 x 60 cm high gray PVC box with open top). The design of the experiment facilitated comparison between environments with different sensory modalities as spatial cues. Visual or olfactory spatial cues were placed on the walls of the open field box which was surrounded by a black curtain to conceal the rest of the room. Twenty-minute recording sessions were repeated twice for each modality, with four total sessions per day, to control for effects of familiarity with the environment apart from the provided salient cues.

The protocol for each session consisted of five minutes of electrophysiological recording while the rat was in its home cage outside of the testing room, followed by 20 mins of electrophysiological and video recording while foraging for chocolate sprinkles in the open field box, then one hour back in the home cage (no recording during this period; Figure 3). A wide-angle low-light camera (ELP 1.3MP USB Camera) was mounted on the ceiling to record

behavior. Two sets of cues for each modality were used to control for effects of specific stimuli, and these were presented on separate days. A large ventilation snorkel was placed over the box within the curtained off area to remove airborne odorants in the hour between sessions. During olfactory foraging sessions red overhead lights were the only lighting used and computer monitors were turned off in order to remove any spatial cues other than the provided olfactory spatial cues. For olfactory spatial cues, the following monomolecular odorants (Sigma Aldrich) were used: amyl acetate and anisole (CAS 628-3-7 and 100-66-3; Stimulus Set 1), ethyl-2-methylbutyrate (EMB) and geraniol (CAS 7452-79-1 and 106-24-1; Stimulus Set 2). Perforated plastic weigh boats containing cotton swab tips saturated in pure odorant were adhered to two of four walls of the open field box. The fourth wall had an empty weigh boat, visually identical to the other three. During visual foraging sessions, three visual spatial cues made of black and white patterns, including diagonal stripes, checkers, and circles, were printed on 8 ½ x 11-inch pieces of paper then laminated and oriented together in different formations (*e.g.*, adjacent, rotated 90 degrees) and adhered to three of four walls of the open field. Red overhead lights and dim lamps outside the curtained area were used to provide dim lighting within the curtained area for visual spatial cue sessions. Rats performed foraging sessions four times per day for two days (Figure 3), alternating modality each session within each day with the order counterbalanced across subjects. The entire box was sprayed with 70% ethanol and wiped down between sessions. Offline tracking for velocity data was conducted *post hoc* using Ethovison XT software (Noldus).

Experiment 2

Behavioral training for Experiment 2 involved allocentric learning (*i.e.,* associations between external spatial cues), which is hippocampal-dependent (Newman et al., 2017). We used a similar manipulation of spatial cue modality as in the foraging task (Experiment 1) by including a comparison of olfactory versus visual spatial cues on learning. Preliminary behavioral data did not show any effect of modality on learning rate ($F_{1,12} = 0.22$, ns).
The static olfactory cues training protocol was implemented for six Long Evans rats on a four-arm radial maze (8-arm maze with 4 accessible arms, and 4 inaccessible platforms Figure 4). Monomolecular odorants served as odor cues: geraniol, ethyl 2-methylbutyrate (EMB), and anisole. Individual cotton swabs were saturated with an odorant and placed in a small plastic lid turned upside-down onto three platforms located equidistant around the maze at an equal height, with the fourth platform containing the same plastic lid and cotton swab but absent any added odor (Figure 4). This produces polarity of spatial cues (Jacobs and Schenk, 2003) and provides uniform visual cues. Training continued until a learning criterion of 9 out of 10 correct consecutive trials, or 90 trials were completed. If the rat did not learn on the first day, training continued the next day. At the end of one arm, stable with respect to the surrounding room and odor cues, there was a sucrose pellet reward on each trial – the pellet was not visible to the rat from across the maze.

For each trial, the rat was placed on a random start arm (one of three arms without a reward) facing away from the center of the maze, towards the curtain (Figure 4). Trials were self-initiated and allowed one choice of arm entry, defined as when the rat traversed to the end of a maze arm to the reward well. Rats were manually removed from the maze and placed back in

their home cages for 10 seconds between trials. The rewarded arm location (any 1 of 4 arms) was counter-balanced across rats and modalities of spatial cues (i.e., olfactory or visual).

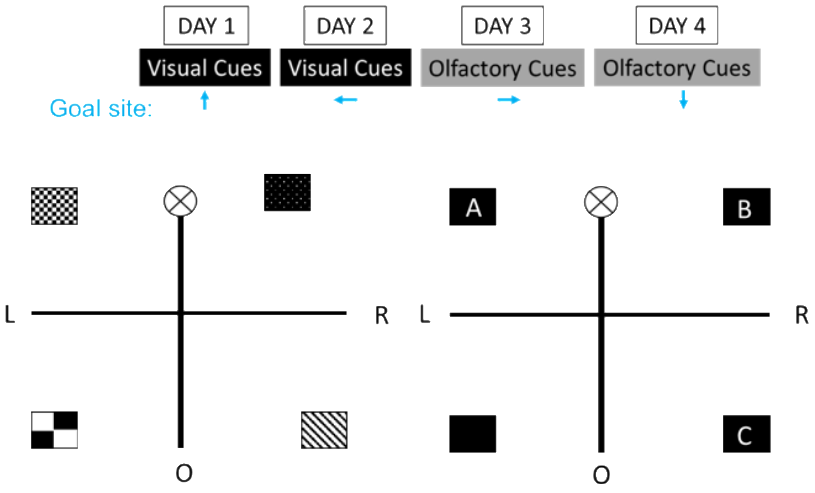

Figure 4. Within-subjects protocol for training on four-arm maze. New goal location learned each day (blue arrows), and with either visual or olfactory spatial cues present for 2 consecutive days. Four-arm plus maze with visual (left) or olfactory (right) spatial cues. R, O, L denotes right, opposite, and left start arms, respectively, in relation to rewarded arm. Boxed letters represent odor cues: A = geraniol; B = ethyl 2-methylbutyrate (EMB); C = amyl acetate; Blank = empty odor container (visual control). Boxed shapes represent symbols on visual cues and their placement around the four-arm maze.

The static visual cues (n = 6) training protocol had the same setup as static olfactory cues, except with 4 visual cues, each two 8” x 11” printouts of black and white shape patterns (circles, checkers, rectangles, and stripes) adhered together in different orientations, laminated, and attached to stands. The cues were placed immediately around the maze, adjacent to the 4 platforms (where odors were placed in the olfactory protocol). One cue is placed between one of the accessible arms and inaccessible platforms, providing polarity of spatial cues (Jacobs and Schenk, 2003; Figure 1B). The training procedure was identical to that for static olfactory cues.

Electrophysiological Methods

For Experiment 1, rats were implanted with bipolar recording electrodes (100 µm stainless steel Formvar insulated, ~1-1.5 mm vertical tip separation, 100-200 kΩ impedance at 1 kHz) following our previously reported methods (Frederick et al., 2016b) in the left main olfactory bulb (OB; 8.5 mm anterior to bregma, 1.5 mm lateral, and ~4.2 mm deep), anterior piriform cortex (PC; 0.5 mm anterior to bregma, 3 mm lateral, and 7.5 mm deep at a 15 degree angle from vertical), dorsal dentate gyrus of hippocampus (DG; 3 mm posterior to bregma, 2.4 mm lateral, 3 mm deep), dorsal CA1 of hippocampus (CA1; 4 mm posterior to bregma, 3mm lateral, 2 mm deep), and primary visual cortex, monocular (V1M; 1.08 mm anterior to interaural line, 2.6 mm lateral, 1.2 mm deep). A thermocouple (0.005 in. Teflon-coated thermocouple, Omega, part #5TC-TTK-36–36) was implanted in the right nasal cavity (7.7 mm anterior to nasal suture) to track the respiratory rhythm (Ranade et al., 2013). Ground and reference screws were secured to head screws in the right parietal and frontal bones. Electrodes were visualized to pierce the pial surface, and signals were recorded as the electrode was lowered. A final location was selected if the signals on each electrode reversed themselves at or near the planned depth. If there was no reversal, the location within the desired stereotaxic depth with largest amplitude was selected. Depths for reversals were previously estimated in acute recording and stimulation experiments (lateral olfactory tract for OB and PC, perforant path for DG and CA1, and lateral geniculate nucleus for V1M). The thermocouple and each electrode were connected to an 18-pin connector (Ginder Scientific). All data were recorded wirelessly with a Multichannel W2100 System, using a 16- or 32-channel head- stage (W16-HS or W2100-HS32) with a digital sampling rate of 2 kHz and MC Rack software. Spike2 Version 6 (Cambridge Electronic Design

Limited) was used to record behavioral videos and synchronize with MC Rack software by sending a 5-V TTL pulse triggered at the start of recording.

For Experiment 2, three of the rats were the same as from Experiment 1. The other three lacked a thermocouple recording and had the same positioned electrodes for the OB, PC and V1M. Additionally, electrodes were implanted in the dorsal part of the HPC at the border of CA1 and DG (3.6 mm anterior to interaural line, 3.5 mm lateral, depth 2.5 mm), secondary motor cortex (M2; 3 mm anterior to bregma, 1.4 mm lateral, depth 1.5 mm), medial entorhinal cortex (mEC; 1.56 mm anterior to interaural line, 3.6 mm lateral, 17 degrees from vertical, depth 8 mm), primary somatosensory cortex of trunk (S1tr; 3 mm posterior to bregma 3.4 mm lateral depth 1.5 mm), and medial parietal association cortex (mPtA; 4 mm posterior from bregma, 1.6 mm lateral, depth 1.2 mm).

Data Analysis

Data Cleaning, Preparation and Spectral Analysis

All analysis was performed in MATLAB R2015b (MathWorks, Natick, MA). The signals from each lead for each rat were assessed. If the two leads for an area showed reversed signals indicating precise positioning across the principal cell layer, then the difference of the two signals was used instead to provide a local reference; otherwise, the cleaner of the two leads was chosen, and if comparably clean or similar amplitude then the longer lead was chosen. A low pass filter at 100 Hz was applied to the respiratory signal to remove chewing artifact. Foraging data was parsed into 10 s half-overlapping windows across each 20 min session and noisy time periods were excluded. Signals were normalized by subtracting the mean and dividing each by its standard deviation.

Average power spectra across all windows for each subject by condition were calculated using the multitaper method implemented in the Chronux version 2.11 toolbox for MATLAB (Bokil et al., 2010). Theory on the multitaper method can be found in several articles and books (Thomson, 1982; Mitra and Bokil, 2008). The multitaper procedure involves a time-bandwidth product of N electrophysiological time series samples, the bandwidth of interest, W, and a selected number of tapers, K, equal to 2NW-1. Computation of the spectrum estimates involves taking the discrete fast Fourier transform of the time series multiplied by the selected tapers and averaging over the tapers (Thomson, 1982). This method multiplies each LFP trace with a series of tapers (Slepian sequences) and then averages them, which has the effect of reducing spurious noise contributions, and works well for short time samples (Bokil et al. 2010). We used 3 and 5 tapers with a time-half bandwidth of 4 and 7 for Experiments 1 and 2, respectively, over a frequency range of 0–18 Hz. More tapers were required for Experiment 2 as data samples were shorter. The number of tapers is optimized to show distinct peaks in spectra without over-smoothing. For Experiment 1, home cage activity was examined from 5 min periods outside of the behavioral room preceding each 20 min foraging session and was also split into 10 s half-overlapping windows (Figure 3). For Experiment 2, home cage activity was also 5 mins, and time windows during spatial learning were 2 s before the decision point, when rats left the center of the maze towards the chosen goal arm (Figure 4).

Coherence measures temporal coordination of oscillatory activity between brain areas associated with perceptual and cognitive processes (Freeman, 2004; Fell and Axmacher, 2011). Coherence was calculated using the *coherencyc* function in the Chronux toolbox (Mitra and Bokil, 2008; Bokil et al., 2010) again using multitaper analysis. Measures of zero coherence reflect no consistent phase relationship and coherence of 1 reflects maximal consistency in phase

and frequency relationships within a given time series (i.e., identical or identical and time-shifted series). Fisher's Z-transform was applied to coherence (Kay and Freeman, 1998; Kay and Beshel, 2010), defined as $\tanh^{-1}$(coherence), to distribute the values from zero to infinity instead of zero to one.

Granger Causality

To extend coherence analysis to the network level and address directional influences, we also used Granger causality, which is an estimation of transfer entropy similar to other measures of functional connectivity between brain regions, including partial directed coherence and the directed transfer function (Florin et al., 2011; Seth et al., 2015). We used the open source multivariate Granger Causality (MVGC) MATLAB© toolbox designed for neuroscience applications (Barnett and Seth, 2014). Granger causality is based on the simple idea that causes both precede and assist in predicting their effects, which can be traced back to Norbert Wiener, was operationalized by the econometrician Clive Granger using vector autoregressive models (Granger, 1969) and later refined for more general uses (Geweke, 1984; Seth et al., 2015). More specifically, Granger causality is an approximation of transfer entropy between variables relying on vector autoregressive (VAR) models of variables as weighted sums of their past (Seth et al., 2015). For example, to determine Granger causality between two variables, from X to Y, conditioned on a third variable, Z, one VAR model is jointly estimated for all variables granting a prediction error for each variable, then a second VAR model is estimated which omits the potential cause, X, in this example. If the prediction error from the first model that includes all

variables is significantly smaller than the one in which X is omitted, then this example would show X Granger-causes Y, conditioned on Z (Seth et al., 2015).

Granger causality generally works better for comparing between experimental conditions than characterizing the directed functional connectivity patterns themselves (Seth et al., 2015), which lends well to our experimental design. A strength of this analysis is that it is unaffected by signal strength, reflected by invariance after rescaling of variables (Seth et al., 2015). Data was first down-sampled to 250 Hz as our 2,000 Hz sampling resolution could result in overfitting (Seth et al., 2015; Nguyen Chi et al., 2016). The model order determines how far back in time data is taken into account to optimally fit the VARs and is estimated using standard techniques with Bayesian information criterion. For Experiment 1 involving up to 20 min recordings, the optimal model order fit of 46 was used as it was the average optimal fit across subjects. This means at 250 Hz a 184 ms timespan was used for the VAR models. For the decision point on spatial learning consisting of only 2 s samples, the optimal model order was 10, meaning 40 ms were taken into account for the VAR models for Experiment 2. First, time-domain pairwise-conditional causalities are generated with Granger causality analysis. Granger causality analysis is then calculated in the frequency domain, first for each rat, then averaged across conditions for the whole spectrum from 0 to 100 Hz. Then, the peaks were converted to the weighting of arrows for network visualizations of the directional interactions at specific frequency ranges. Integrating Granger causality across all frequencies, up to the Nyquist frequency, should recover the time-domain Granger causality (Seth et al., 2015)

Phase-Amplitude Coupling

Slow oscillations in one brain area can drive similar activity in another, which was examined using coherence and granger methods. However, slow oscillatory processes can also induce changes in neural activity in other frequency bands within and across cortical areas. We therefore examined the degree to which fast oscillatory activity is related to the phase of slower activity using phase amplitude coupling. To quantify the amplitude modulation by phase, Tort *et al.* (2008) created a modulation index (MI) based on a normalized entropy measure previously used to detect phase-locking episodes in neural oscillations (Hurtado et al., 2004; Tort et al., 2008). I used the open source package by Tort et al., (Tort et al., 2010) for phase-amplitude coupling analyses of data from Experiments 1 and 2 to characterize how respiratory and theta rhythms modulate faster neural oscillations.

The data are first filtered at amplitude and phase frequency ranges, f_A and f_p, respectively. Using the standard Hilbert transform, the time series of the phases is obtained. The Hilbert transform is also applied to the time series of the amplitude envelope extracted from f_A, forming a composite time series with each phase of the f_p oscillation informing the amplitude of the f_A rhythm. The mean f_A is then calculated over eighteen bins of 20˚intervals (0˚to 360˚). Then, the entropy measure H is first applied to the phase amplitude bins, the maximum possible entropy (H_{max}) value is then obtained for a uniform distribution, and the MI is finally obtained by normalizing H by H_{max}. An MI value of 0 reflects lack of phase-to-amplitude modulation, and larger MI values show stronger phase-to-amplitude modulation. Data are presented in comodulogram plots which represent in pseudocolor scale the MI values of f_p calculated in 1-Hz steps with 4-Hz bandwidths and f_A in 2-Hz steps with 20-Hz bandwidths.

Experimental Design and Statistics

Behavior and recordings were conducted within-subjects with the order of modality for spatial navigation counterbalanced in Experiment 1, and similarly with the order of modality for spatial learning counterbalanced in Experiment 2. Confidence levels at $p > 0.05$ were generated by 1,000 bootstrap permutations of the data across the 6 rats for comparisons between conditions and chance coherence. Data was shuffled by as many mismatched as actual trials for each condition for chance coherence. Surrogate analyses were also used for Granger causality as they are required in the frequency domain (Seth et al., 2015). Surrogate analyses were also implemented for phase-amplitude coupling as they are also necessary for phase amplitude coupling analyses, especially for short time windows (Tort et al., 2010) like those collected in Experiment 2.

Chapter 3: Respiratory and theta networks during spatial navigation

I studied respiratory and brain rhythms in olfactory, visual and hippocampal areas and the relationships between these areas, with a focus on respiratory and theta rhythm frequency bands. In order to describe dynamic network states that might depend on the rats' perceptual state (visual or olfactory cues), we recorded nasal respiration and LFPs in olfactory and visual primary sensory cortices and in hippocampal areas while rats freely explored different environments. I recorded all channels simultaneously while rats explored their home cage and foraged with salient olfactory spatial cues in the dark or visual spatial cues in dim light. Of the seven rats implanted with electrodes in olfactory and hippocampal areas, four were also implanted with electrodes in V1M (n=4). Signals were recorded from each rat during eight home cage activity and eight foraging sessions across two days (see Methods; Figure 1). One rat was excluded from analysis due to bridged electrodes. I use spectral analysis to characterize the presence of both respiratory and theta rhythms and to examine coherence structure across pairs of brain regions. I then use Granger causality analysis to examine the directionality of influence across all recorded nodes. This chapter, by characterizing networks related to basal activity and passive exploration, sets the foundation for future chapters comparing these networks during spatial learning.

Results

Power and coherence spectral analyses are presented first. Then directional analyses using Granger causality are characterized. Comparisons between home cage activity, modality of spatial cues during foraging, and interactions between all pairs of recorded brain regions are conducted.

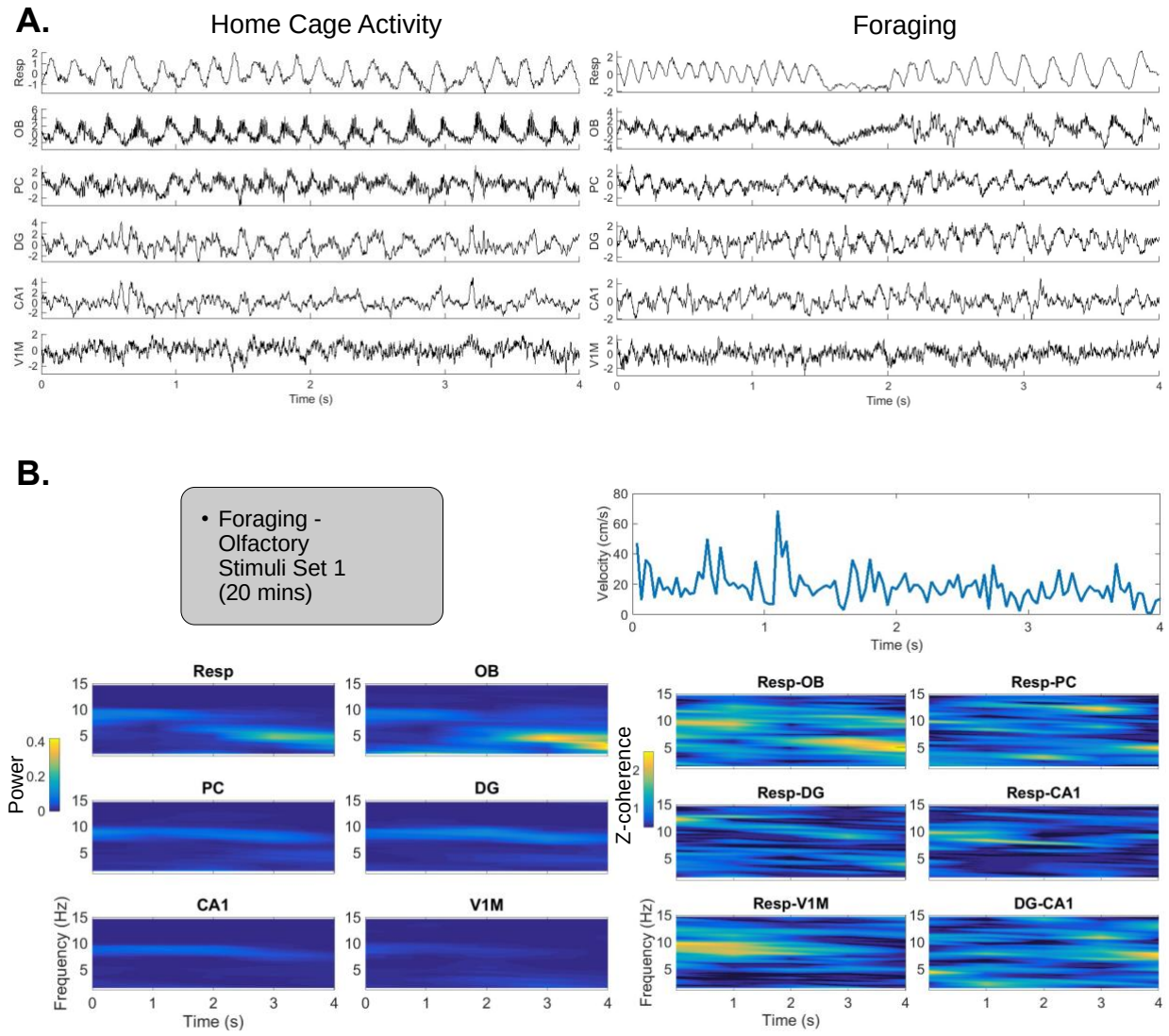

Figure 5. Representative data during foraging. (A.) Example of signals from one rat during home cage activity (left) and foraging (right). Resp – nasal thermocouple, OB – olfactory bulb, PC – piriform cortex, DG – dentate gyrus, CA1, V1M – primary visual cortex, monocular. Note 4-6 Hz respiratory frequency in the home cage. During foraging, faster respiration around 9 Hz is seen in the first second of this example, while 2-4 s show slower respiration around 6 Hz. (B.) Velocity, power, and coherence across time for the same sample of signals during foraging shown above.

Spectral analysis – power and coherence:

Power in the 2-18 Hz band was compared across the three behavioral conditions, with signals normalized by their own standard deviation (Figure 3). During home cage baseline activity (Figure 6) respiratory (Resp) and OB power was centered around 6 Hz. Power at 7 Hz was apparent in both DG and CA1, consistent with the range of hippocampal theta rhythms (Newman et al., 2013; Agarwal et al., 2014). The PC exhibited lower power at theta frequency, and V1M power was negligible (Figure 6.

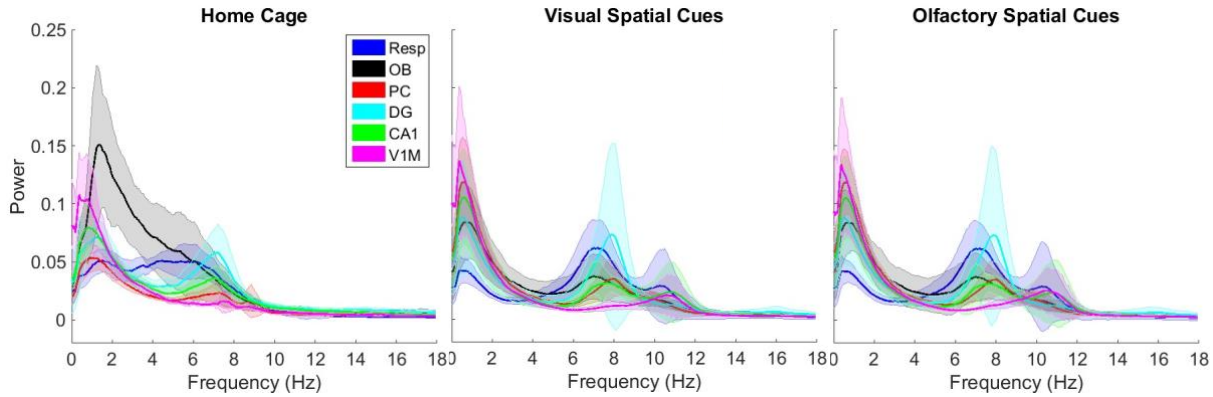

Figure 6. Power during home cage activity and foraging. Resp – nasal thermocouple, OB – olfactory bulbs, PC – piriform cortex, DG – dentate gyrus, CA1 are in top row, V1M – primary visual cortex, monocular. For all regions other than V1M, n = 6; for V1M, n= 4. Power is averaged across all sessions by condition for each rat, with bootstrap 95% confidence intervals from 1,000 permutations across the 6 subjects.

During foraging, all regions exhibited power at 6-8 Hz and 10-12 Hz in both olfactory and visual conditions (Figure 6). V1M showed a smaller peak than other regions for the 6-8 Hz band, and DG showed a smaller peak in the 9-12 Hz band. The CA1 showed a clear peak in both frequency bands and in both foraging modalities. Both of these frequencies can also be seen in the signals during foraging on the right side of Figure 2A. Velocity was low (~15-16 cm/s) in both conditions, with no difference in velocity between foraging conditions ($F_{1,5} = 1.87$, ns).

Coherence reveals the degree of phase coordination between two oscillatory signals as a ratio of 0 to 1, with 1 being maximal coherence where the signals are identical and may be shifted in phase. We normalized coherence using the Fisher Z-transform which results in a scale from 0 to infinity (Kay & Freeman, 1998). Low-frequency coherent neural oscillations are suggested to facilitate coordinated activity between brain areas (Fell and Axmacher, 2011). Examination of coherence across the three behavioral conditions therefore allows us to understand how the network might configure itself to share activity flexibly depending on momentary behavioral or cognitive needs.

In the home cage, respiratory coherence with OB (Resp-OB) in the 4-6 Hz range was very high, as expected (Rojas-Libano et al., 2014), along with a slightly smaller peak at 6-8 Hz (Figure 7). This resembles peak power of respiration (Resp) at 4-8 Hz during home cage activity shown above (Figure 2A). Moderate coherence is seen for other pairs with respiratory drive during home cage activity at 6-8 Hz including Resp-PC, Resp-DG, and Resp-CA1. OB coherence with hippocampal areas DG and CA1 is near chance levels (95% confidence level from these data for chance Z-coherence is 0.48), as seen elsewhere when rats are mostly immobile and not engaged in odor discrimination learning (Kay, 2005). OB-PC coherence is significant but low. PC shows high coherence with the DG and moderate coherence with CA1 at 6-8 Hz. Within the hippocampus, DG-CA1 coherence was high at 6-8 Hz, consistent with the range of hippocampal theta rhythms as seen above for power (Newman et al., 2013; Agarwal et al., 2014). Areas paired with V1M show low coherence levels at or near chance for home cage activity.

Coherence during foraging primarily occurred in two low-frequency bands. As expected, respiratory activity shows the most robust coherence for Resp-OB coherence which peaked at 6-

8 Hz and 9-12 Hz in both olfactory and visual foraging conditions (Figure 7), although coherence magnitude for 9-12 Hz was significantly lower in the visual condition. Respiratory activity shows moderate to high coherence with hippocampal areas; both Resp-CA1 and Resp-DG show a moderate peak from 6-12 Hz in the visual condition, while Resp-CA1 also shows a high peak from 9-12 Hz in the olfactory condition. Resp-PC shows a broader frequency large peak from 6-12 Hz. The other pairs with OB (OB-PC, OB-DG, OB-CA1; Figure 7) also show coherence from 6-8 Hz and a more distinct peak from 9-12 Hz during foraging, with a larger peak from 9-12 Hz for the olfactory condition. For the remaining pairs between the PC and the hippocampus (Figure 7), there is moderate to high coherence between PC and both CA1 and DG at 6-8 and 9-12 Hz bands, and larger PC-DG coherence at the 9-12 Hz band in the olfactory condition. Within the hippocampus, DG-CA1 show two distinct bands of high coherence from 6-8 and 9-12 Hz in both conditions. V1M-Resp and V1M-OB show low power coherence at 6-8 Hz in both olfactory and visual conditions (Figure 7). All pairs with V1M showed high coherence at the higher frequency around 9-12 Hz. The 9-12 Hz activity reported here is likely not due to velocity, as the rats mostly moved too slow for speed modulation of theta (Figure 5; Hinman et al., 2011). Also, there was no correlation between

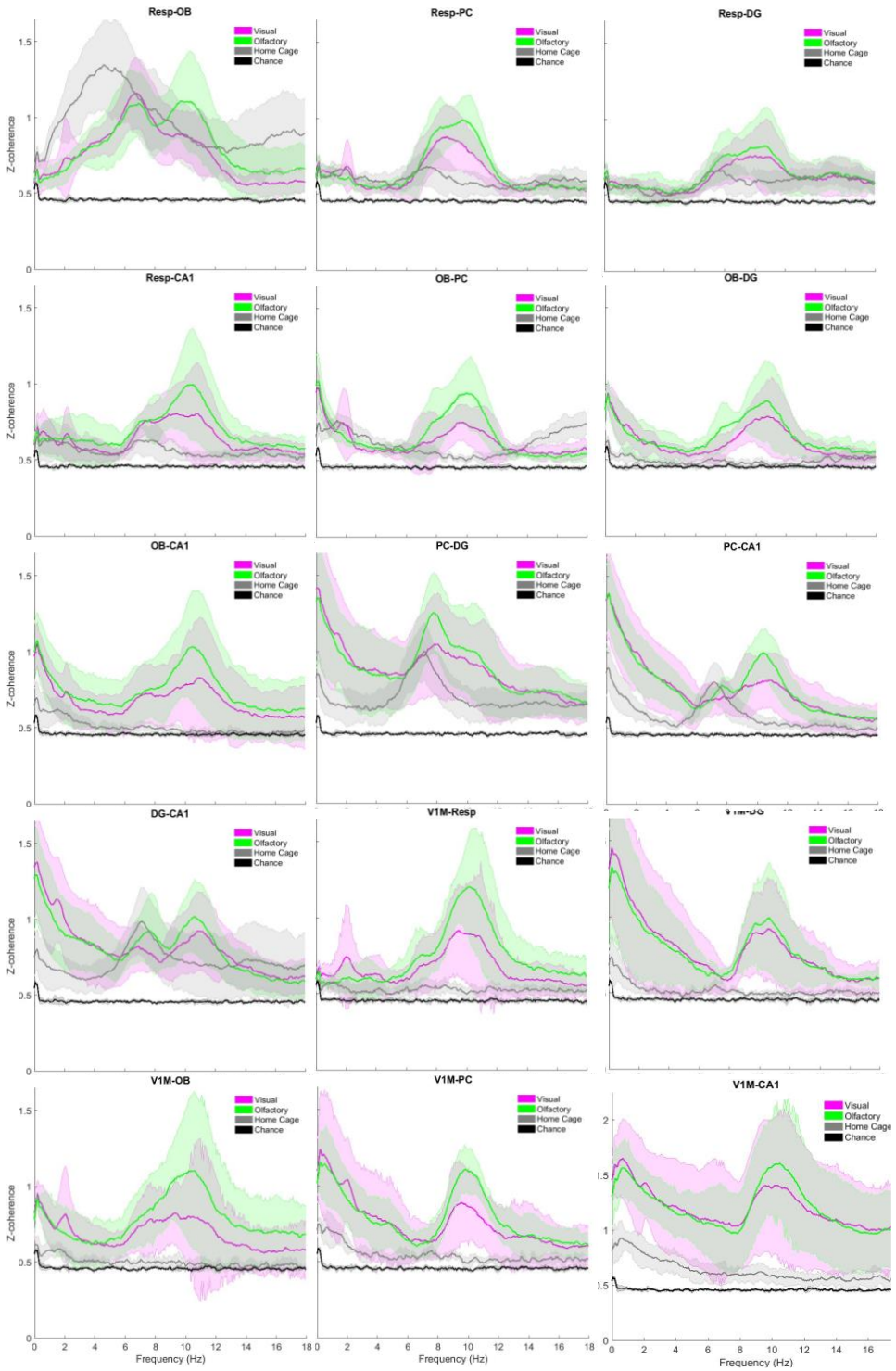

Figure 7. Coherence during home cage activity and foraging. Resp – nasal thermocouple, OB – olfactory bulbs, PC – piriform cortex, DG – dentate gyrus, CA1, V1M – primary visual cortex, monocular, listed as pairs of brain regions. Less rats had V1M recordings (n=4), while the rest of the pairs were recorded in all rats all rats (n=6). Note difference in scale of y-axis for V1M-CA1 in bottom right panel.

Resp-OB or DG-CA1 peak coherence frequency with velocity or acceleration (Kropff et al., 2021).

Respiratory state

Because respiratory frequency can be used to track different behavioral states (Rojas-Libano et al, 2014), we used this frequency to bin the data in order to understand possible network states that might be associated with different behavioral states associated with slow or fast respiration. The frequency of Resp-OB coherence was used as a proxy for respiratory frequency, because it is the measure of the frequency that the OB produces in response to input from the sensory nerve. We indexed times from coherence spectrograms at which Resp-OB coherence peaked within select frequency bands. Data were binned in two respiratory frequency bands (Figure 8), since average Resp-OB coherence occurred primarily in these two bands for each condition (Figure 7). Within each respiratory frequency state, there is also evidence of lower power events at different frequencies. This means that a low frequency respiratory period representing a relatively quiet behavioral state may contain activity at higher frequencies, which would still show up in the network but with a lower probability than lower frequency events. The probability of Resp-OB coherence is maximal at the frequency identified for each bin, however (Figure 7). Most pairs of regions involving respiratory or olfactory areas (Resp, OB, PC) show probability of peak coherence aligned to the frequency of respiration at which the data is binned, which is more prominent for the fast respiration bin. Within the hippocampus (DG-CA1) and DG-PC, however, show similar probabilities of peak coherence at slow (6-8 Hz) and fast (9-12 Hz) frequencies in the fast respiratory bin, suggesting synchronous respiratory and theta

oscillations in the hippocampus as reported previously (Nguyen Chi et al., 2016; Tort et al., 2018b).

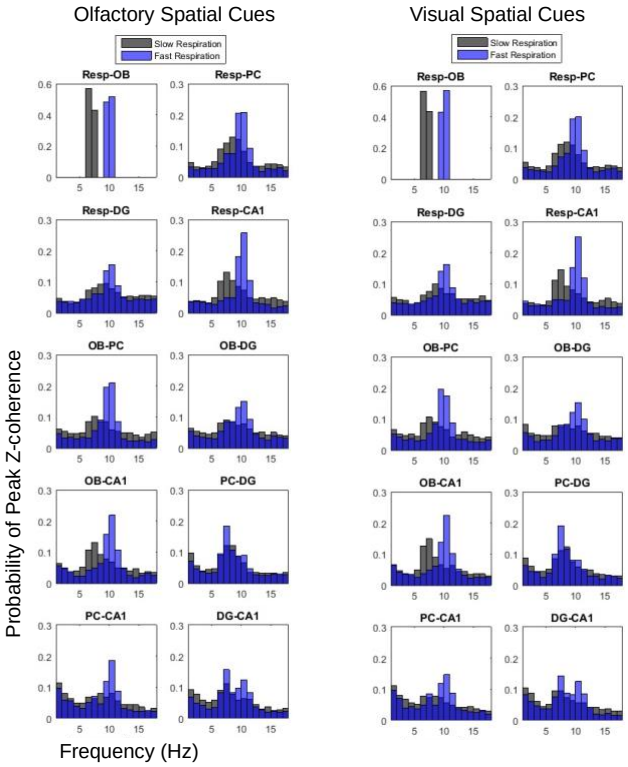

Figure 8. Probability of peak coherence after binning by respiratory rate. Resp – nasal thermocouple, OB – olfactory bulbs, PC – piriform cortex, DG – dentate gyrus, CA1, V1M – primary visual cortex, monocular. Data are indexed by peak Resp-OB coherence at fast (9-11 Hz) and slow (6-8 Hz) respiration (Resp-OB panels in top left corners) across the whole time series from 2 s moving windows stepped by 1 s, then the probabilities of peak coherence during the different respiratory bins are calculated. Probabilities are shown in black for slow respiration, and blue for fast respiration, compared between olfactory (left) and visual (right) foraging conditions.

Granger causality

We used Granger causality for measures of directionality in functional connectivity (Barnett and Seth, 2014) as was used in recent reports on respiratory rhythm coherence with neural oscillations (Nguyen Chi et al., 2016). We estimated directionality at each Granger frequency for each pair of brain areas and directionality across all sessions within a behavioral

condition (home cage, olfactory, visual) for each subject. These spectra were averaged across subjects resulting in an averaged spectrum for each pair of brain areas and directional influence for each of the three behavioral conditions.

Peaks in Granger analysis mirror what appeared in the coherence results. During home cage activity (Figure 9), all causality peaks were in the lower frequency band from 5-8 Hz. For pairs with Resp, there was high magnitude causality from Resp to OB, weak causality from Resp to PC, and weak causality from DG and CA1 to Resp. The OB received moderate causality from PC and DG. For other pairs with PC, there was moderate causality from the PC to CA1, and moderate causality towards V1M. Within the hippocampus, there was moderate causality from DG to CA1. The CA1 showed weak causality on the V1M. There were no 9-12 Hz Granger causality interactions during home cage activity. In summary, influences are relatively weak during home cage activity except for respiratory drive to the OB, and there is relatively weak

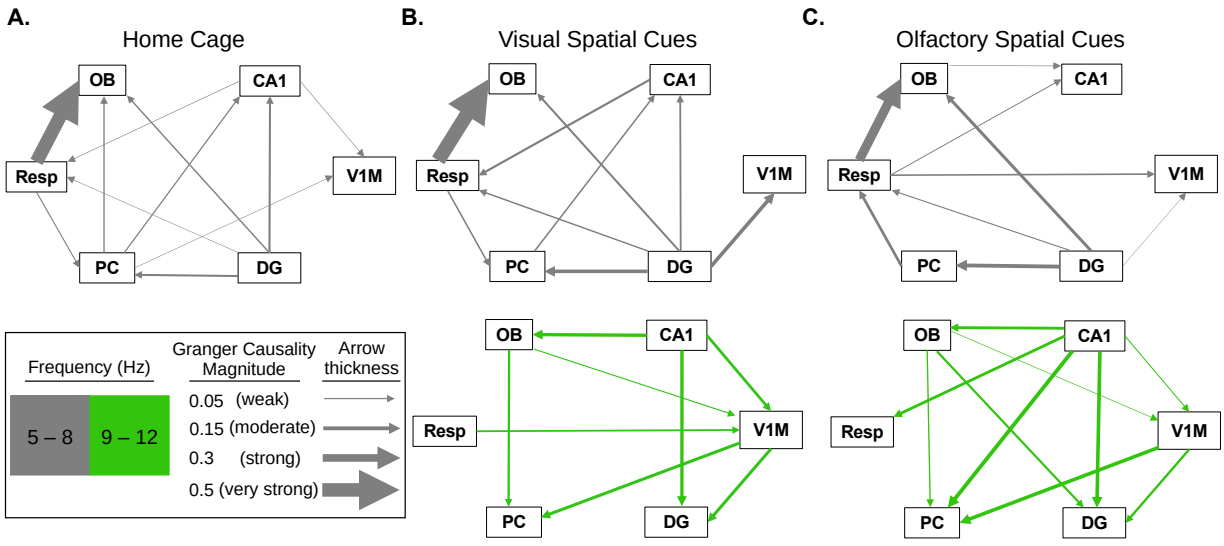

Figure 9. Granger causality across the three behavioral conditions. Resp – nasal thermocouple (respiration), OB – olfactory bulb, PC – piriform cortex, DG – dentate gyrus, CA1, V1M – primary visual cortex, monocular. Direction of arrows show which direction had greater causal influence, color denotes frequency, and the thickness of arrow denotes causal magnitude (see legend).

effective connectivity between the olfactory and hippocampal systems, except for the influence of DG onto PC.

Causal influences between brain areas during foraging were also characterized by frequency bands similar to those seen with coherence analysis (5-8 Hz and 9-12 Hz). We begin with the lower frequency band (5-8 Hz; Figure 8, upper row, gray arrows). The network of Granger connections seen in the lower frequency band during visual foraging is similar to that in the home cage (Fig. 8A,B). There are some notable differences during olfactory foraging, which we highlight below. Respiratory influences on the OB are present in all three conditions. There is weak Granger causality from Resp to PC than Resp to OB during home cage activity and visual foraging, and this connection is reversed from PC to Resp during olfactory foraging. Both hippocampal areas show a similarly weak influence on respiration in the home cage and during visual foraging, that is moderate during olfactory foraging. CA1 shows weak causality towards Resp in home cage that is similarly strong during visual foraging, and this interaction reverses and is weak in the olfactory condition. In this lower frequency band, the OB does not have causal connections towards any higher cortical areas except for a weak connection onto CA1 during olfactory foraging. Instead, OB receives causal influence from PC in the home cage and from DG in both foraging conditions. PC shows weak causal influence on CA1 in the home cage and during visual foraging. PC receives moderate causal influence from the DG in both visual and olfactory foraging conditions. DG shows a weak connection to OB during home cage activity and visual foraging which is moderate during olfactory foraging. Similarly, DG shows moderate causality to V1M during visual foraging which is weak during olfactory foraging. DG also shows moderate causality to PC and CA1 in these same two conditions but lacks causal connection to CA1 during olfactory foraging. Involvement of V1M in this circuit at lower frequencies varies

between home cage and foraging conditions. CA1 and PC influence V1M weakly during home cage activity. During visual and olfactory foraging, only the DG shows a causal connection to V1M which is stronger during visual foraging. Overall, the most prominent interactions in this frequency band (5-8 Hz) are consistent Resp to OB causality in all three conditions, DG causality onto V1M during foraging, and DG causality onto OB and PC in all three conditions but stronger during foraging than in the home cage.

A major difference between foraging and home cage activity was the emergence of high frequency (9-12 Hz) Granger connections in both foraging conditions, similar to what we saw with coherence (Figure 8, lower row, green arrows). Respiratory activity plays very different roles in the two foraging conditions in this frequency band. During olfactory foraging there is moderate causality on Resp from CA1, while during visual foraging Resp shows moderate causality on V1M. OB shows low causal influence on PC and receives moderate influence from CA1 in both olfactory and visual conditions. However, OB shows a moderate causal influence on DG only in the olfactory condition. PC receives moderate causality from V1M in both foraging conditions, and additionally moderately strong influence from CA1 in the olfactory condition. CA1 shows moderately high causality towards DG in both visual and olfactory conditions. This analysis shows that hippocampal interactions with V1M are stronger during foraging with visual vs. olfactory spatial cues. Specifically, CA1 shows moderately high causality to V1M which itself shows moderately high causality to DG in the visual condition. These same directional interactions are of lower magnitude in the olfactory condition. This is also true for 5-8 Hz for DG to V1M, as mentioned above.

Overall, the most notable interactions in the higher frequency band (9-12 Hz) are from CA1 towards OB, DG, and V1M during visual foraging, with the same interactions present

(although weaker towards V1M) during olfactory foraging, plus the addition of CA1 influence on PC and Resp during olfactory foraging. Furthermore, OB causality on DG is only present in the olfactory foraging condition for this frequency band. The top-down influences from CA1 towards Resp and PC are present only in the olfactory foraging condition in this frequency band.

Discussion

There was a clear change in network connectivity patterns based on behavioral context, with less interactions during home cage activity compared to foraging conditions. OB-hippocampus coherence was low during home cage activity (Figure 7), but there was significant hippocampal-respiratory coupling in the home cage similar to that reported elsewhere (Tort et al., 2018b). During foraging with either olfactory or visual cues we found distal interactions between respiration, primary sensory, and hippocampal areas. Coherence among these areas was elevated in either condition in two frequency bands (6-8 Hz and 9-12 Hz), matching the frequency range in recent reports of respiratory coupling between hippocampal and neocortical areas (Tsanov et al., 2014; Rojas-Líbano et al., 2018; Tort et al., 2018b). We saw some effects of modality, with increased Granger causality in the 9-12 Hz frequency band between the hippocampus and V1M during visual foraging and increased influence from DG to OB at 5-8 Hz and from OB to DG at 9-12 Hz during olfactory foraging. Furthermore, we found CA1 influence on respiration during olfactory foraging, and respiratory influence on V1M during visual foraging.

The widespread coherence during foraging is striking. We chose this task to engage the hippocampal system, because open field foraging activates hippocampal place cells and theta oscillations (J.O'Keefe and Recce, 1993). Place fields have been shown to map to olfactory

spatial cues in an open field environment (Save et al., 2000; Zhang and Manahan-Vaughan, 2015), and the olfactory system may have evolved in parallel with the hippocampus as a scaffold for space (Jacobs, 2012). Hippocampal theta phase encodes position as well or more accurately than place cells (Agarwal et al., 2014), so theta coherence with other regions may facilitate navigation through sensory representations of space via coherence at distinct phases. This hypothesis aligns with recent findings in humans that the topography of alpha oscillations tracks spatial working memory content (Foster et al., 2016). Thus, respiratory phase could play an important role in coordinating sensory information with hippocampal activity for navigation and memory, as suggested in other behavioral contexts (Macrides et al., 1982; Forbes and Macrides, 1984; Vanderwolf, 1992; Kay, 2005). This is supported by our findings that engagement of olfactory and visual systems with the hippocampus depends on the primary sensory modality used in foraging (Figure 8). Motor activity related to navigation, including sensorimotor whisking, head and orofacial orientation, shows coherence with respiration (Moore et al., 2013; Kleinfeld et al., 2014), and motor signals show up in sensory areas (Parker et al., 2020), which suggests that there may be additional sensorimotor pathways by which the distal coherence reported here could occur.

Chapter 4: Respiratory and theta networks during spatial learning

Respiratory drive has been shown to interact with brain rhythms during waking activity in rodents and humans (reviewed in Chapter 1). However, apart from studies on fear conditioning in rodents (Moberly et al., 2018), only human studies have investigated cognitive roles of respiratory and neural oscillatory interactions (Zelano et al., 2016; Arshamian et al., 2018; Perl et al., 2019) including enhancements of episodic memory related to nasal respiration (Zelano et al., 2016; Arshamian et al., 2018). Therefore, it is important to compare characterizations of respiratory and theta networks during navigation (Chapter 3) to studies of memory. Rodent spatial memory is a model system for human episodic memory. Chapter 4 characterizes dynamic network states during spatial learning with visual compared to olfactory spatial cues. Spatial cognition can be both latent, as in the last chapter, or involve explicit learning of places, as is addressed in this chapter. In the last chapter, I showed that spatial exploration involved strong interactions between limbic and primary sensory areas at primarily one low frequency during home cage exploration, and two low frequencies (<15 Hz) during both visual and olfactory foraging. I extend those findings here with further within-subjects comparisons in another hippocampal-dependent behavior that is more cognitively demanding, spatial learning.

Experiments in Chapter 4 make similar comparisons of modality for spatial cognition as Chapter 3, now with spatial cues used to learn a single location within a four-armed maze (Figure 4). Rats were trained to a new goal location each day, with either visual or olfactory spatial cues present, in dim light or only red light outside of the rat visual spectrum, respectively. This is a spatial, or allocentric (*i.e.,* associations between external objects), hippocampal-dependent task, and not a response, or egocentric (*i.e.,* associations relative to self), striatal-

dependent task (Gold, 2004). For spatial learning, rats start each trial at a random location with reinforcement at a single goal location, rather than response learning which reinforces consistent turns relative to position (*e.g.*, always go left). While studies of hippocampal-dependent place learning standardly use visual spatial cues, we compared coordinated oscillatory activity among olfactory, visual, and hippocampal systems as it may contribute to learning with visual and olfactory spatial cues.

There were two groups of rats for this experiment. Three rats were from Experiment 1 and had been chronically implanted with electrodes and a thermocouple for recordings of local field potentials (LFPs) and respiration, respectively. Therefore, the same sites were recorded for Experiment 2, including nasal respiration (Resp), and LFPs in the olfactory bulb (OB), piriform cortex (PC), dentate gyrus (DG) and CA1 of the hippocampus, and primary visual cortex, monocular (V1M). Three more rats were implanted with four additional cortical areas but lacked DG and respiratory recordings, although OB LFPs can be used as a proxy for respiration since it tracks all breathing frequencies in rats (Rojas-Líbano et al., 2014). These rats were implanted in areas OB, PC, CA1, and V1M as in the other group of rats. Additional cortical areas in this second group of rats were ipsilateral medial entorhinal (EC), secondary motor (M2), medial parietal association (mPtA), and primary somatosensory (S1) cortices. We recorded all channels simultaneously while rats (n=6) explored their home cage and then acquired spatial learning of rewarded locations within a four-arm maze. During spatial learning, there were either olfactory spatial cues in the dark or visual spatial cues in dim light, similar to comparisons during spatial navigation for experiments in Chapter 3. Respiratory and theta networks during spatial learning and memory were characterized with spectral analyses and Granger causality.

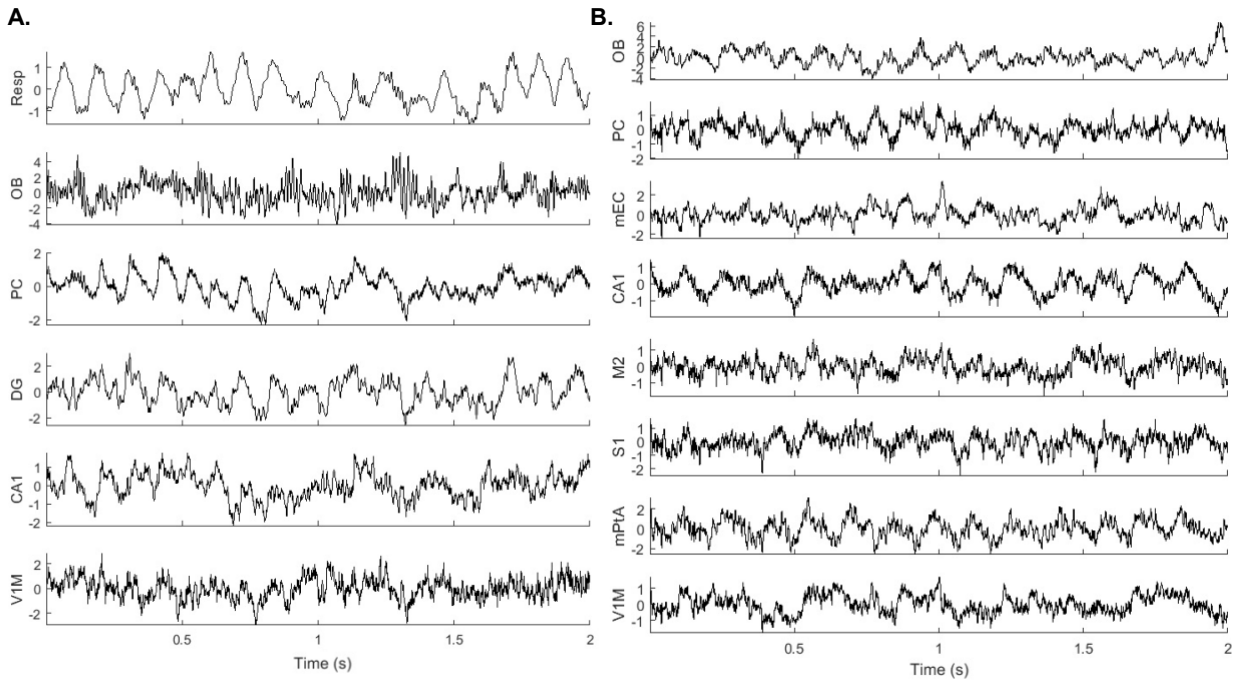

Figure 10. Raw data samples during spatial learning. Data is from one of three rats with respiratory and DG recordings (A.), and one of three rats with additional cortical areas (B.), centered around 2 s before leaving the center decision area of the maze. Both examples are from the naive state of spatial learning with visual spatial cues.

Results

Spectral analysis will be presented first, including power and coherence, limited to a slow frequency range (0-18 Hz). Then, directional interactions will be assessed with Granger causality, including faster frequencies up to 100 Hz. Comparisons between modality of spatial cues and learning state, and interactions between sensory and hippocampal systems, will be characterized. Within-subjects analyses continued for three of the rats from the previous chapter, along with three additional rats with more cortical areas relevant for spatial cognition. After pilot analyses, the behavioral epoch of focus will be two seconds before rats leave the center area of the maze, as a decision point in spatial learning and memory.

Spectral analysis – power and coherence:

An example of respiratory and hippocampal theta power is shown in Figure 10. Power was normalized by dividing each signal by its own standard deviation and shown for the three rats that had respiratory (Resp) and dentate gyrus (DG) recordings from Experiment 1. Rats were trained to a new goal location for each of four days, with visual spatial cues present two consecutive days, and olfactory spatial cues present for two consecutive days, with order counter-balanced. The same stimuli were used within modality for each subject, and the configurations of stimuli with respect to each other and goal locations were different for each rat. Power spectra are calculated for each subject across the two days for each modality, then averaged across subjects with 95% confidence intervals from 1,000 bootstrap permutations shown. Power is compared between home cage activity and spatial learning, between the first block of ten trials (naive) and the last block of ten trials (learned), when accuracy was 90%. Unlike foraging in Experiment 1, where two frequencies of respiratory and theta oscillations were present, spatial learning shows one slower respiratory frequency, peaking near 8 Hz. These peaks are slightly slower during home cage activity, similar to what we saw in Experiment 1 in the previous chapter. Power is consistent in Resp and DG throughout spatial learning, except Resp power at 8-10 Hz appears more prominent in naive than learned olfactory spatial learning and home cage activity (Figure 10).

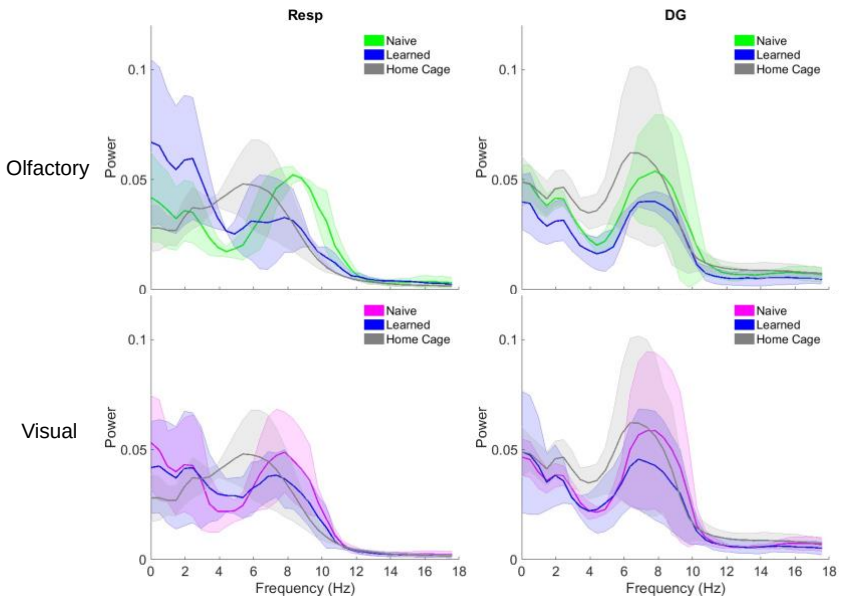

Figure 11. Examples of power in respiratory and hippocampal signals. Normalized power is averaged across the first group of subjects (n=3) with 95% confidence intervals shown for respiratory (Resp) and dentate gyrus (DG). Naive is the first block of ten trials; learned is the last block of trials which were 9 out of 10 correct.

Some examples of respiratory and theta coherence from these same three animals are shown in Figure 12. Coherence was transformed to z-coherence using the inverse hyperbolic tangent ($atan^{-h}$) transform. Data were shuffled by mismatching trials to calculate chance z-coherence levels. Confidence levels at $p > 0.05$ were generated for all z-coherence data with 1,000 bootstrap permutations across the 6 rats. Similar to the more prominent 8-10 Hz respiratory power in the naive state of olfactory spatial learning (Figure 11), Resp-PC coherence is slightly higher at 10 Hz in the naive state of spatial learning with olfactory spatial cues than coherence levels at learned and home cage states (Figure 12). Similarly, V1M-DG coherence peaks at 10 Hz in the naive state above coherence levels seen once learning criterion is reached and in the home cage. Resp-OB and DG-CA1 coherence was far above chance during home cage

activity and throughout both conditions of spatial learning (data not shown), similar to that seen in Experiment 1 during spatial navigation, although only at one frequency band peaking around 8-9 Hz during spatial learning. PC-DG and DG-CA1 showed a prominent peak in coherence centered at 8 Hz during home cage activity, and throughout spatial learning with either modality of spatial cues (data not shown), similar to that seen during foraging (Experiment 1, Chapter 3).

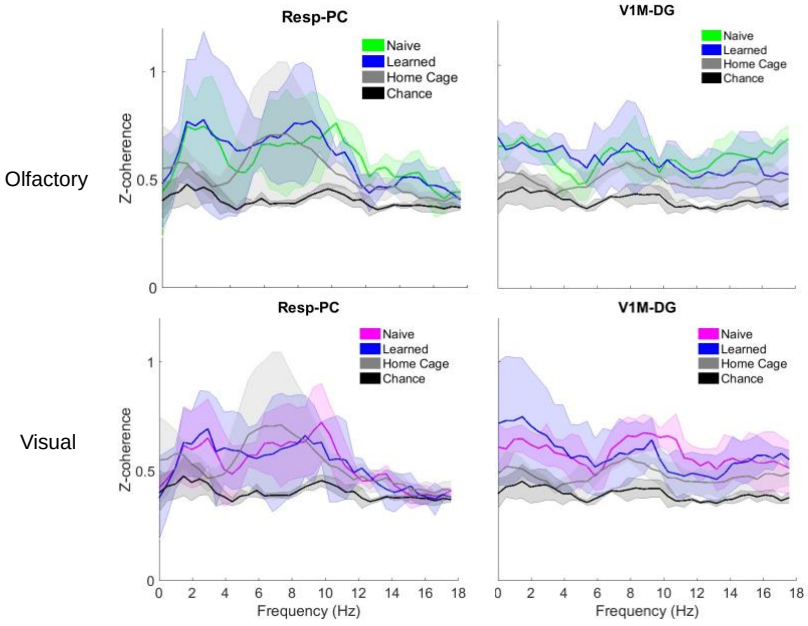

Figure 12. Examples of respiratory and theta coherence throughout spatial learning. Coherence is transformed to Z-coherence and is calculated across days for each subject, then averaged across subjects with 95% confidence intervals from 1,000 bootstrap permutations shown, similar to power. Areas are abbreviated as follows: respiratory (Resp), piriform cortex (PC), primary visual cortex, monocular (V1M), and dentate gyrus (DG).

We now turn to coherence measures for pairs of areas that were recorded in all 6 rats during spatial learning (Figure 13). Early in spatial learning some pairs show elevated coherence at theta frequency (6-12 Hz), including OB-V1M, PC-V1M, and CA1-V1M, with olfactory or visual spatial cues (Figure 13, top). Once spatial learning criterion is reached, OB- and PC-V1M coherence remains high, while CA1-V1M no longer is elevated above home cage levels.

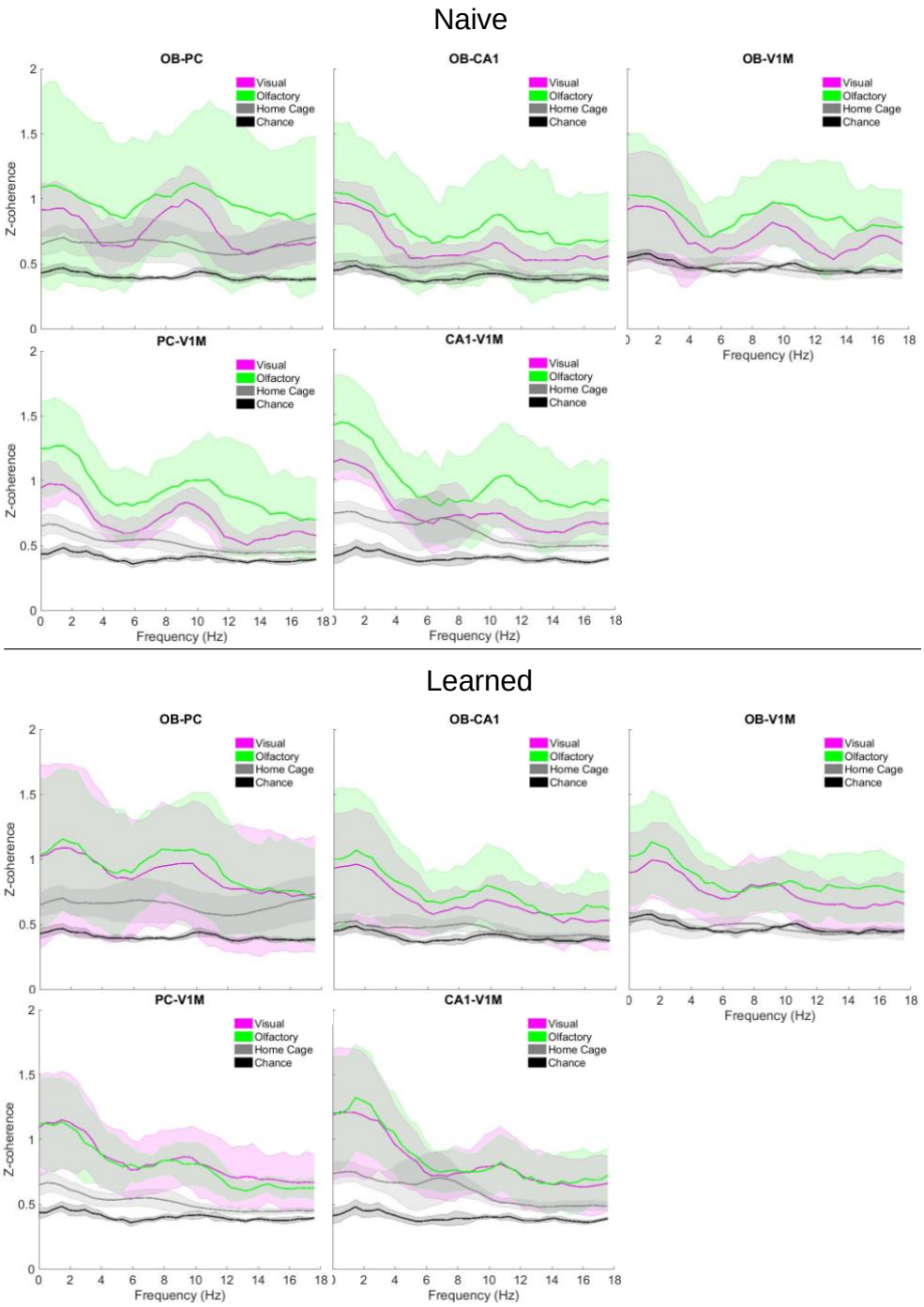

Figure 13. Coherence during spatial learning for areas recorded in all subjects (n=6). Data is averaged across all rats for each pair. Chance data is coherence from trial mismatched shuffled data of the same number of trials used for the other conditions. Confidence intervals at 95% are shown from 1,000 bootstrap permutations across all subjects (n=6).

Three rats had additional electrodes in more areas relevant for spatial cognition (mEC, S1, M2, and mPtA). Examples of coherence between some of these areas during the different behavioral conditions compared to chance levels are shown in Figure 14. Many areas show peaks in theta coherence during home cage activity and throughout spatial learning in both types of spatial cues. This was especially true for CA1, S1, and mPtA, which had high CA1-S1, CA1-mPtA, and S1-mPtA theta coherence in all conditions. mEC and M2 showed significant theta coherence only during spatial learning and not during home cage activity (Figure 14).

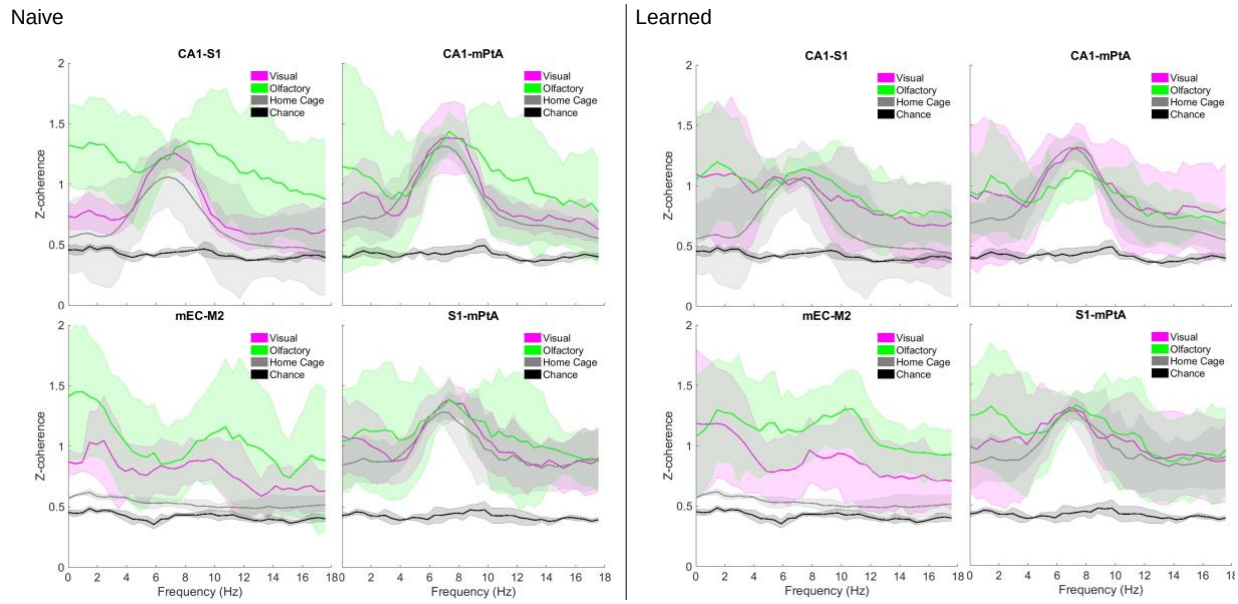

Figure 14. Coherence from three rats with CA1, mEC, mPtA, S1, and M2 electrodes.

Granger Causality:

Directional interactions were characterized using Granger causality, a statistical method that estimates causality based on the predictability of one variable's past on the future of another variable. Granger causality data is presented separately for the two groups of animals. These are first shown in Figure 14 for the three rats that also completed Experiment 1, which had Resp and DG recordings. Figure 14A shows the time-domain pairwise-conditional causalities compared

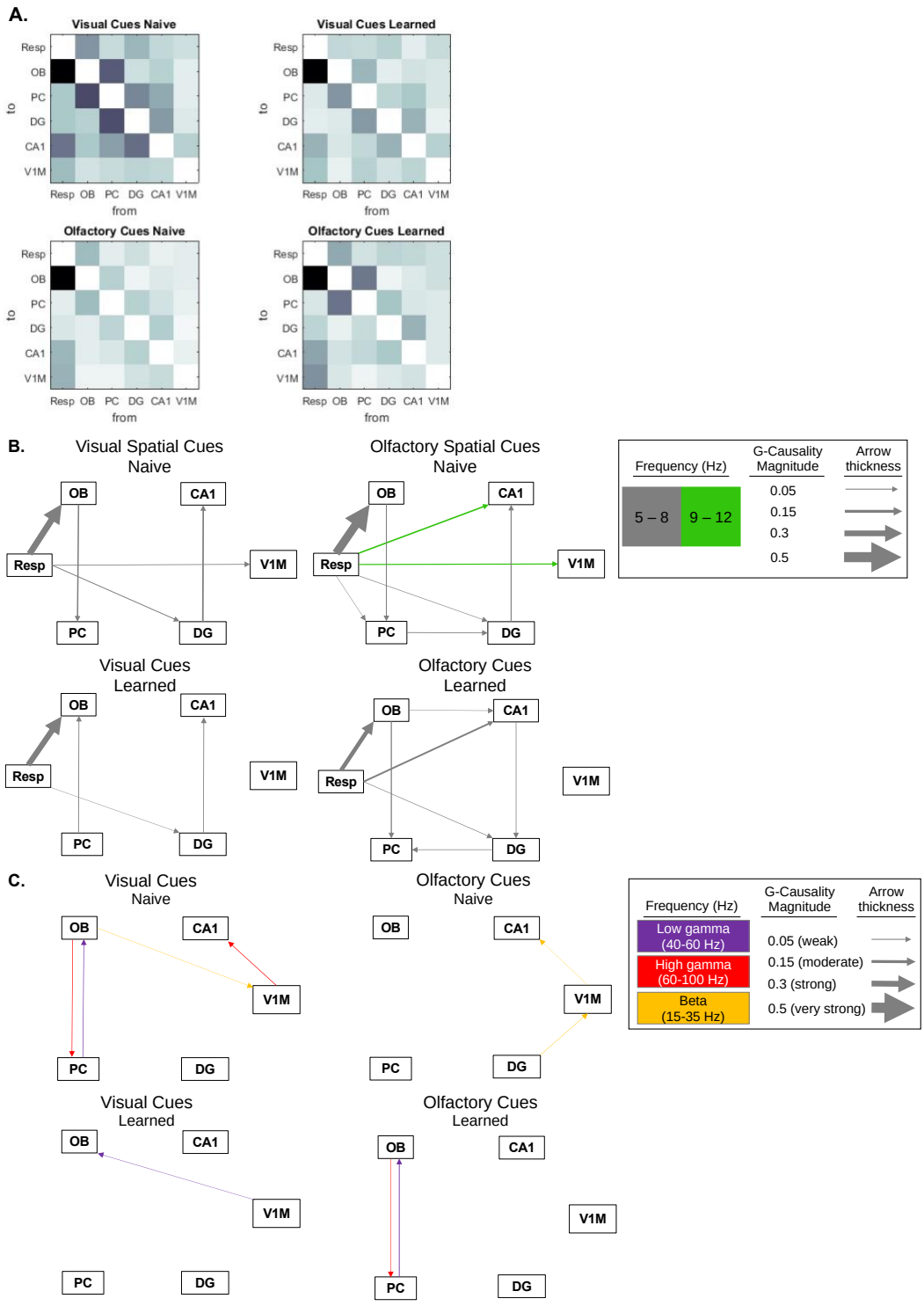

Figure 15. Granger causality for the rats (n=3) that were also used in Experiment 1. A.) Time-domain pairwise-conditional causalities compared throughout spatial learning. B.) Frequency-domain granger causality in the low frequency band of 5-12 Hz. C.) Frequency-domain granger causality in the higher frequency bands.

between spatial learning states with olfactory versus visual spatial cues (darker shading indicates stronger causality). Note the strong causality from Resp to OB throughout all conditions, while OB to PC causal influence is more dynamic, with changes following learning in olfactory and visual spatial conditions. PC-DG and DG-CA1 show some decreases in causal strength with learning under visual spatial cues.

We also characterized the frequency domain of these Granger causal interactions, with the slower frequency band (5-12 Hz) shown in Figure 15B, and the faster bands, including beta (15-35 Hz), low gamma (40-60 Hz), and high gamma (60-100 Hz) shown in Figure 15C. Respiration shows causal influence on the OB and hippocampus, specifically the DG, in all conditions, with very strong causality overall seen from Resp to OB. Note the higher frequency of respiratory drive to CA1 and V1M at 9-12 Hz only during the naive state of spatial learning with olfactory spatial cues (Figure 15B), similar to that mentioned above for respiratory power (Figure 11) and coherence between Resp and PC (Figure 12B). The OB also shows causal influence on the PC in all conditions. The PC shows weak causality towards the DG initially in olfactory spatial learning, and this reverses from DG to PC once learning criterion is reached with olfactory spatial cues.

There are relatively few fast frequency causal interactions (Figure 15C) compared to slow frequency interactions (Figure 15B). However, there are still more interactions at these higher frequencies during spatial learning than during foraging, evidenced by the absence of any interactions at these faster frequencies in Experiment 1. Causal influences are seen in high gamma (60-100 Hz) from OB to PC and low gamma (40-60 Hz) from PC to OB early in visual and late in olfactory spatial learning. Weak causality from OB to V1M at beta frequency (15-35 Hz) is present in the naive state of visual spatial learning, and this reverses from V1M to OB at

low gamma once the location is learned in the visual condition. V1M shows weak high gamma to CA1 early in visual spatial learning. Also, DG shows weak beta to V1M, which also exhibits weak beta causality to CA1 early in olfactory spatial learning (Figure 15C).

The other three rats that only participated in Experiment 2 were analyzed separately for Granger due to several additional neocortical areas. First, interactions in the slower frequencies (5-12 Hz) are characterized (Figure 15). During home cage activity, there is low frequency (5-8 Hz) causality from PC and mEC to OB. PC also shows moderate 9-12 Hz causality to CA1 in this condition. A network of theta oscillations from CA1 to neocortical areas is active during home cage activity, with moderate causality towards mPtA and S1, and weak causality towards V1M, at 8 Hz. This suggests CA1 drives theta coherence with mPtA and S1 during home cage activity as seen in Figure 14. These neocortical areas also interact at theta, with weak causality from mPtA to S1 and V1M, and from V1M to S1, also at about 8 Hz.

Spatial learning patterns are different from network activity in the home cage, as they were for foraging in Experiment 1. There are few significant connections at slower frequencies during visual spatial learning, with only mEC showing weak 9-12 Hz causality to S1 in the naive state, and M2 showing weak 5-8 Hz causality to V1M in the learned state. Conversely, there is a network of moderate strength causality early in olfactory spatial learning in these slower frequencies (5-12 Hz) that overlap with respiratory and theta rhythms. OB shows moderate causality towards V1M at 5-8 Hz, as does PC to OB. PC also shows moderate 9-12 Hz causality towards CA1 and V1M. V1M also exhibits 5-8 Hz causal interaction towards M2. Once the learning criterion is reached with olfactory spatial cues, this slow frequency network is sparser, with weak 9-12 Hz causality from V1M to OB and 5-8 Hz causality from V1M to PC. The only other significant causal connection is weak from PC to mEC from 9-12 Hz (Figure 15).

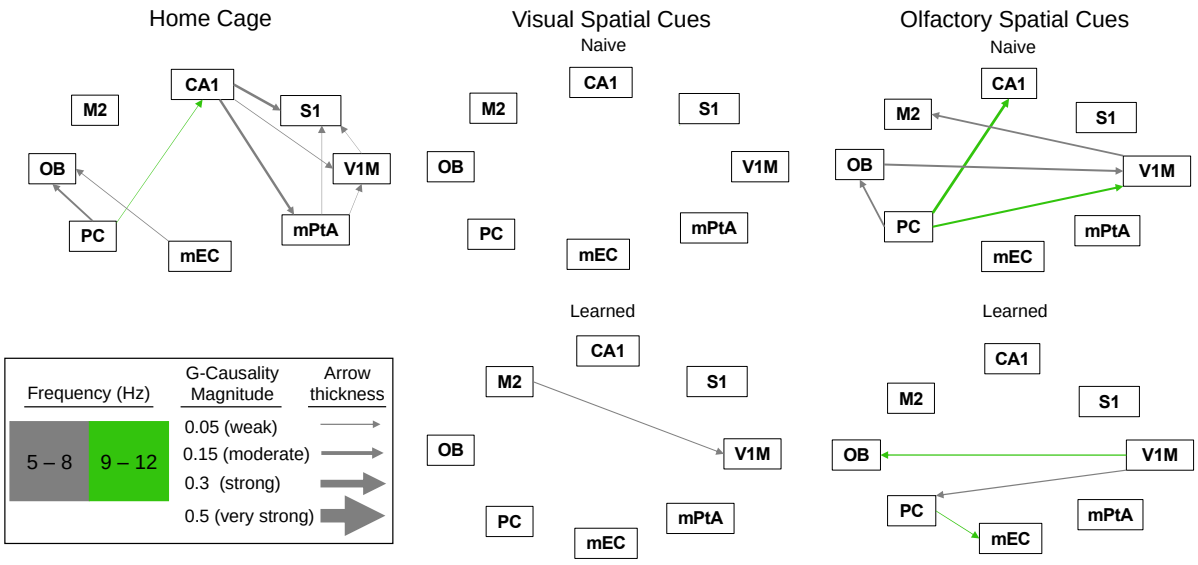

Figure 16. Granger causality for lower frequencies (5-12 Hz) during home cage activity and spatial learning with visual versus olfactory spatial cues. Recordings in OB, CA1, PC, mEC, mPtA, V1M, and S1. N = 3 rats.

The higher frequency interactions for this second group of rats showed significant effects involving the several additional neocortical areas. Home cage activity and the naive state of spatial learning with olfactory or visual spatial cues showed significant interactions in beta and gamma bands (Figure 16A). During home cage activity, there is moderate beta (15-35 Hz) causality from PC to mEC, and weak beta causality from OB to PC. PC also shows moderate low gamma (40-60 Hz) causality to OB, which exhibits weak low gamma causality to M2. M2 also receives weak beta causality from mEC in the home cage (Figure 16A, left). Early in visual spatial learning, there is only weak PC beta causality to S1 in these higher frequency bands (Figure 16A, right). There were no causal interactions at these faster frequencies early in olfactory spatial learning, so no network diagram is shown for the olfactory condition.

Higher frequency causal interactions once learning is reached with olfactory or visual spatial cues are shown in Figure 16B. Due to the density of the network these are separated by beta (top) and gamma (bottom) frequency bands. A dense beta network emerged between

somatosensory, motor, and sensory cortices once rewarded locations were learned with visual spatial cues. Specifically, M2 shows moderate beta causality to V1M and S1, along with weak beta causality to PC, mEC, and mPtA. S1 also shows moderate beta causality, but towards OB, PC, and mEC. PC exhibits weak beta causality towards mPtA and S1. A dense gamma network also emerged between these areas, specific to the visual cue condition. M2 exhibits moderate gamma causality to V1M and S1. There is also moderate gamma causality from mPtA to M2 and S1, weaker causality towards PC, mEC and V1M, and weak bidirectional gamma activity between mPtA and OB. PC and S1 show weak low gamma to M2, as does mPtA to S1. Thus, a highly connected network of beta and gamma oscillations emerges among somatomotor and sensory areas following allocentric learning with visual spatial cues (Figure 16B, middle).

A sparser high frequency network emerged following olfactory spatial learning (Figure 16B, right) compared to visual spatial learning. Once a location is learned with olfactory spatial cues, OB shows moderate beta causality to M2, and weaker beta causality to V1M. There is also some beta causality from mPtA to CA1 and to V1M. Very few gamma interactions are seen between the neocortical areas which densely interacted at these faster frequencies following visual spatial learning. There is weak causality from V1M to S1 at high gamma, and from S1 to CA1 at low gamma. Otherwise, causal interactions are absent at these higher frequencies during olfactory spatial learning, among the same network where causal interactions at these frequencies were strong during visual spatial learning.

The time-domain pairwise-conditional causalities summarize these changes at a coarser level (Figure 16C). Most notably, there is strong OB to M2 causality throughout visual spatial learning, but this interaction is only strengthened to that level once criterion is reached for olfactory spatial learning. CA1 initially shows strong causality to mPtA and S1 in visual spatial

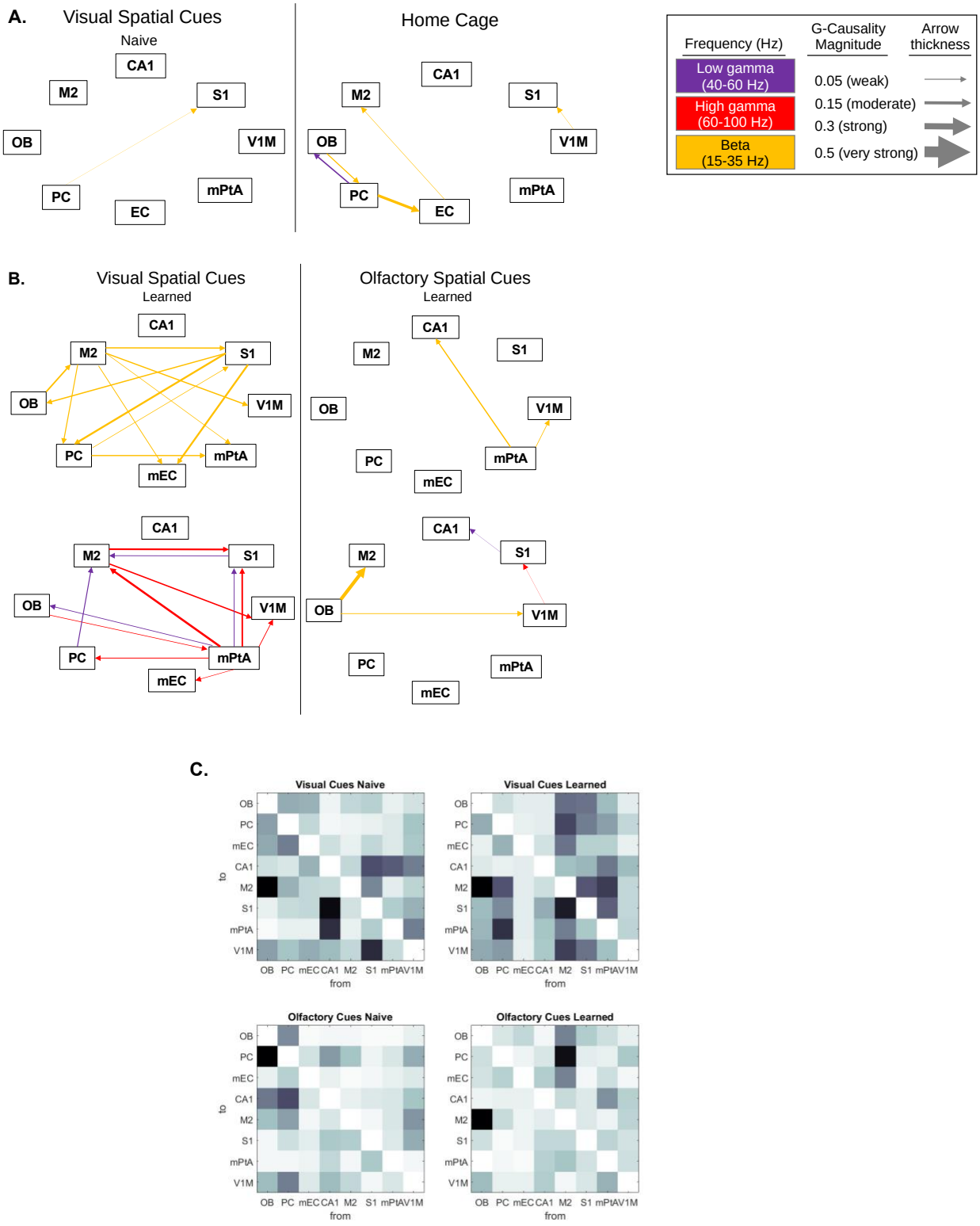

Figure 17. Granger causality for faster frequency bands including beta (15-35 Hz), low gamma (40-60 Hz), and high gamma (60-100 Hz) during home cage activity and spatial learning with visual versus olfactory spatial cues.

learning, but this weakens with learning. Conversely, causality is strengthened from M2 to S1, mPtA, mEC and V1M, along with olfactory areas OB and PC. S1 also shows increased causality upon visual spatial learning with olfactory areas OB and PC. mPtA shows increases with M2 and S1 following visual spatial learning. During olfactory spatial learning, these neocortical areas are largely absent except for M2, which shows increased causal influence from OB following olfactory spatial learning. M2 also shows strengthened causal input to the olfactory system following allocentric learning with olfactory spatial cues, including to PC and OB (Figure 17C).

Discussion

Distal interactions between primary olfactory and visual areas were seen during spatial learning in rats, shown by coherent neural oscillations around 8-10 Hz, and by directional Granger causality analyses. Interactions detected by coherence at slow respiratory and theta frequencies were generally less prominent than during spatial navigation shown in Chapter 3. Basal theta networks were detected between CA1, S1, and mPtA, which maintained prominent coherent theta oscillations (~8 Hz) during all behavioral conditions, including home cage activity and spatial learning with visual and olfactory spatial cues (Figure 14). This network appeared to be driven by hippocampal networks during home cage activity, since CA1 showed Granger causality at theta frequency towards S1 and mPtA in this condition (Figure 16). mEC-M2 coherence was elevated above home cage and chance levels throughout spatial learning in both conditions, which suggests hippocampal circuits may interact with motor areas in special circumstances during spatial decision making.

Granger causality analyses were presented separately for rats that had Resp and DG recordings and rats that had additional cortical areas recorded. Some discrepancies between other

areas common to these two groups arose. For example, OB and PC interact at slow frequencies in all spatial learning conditions in the first group (Figure 14), and only in one spatial learning condition in the second group of rats, where PC-V1M interactions are also only seen (Figure 16). Granger causality analyses were run on each rat separately and then averaged within groups. Each jointly estimated regression looks at two variables of interest at a time, conditioned on the rest of the variables. Therefore, it is possible that the presence of different conditioning variables between the two groups of rats may affect the causal interactions detected by Granger causality, and future studies will include a combined analysis of the common areas. Preliminary analysis suggests moderate OB to CA1 interactions may emerge upon acquisition of olfactory spatial learning when conditioned with common sites across all rats, which was only detected as a weak interaction in the first group of rats in these analyses (Figure 14).

Differences between common sites like OB and PC interactions are also present in higher frequency Granger causality interactions shown. However, no high-frequency Granger causality interactions were seen during foraging in the previous chapter, while three of these same rats show OB to V1M beta causality and bidirectional OB-PC gamma causality, along with V1M gamma to CA1, during visual spatial learning (Figure 14C). The additional recording sites from this experiment also showed robust higher-frequency interactions, which mostly emerged once learning criterion was reached with visual spatial cues (Figure 17). Visual, motor, and somatosensory areas showed dense networks of beta and gamma causality interactions, with input to mEC, an important area for spatial navigation and memory (Buzsáki and Moser, 2013). Beta oscillations have been related to motor tasks (Hermer-Vazquez et al., 2007; Balasubramanian et al., 2020) and motor planning on spatial tasks (Caplan et al., 2003), so the beta interactions reported here could be especially important during the decision epoch of a

spatial task where rats decide direction of movement based on memory. Olfactory spatial learning also leads to directional interactions in the beta band, especially from OB to M2, which was also present in visual spatial cues. The moderate OB to M2 beta causality is reminiscent of beta coherence between OB and primary motor cortex on an olfactory-driven reach task (Hermer-Vazquez et al., 2007). Furthermore, OB to M2 beta causality was only seen after learning with olfactory spatial cues, similar to the beta and gamma networks that emerged with visual spatial learning.

In summary, Chapter 4 shows dynamic network interactions that depend on behavioral and learning state which are unique from those seen during foraging in the previous chapter. Robust high-frequency interactions occur between cortical areas at the decision point of a learned spatial task, with differences in frequencies of interactions and network density. This chapter shows more dramatic changes to network configuration related to the modality of spatial cues used to navigate to a learned goal, than on the modality of similar spatial cues used for exploratory navigation in the previous chapter.

Chapter 5: Respiratory and theta phase-amplitude coupling with faster neural oscillations

Respiration has been shown to modulate faster rhythms, emerging from local activity, in rodents and humans differently during different behavioral states including sleep stages, exploration, and learning (Rojas-Líbano et al., 2014; Zelano et al., 2016; Tort et al., 2018b). Low frequency oscillations are larger amplitude and better for longer range interactions (Von Stein and Sarnthein, 2000; Buzsáki and Draguhn, 2004), while high frequency oscillations appear to represent local activity (e.g., multi-units equal high frequency LFP). For example, gamma oscillations (40-100 Hz) in the rodent primary olfactory system emerge locally (Freeman, 1968) from excitatory-inhibitory circuit interactions (Eeckman and Freeman, 1990). Similarly, hippocampal pyramidal cells in CA1 display high frequency oscillations (<100 Hz) during behavioral immobility, consummatory behaviors, and slow-wave sleep (Buzsaki et al., 1992), and gamma oscillations couple regions CA3 and CA1 of the hippocampus during spatial memory (Montgomery and Buzsáki, 2007). Slow and fast oscillations can interact, with low frequency oscillations modulating the amplitude of high frequency oscillations, detectable by measure of phase-amplitude coupling (Jensen and Colgin, 2007; Tort et al., 2010). Hippocampal LFP oscillations exhibit phase-amplitude coupling with the striatum during spatial learning (Tort et al., 2008).

I characterized distal interactions between brain areas important for sensation and memory, limited to slower oscillations in rodent respiratory and theta frequency bands (4-12 Hz). Here, in Chapter 5, I analyze phase-amplitude coupling of low and high frequency oscillations during the spatial navigation and learning tasks from experiments and data described in Chapters 3 and 4. I compare respiratory and theta modulation of faster cortical oscillations in exploratory versus learned behaviors using visual versus olfactory spatial cues. I used the open source

package by Tort et al., (Tort et al., 2010) to quantify phase-amplitude coupling between pairs of recording sites (Chapter 2: Methods). The behavior protocol for foraging is outlined in Figure 3, and for spatial learning in Figure 4, of Chapter 2. Data collected during rat foraging and spatial learning behaviors that were characterized in Chapters 3 and 4, respectively, with spectral and Granger causality analyses of respiratory and theta networks, are additionally analyzed for phase-amplitude coupling with faster oscillations here. The high-frequency Granger causality results for spatial learning (Figure 17) suggest involvement of faster oscillations especially for spatial learning. Phase-amplitude coupling analysis is presented first while rats foraged (Experiment 1, Chapter 3), then while rats underwent spatial learning (Experiment 2, Chapter 4), with visual versus olfactory spatial cues.

Results

Phase-Amplitude Coupling: Foraging

The first set of analyses is on data from Chapter 3, which involved spectral analyses of power and coherence, along with Granger Causality, during foraging behavior. There were no high frequency interactions detected with Granger causality, but spectral analyses were limited to slow frequencies (0-18 Hz) in Chapter 3. Six rats made up this dataset, with LFPs recorded in olfactory bulb (OB), piriform cortex (PC), dentate gyrus (DG) and CA1 of hippocampus in all six rats, and primary visual cortex (V1M) was recorded in four of the rats. Nasal respiratory (Resp) recordings were also collected in all six rats. Phase-amplitude coupling data is presented in comodulogram plots which represent in pseudocolor scale the modulation index (MI) values (Chapter 2), by pairs of areas shown with the phase of one area to the amplitude modulation of

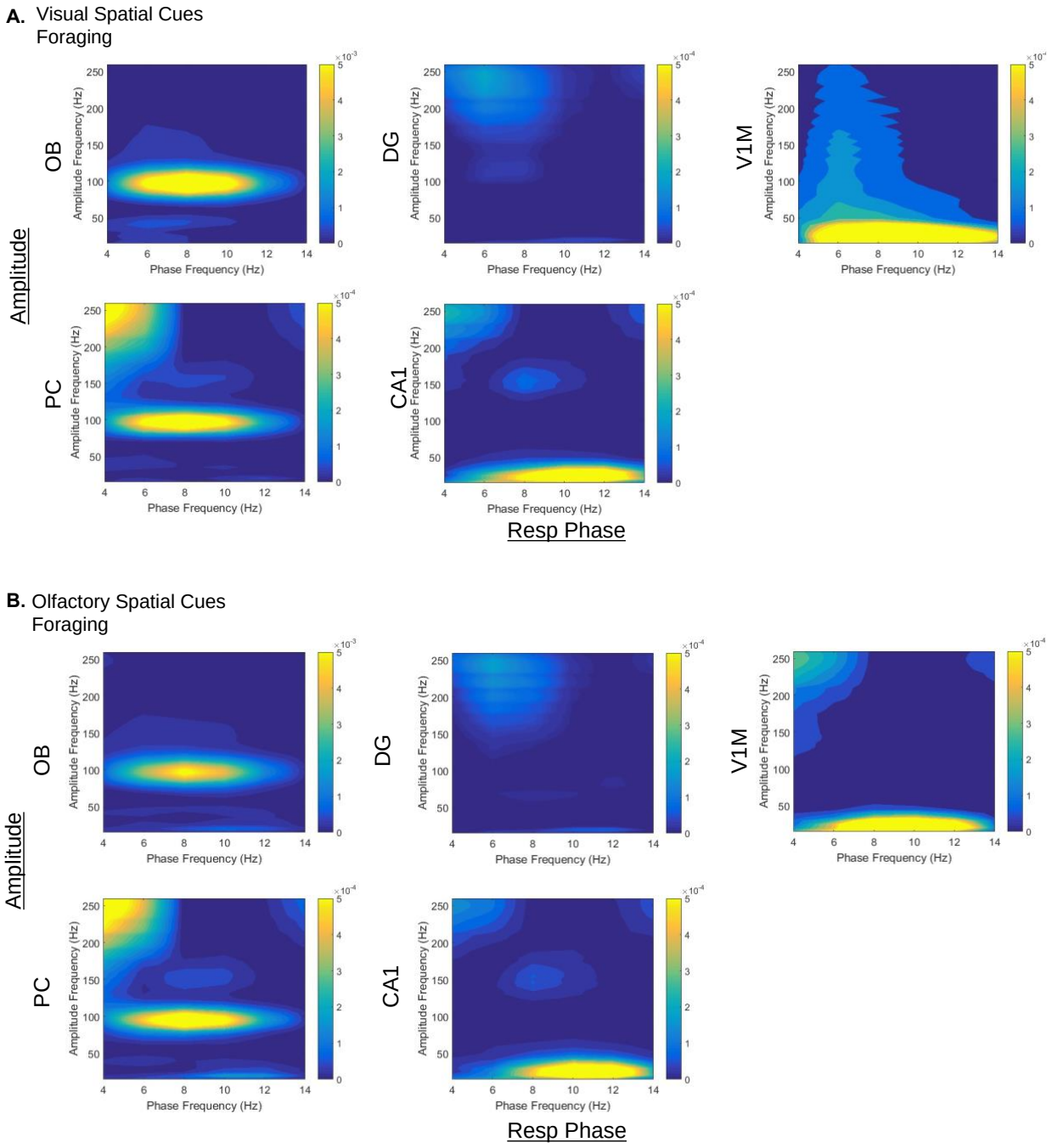

Figure 18. Respiratory phase-amplitude coupling during foraging with visual (A.) and olfactory (B.) spatial cues. Y-axes range from 15-250 Hz. Note color axis is an order of magnitude larger for Resp-OB. N=6 for OB, PC, DG, and CA1. N=4 for V1M.

all others, at phase frequencies of 4-12 Hz and amplitude frequencies of 15-250 Hz. Each comodulogram is from data concatenated across subjects by condition. Subtracted out from these are the average plus two standard deviations of comodulograms from shuffled data, so all phase-amplitude couplings are significant at $p < 0.05$. Home cage activity was characterized in addition to foraging, but will only be discussed and not visually presented here.

Respiratory phase-amplitude coupling patterns are strikingly similar between foraging with visual (Figure 18A) and olfactory (Figure 18B) spatial cues. Respiratory phase showed the strongest modulation of OB and PC amplitude, with the color scale shown an order of magnitude larger for OB than the rest of the plots. The phase of respiratory frequency at 4-12 Hz modulated the amplitude of high gamma (~100 Hz) oscillations in the OB and PC during foraging with either visual (Figure 18A) or olfactory (18B) spatial cues. Respiratory phase modulates CA1 beta oscillations (15-35 Hz) at 8-13 Hz, and V1M beta oscillations at 4-13 Hz. During home cage activity (data not shown), respiratory modulation of OB and PC gamma was similar, while modulation of CA1 and V1M beta was absent.

Coupling to slow olfactory rhythms

Using the OB LFP signal instead of the respiratory signal to provide the slow oscillation (phase) component of the analysis shows similar patterns to respiratory phase-amplitude coupling (Figure 19). Again, phase-amplitude coupling appears similar for OB phase with other areas in both visual (Figure 19A) and olfactory (Figure 19B) foraging conditions. Note OB-OB coupling is on a color scale an order of magnitude larger than the other panels. The OB exhibits 4-10 Hz phase-amplitude coupling to its own high gamma oscillations (~100 Hz) and those of

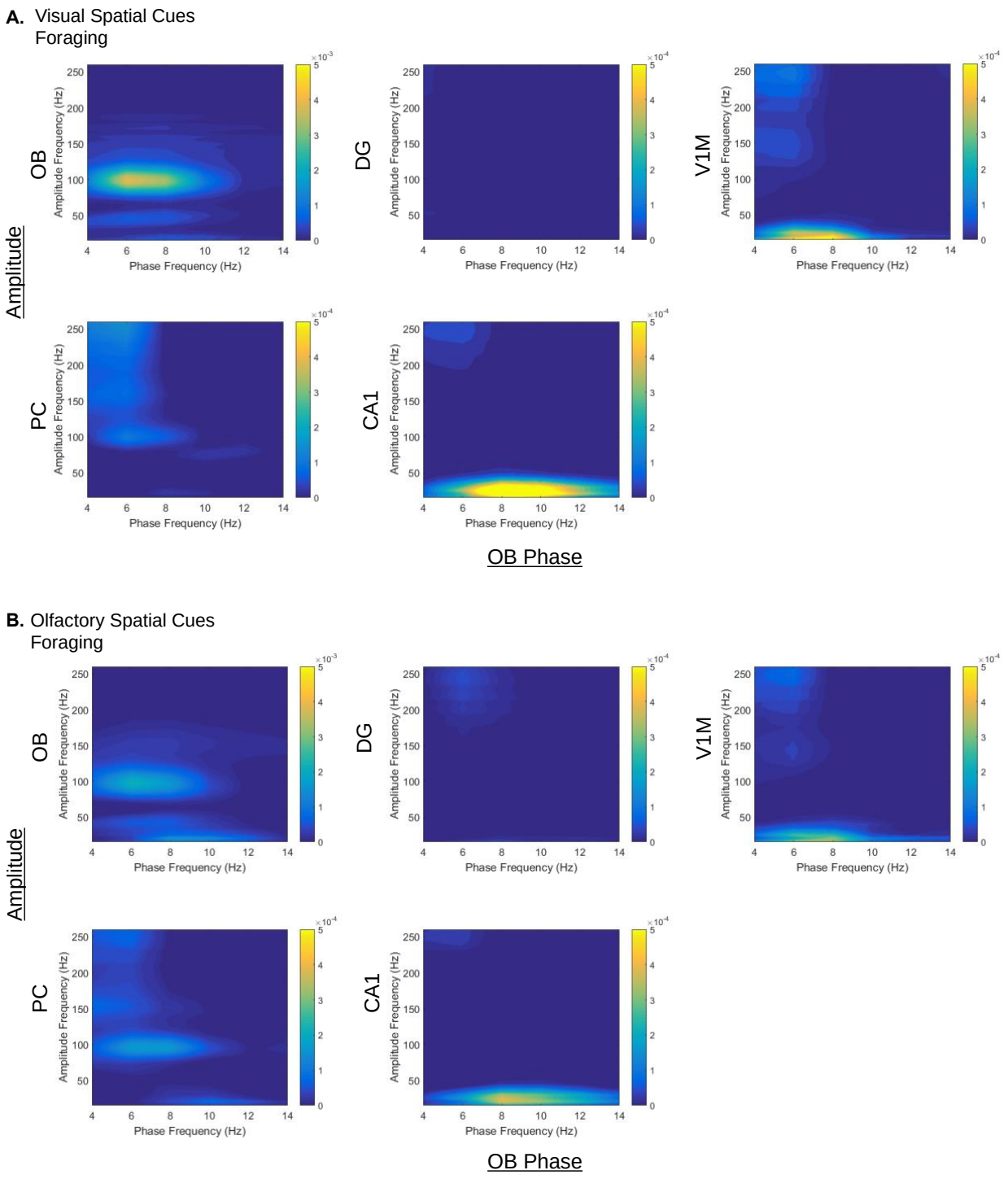

Figure 19. OB phase-amplitude coupling compared during foraging with visual (A.) and olfactory (B.) spatial cues. Y-axes range from 15-250 Hz. Note color axis is an order of magnitude larger for OB-OB. N=6 for OB, PC, DG, and CA1. N=4 for V1M.

the PC, similar to those reported elsewhere (Rojas-Líbano et al., 2014). OB oscillations at 6-12 Hz phase-amplitude couple with CA1 beta, and similarly at 6-8 Hz for V1M beta oscillations. As was the case for respiratory phase-amplitude coupling, only the coupling between OB-OB and OB-PC were also present during home cage activity.

Phase-amplitude coupling between OB and PC may be bidirectional, because PC phase at 4-10 Hz also couples with OB high gamma in both foraging conditions and during home cage activity at 4-6 Hz (Figure 20). However, because OB-PC signals are coherent in the low frequency range, and Granger analysis shows causal influence only from OB to PC, it is unlikely that this drive is bidirectional (Chapter 3). PC-PC shows phase-amplitude coupling in the 6-12 Hz band, also at high gamma around 100 Hz, during foraging with visual spatial cues (Figure 20A), and this appears more prominently with olfactory spatial cues (Figure 20B). There is weak but significant low gamma (~50 Hz) and beta (~20 Hz) coupling in the visual condition between PC and OB and PC, at PC phase frequencies of 8-12 Hz (Figure 20A). PC phase-amplitude coupling with OB beta is more prominent during olfactory foraging (Figure 20B), along with coupling with PC beta. Similar to Resp and OB, PC shows phase-amplitude coupling with CA1 and V1M beta oscillations at 8-12 Hz. Additionally, PC low frequency activity couples with CA1 and V1M high frequency rhythms (approximately 150 Hz), at a slower frequency range (6-8 Hz), in both foraging conditions (Figure 20). PC phase at 6-8 Hz also couples with DG very high frequency rhythms (200-250 Hz) in both foraging conditions.

Coupling to slow hippocampal rhythms

In the visual foraging condition, DG phase couples with the amplitude of OB high gamma oscillations (~100 Hz) at theta frequency (6-12 Hz). The DG, similar to the PC, exhibits

low gamma (~50 Hz) and beta (~20 Hz) phase-amplitude coupling in the visual condition with OB at 8-12 Hz (Figure 20A). There is subtle DG-OB coupling of beta oscillations at 8-12 Hz in the visual condition, which is clearly seen during olfactory foraging, similarly for DG-PC but to a lesser extent (Figure 20B). DG couples at 6-12 Hz with CA1 and V1M beta oscillations in both

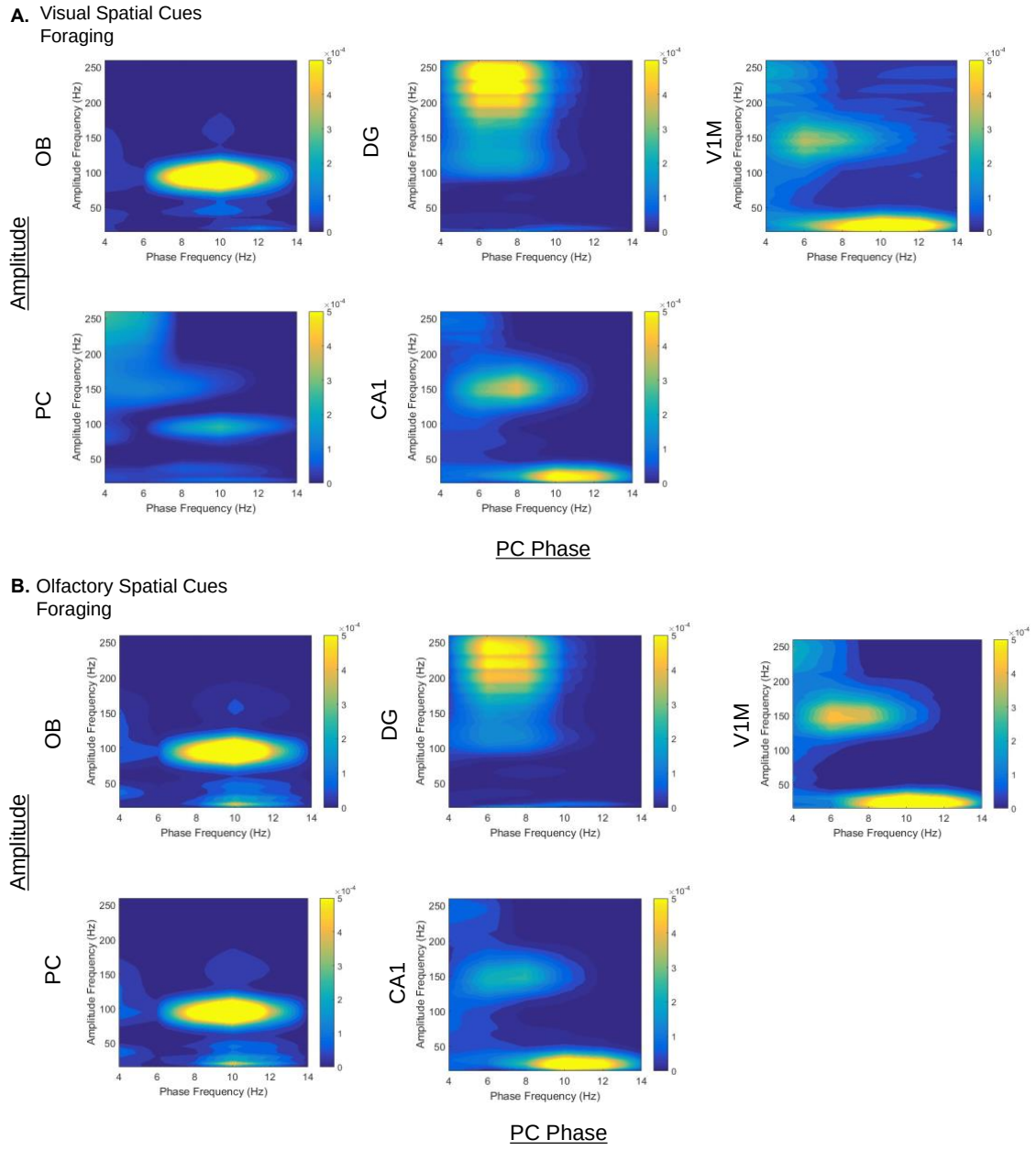

Figure 20. PC phase-amplitude coupling compared during foraging with visual (A.) and olfactory (B.) spatial cues. N=6 for OB, PC, DG, and CA1. N=4 for V1M.

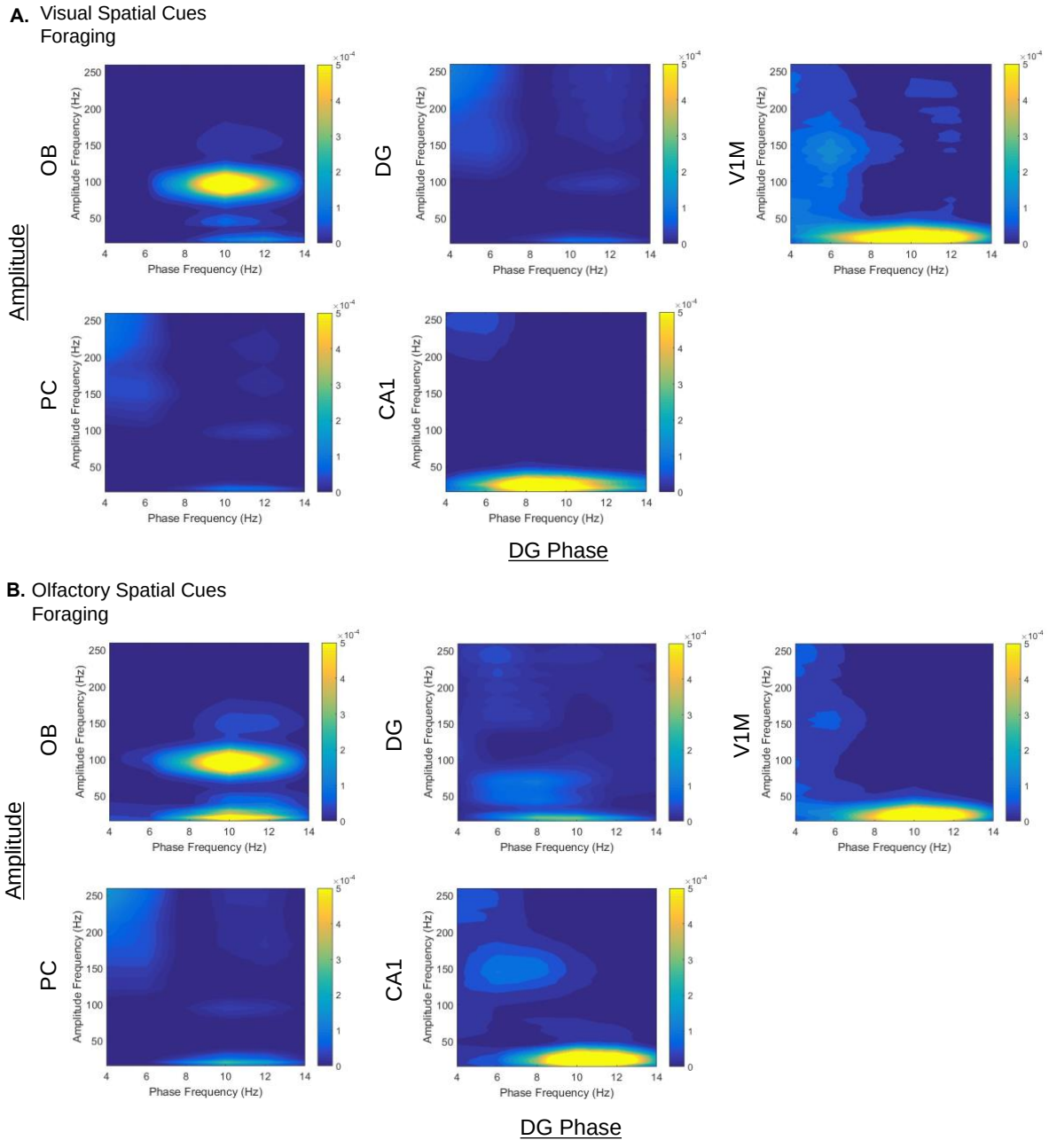

Figure 21. DG phase-amplitude coupling during foraging with visual (A.) and olfactory (B.) spatial cues. N=6 for OB, PC, DG, and CA1. N=4 for V1M.

visual and olfactory conditions. During visual foraging, there is weak coupling of high frequency (~150 Hz) of V1M oscillations to 6 Hz DG phase (Figure 21A), and during olfactory foraging there is high frequency coupling (~150 Hz) of CA1 oscillations to the phase of 6 Hz DG oscillations. None of these interactions were present during home cage activity.

CA1 shows a similar pattern to DG in relation to OB during foraging: prominent high gamma coupling between CA1 low frequency phase and high frequency amplitude in OB in both conditions, and stronger beta coupling with olfactory spatial cues (Figure 22). CA1 also showed weaker modulation of low gamma in OB with visual spatial cues. However, these occurred at a wider range of phase frequencies (4-12 Hz) for CA1 than for DG (8-12 Hz; Figure 22). There was 4-12 Hz phase-amplitude coupling from CA1 to PC gamma and higher frequency oscillations in both conditions. Similar to the other areas, V1M and CA1 beta amplitude was modulated by CA1 oscillations at 4-12 Hz (Figure 22). There is some modulation of high frequency oscillations in V1M DG and CA1, from CA1 oscillations at 6-8 Hz.

Coupling to slow visual cortex rhythms

Interestingly, V1M shows phase-amplitude coupling with OB, CA1, and V1M beta oscillations in both visual and olfactory foraging conditions, at 6-12 Hz (Figure 22) and with the DG during olfactory foraging (Figure 22B). This is accompanied by V1M coupling with OB high gamma, also at 6-12 Hz and in both conditions. V1M only shows 6-12 Hz coupling with DG high gamma in the olfactory condition (Figure 22B).

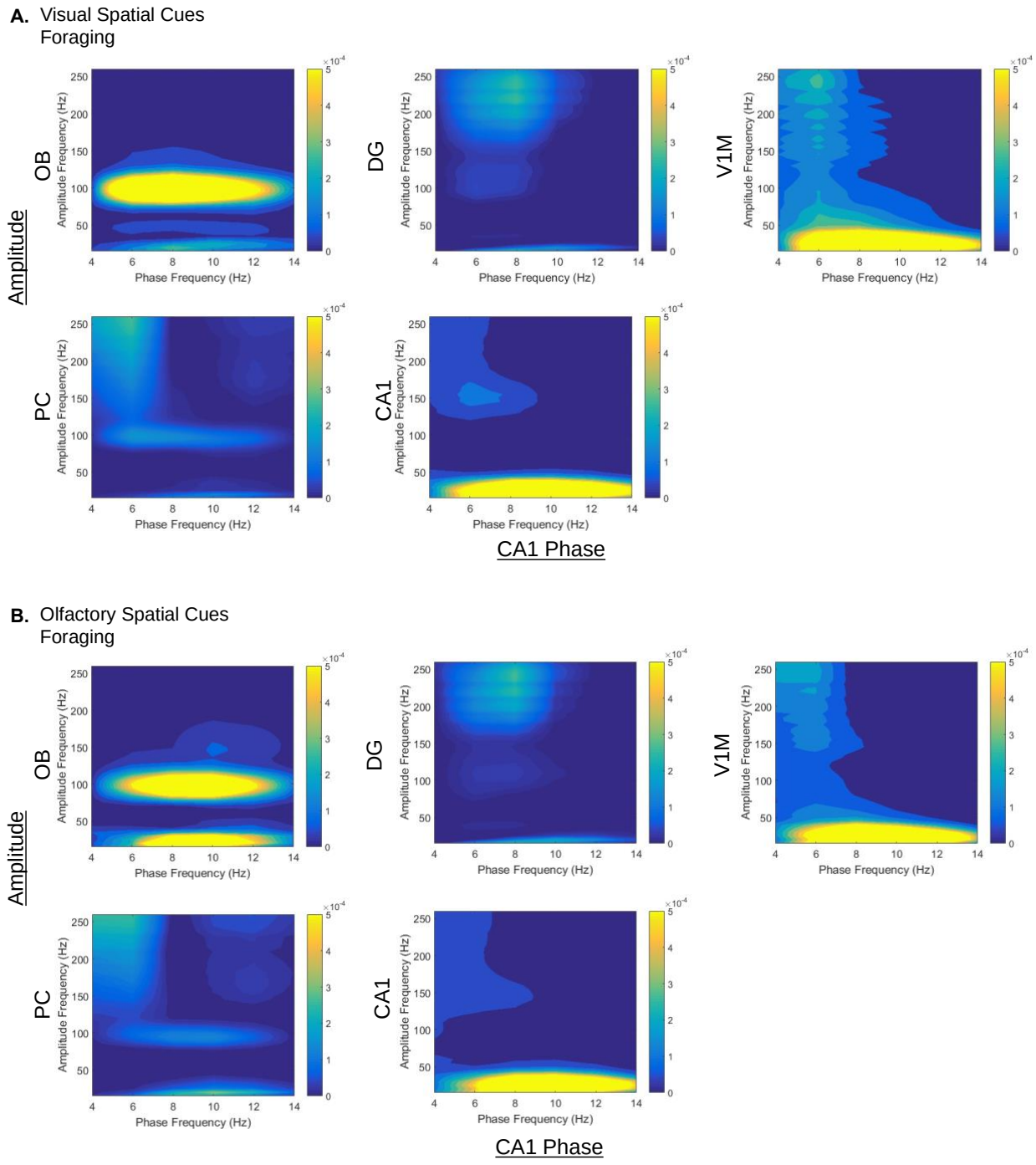

Figure 22. CA1 phase amplitude-coupling during foraging with visual (A.) and olfactory (B.) spatial cues. N=6 for OB, PC, DG, and CA1. N=4 for V1M.

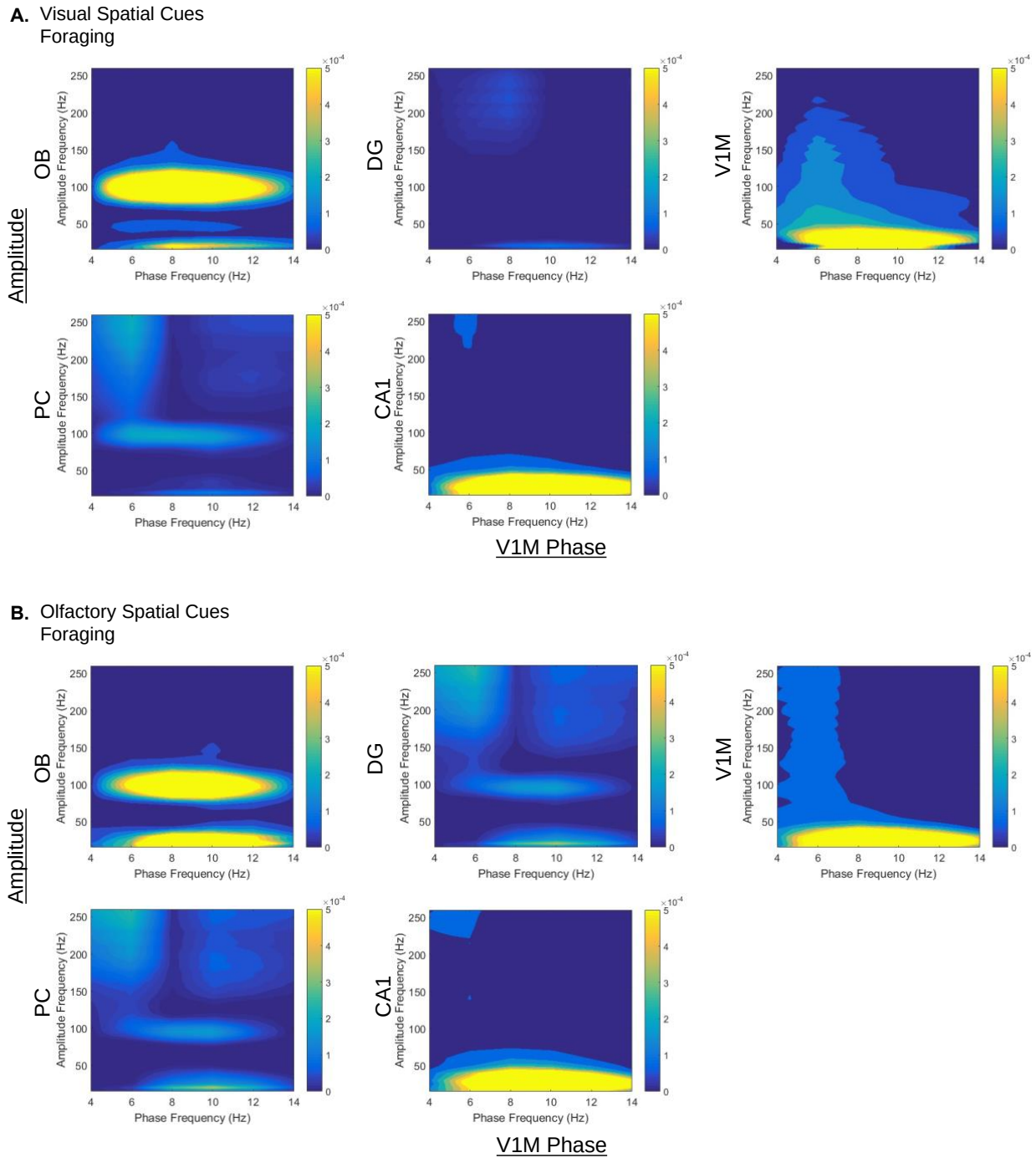

Figure 23. V1M phase-amplitude coupling during foraging with visual (A.) and olfactory (B.) spatial cues. N=4.

Phase-Amplitude Coupling: Spatial Learning

The second set of phase-amplitude coupling analyses focus on recordings made during spatial learning from Chapter 4. The task involved allocentric learning (*i.e.,* assocations between external objects) compared between visual and olfactory spatial cues. Data are presented for respiratory (Resp) and dentate gyrus (DG) interactions from three of rats from the foraging study who also completed the spatial learning study, and for areas that were common to all six rats trained on spatial learning. These areas include OB, PC, CA1, and V1M. Phase-amplitude coupling measures are compared between modality (visual vs. olfactory spatial cues) and cognitive behavioral states (naive vs. learned).

The phase of the respiratory frequency at 6-12 Hz couples with high gamma amplitude in OB and PC throughout spatial learning with both visual (Figure 23) and olfactory (Figure 25) spatial cues. High frequency DG oscillations around 150 Hz that are coupled to 4-8 Hz respiratory phase emerge once the goal locations are learned with visual spatial cues (Figure 23). Conversely, respiratory phase-amplitude coupling with CA1 gamma is present early but not late in visual spatial learning. There is weak respiratory phase-amplitude coupling with DG high gamma and CA1 high frequency oscillations (~150 Hz) throughout olfactory spatial learning (Figure 25), at around 4-8 Hz respiratory frequency.

DG theta at 8-10 Hz couples with OB high gamma around 100 Hz throughout spatial learning with visual cues, while DG to PC coupling of this same type only occurs once learning criterion is reached (Figure 26). V1M shows high frequency oscillatory coupling (~150 Hz) to the phase of DG theta oscillations early but not late in visual learning. Conversely, DG couples to its own high frequency oscillations (>100 Hz) from the phase of 8-10 Hz theta in the naive state, which appear more prominent as higher frequency DG oscillations emerge coupled to the

phase of slower 4-8 Hz oscillations in the learned state. DG also shows weak coupling with CA1 high frequency oscillations throughout spatial learning with visual spatial cues.

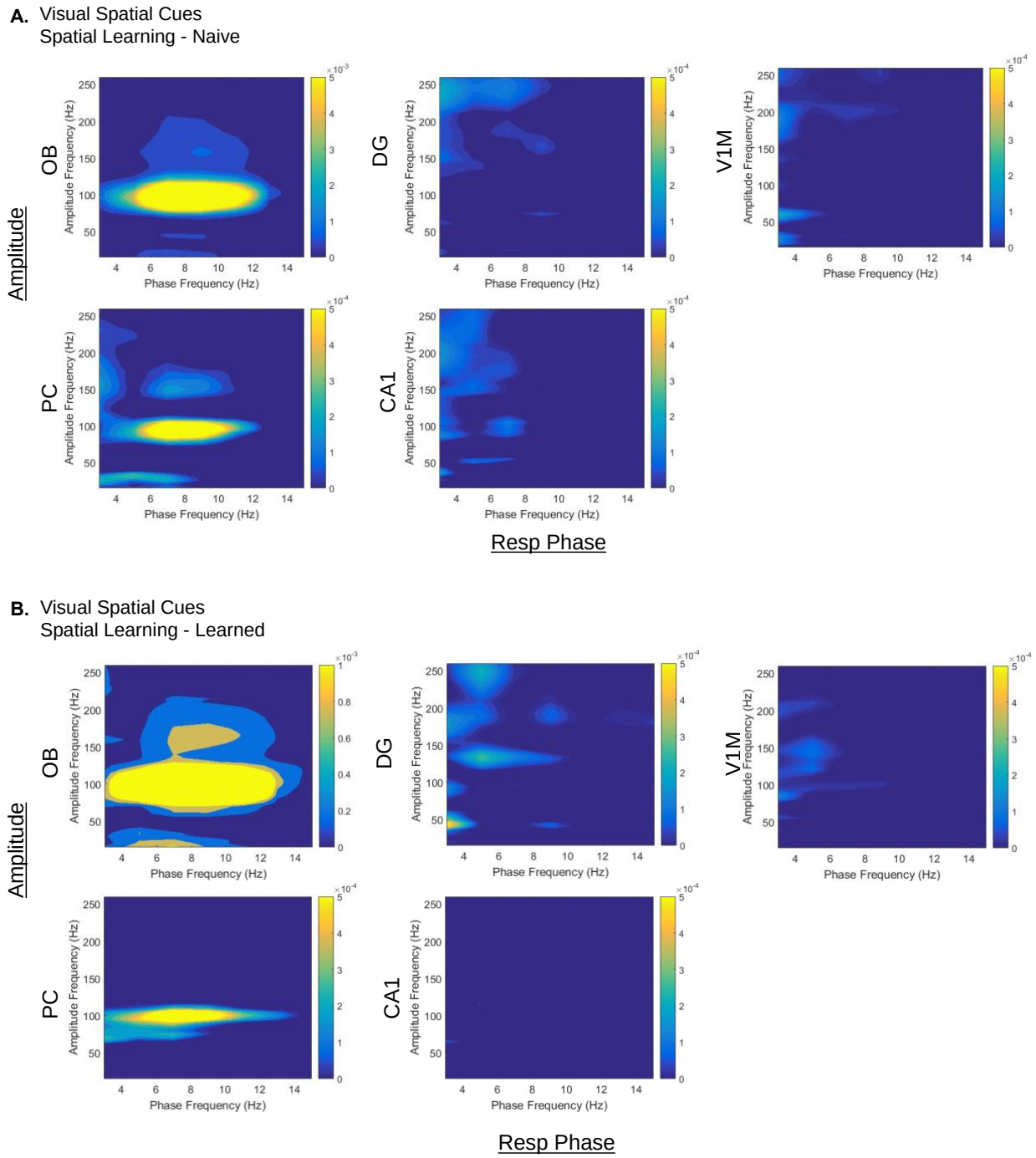

Figure 24. Respiratory phase-amplitude coupling throughout spatial learning with visual spatial cues. Note Resp-OB has an order of magnitude larger color scale. N=3.

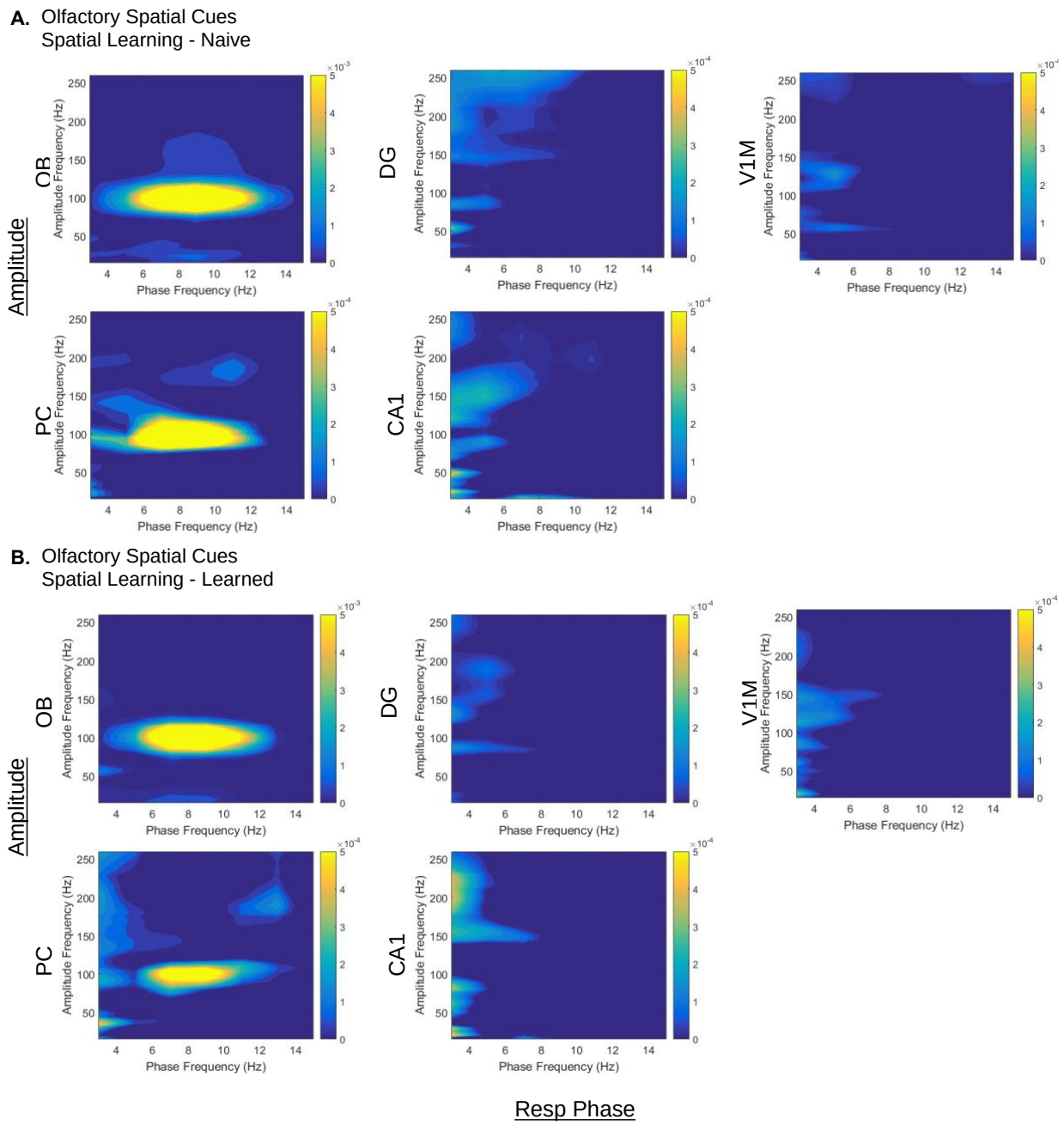

Figure 25. Respiratory phase-amplitude coupling throughout spatial learning with olfactory spatial cues. Note Resp-OB has an order of magnitude larger color scale. N = 3.

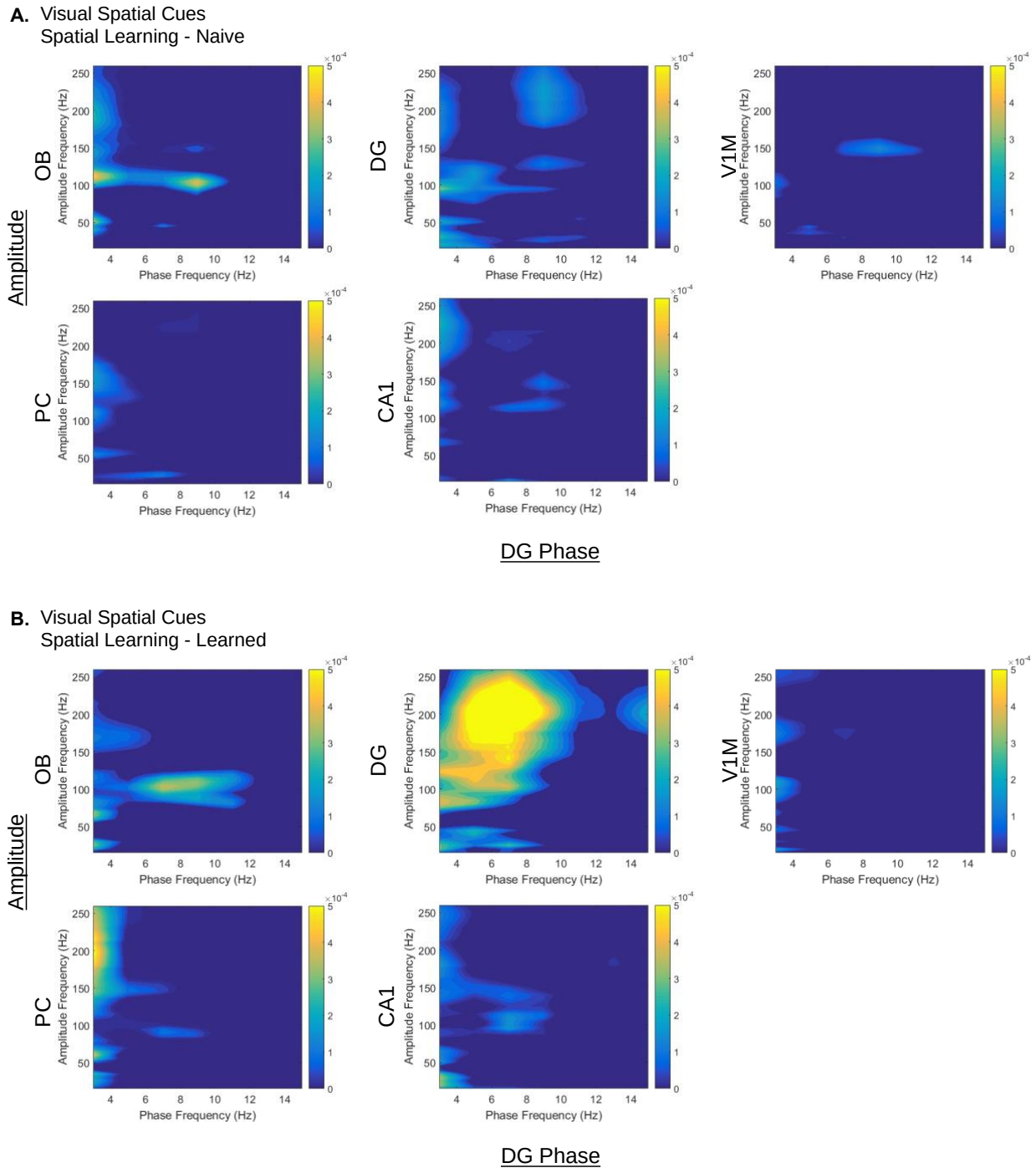

Figure 26. DG phase-amplitude coupling during spatial learning with visual-spatial cues. N=3.

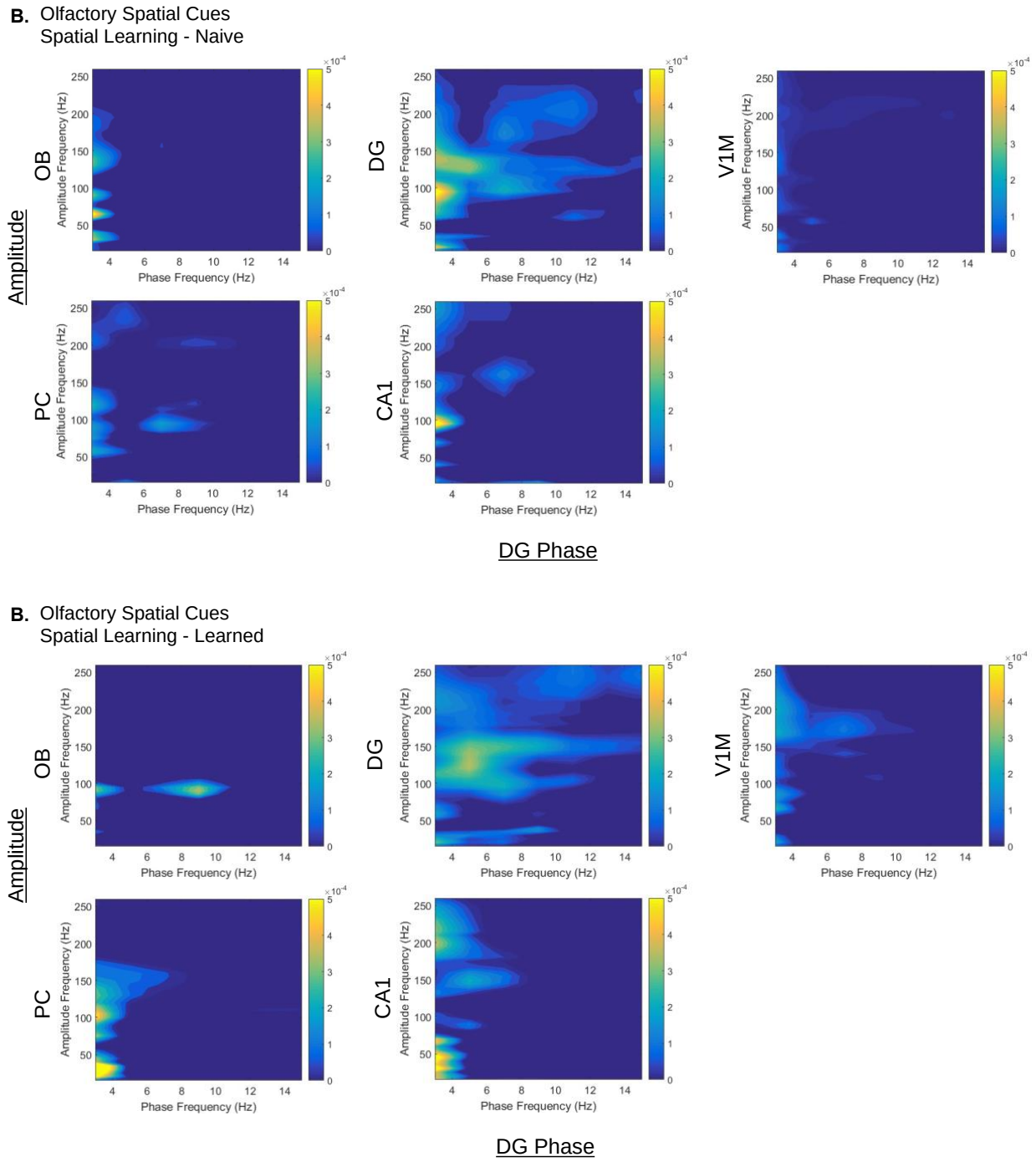

Figure 27. DG phase-amplitude coupling during spatial learning with olfactory spatial cues. N=3.

A different picture emerges for DG phase-amplitude coupling during spatial learning with olfactory cues (Figure 27). The phase of 6-10 Hz DG oscillations couples with OB high

gamma only once the location is learned with olfactory spatial cues (Figure 27B), and not in the naive state (Figure 27A). Interestingly, the opposite relationship is seen with PC, with DG phase-amplitude coupling at 6-8 Hz with PC high gamma around 80-100 Hz only is present in the naive but not learned state with olfactory spatial cues (Figure 27). High frequency oscillations in DG and CA1 couple to DG phase at 6-8 Hz throughout olfactory spatial learning, but V1M only shows this same coupling once learning criterion was reached. Figure 28 shows that PC phase-amplitude couples with DG high frequency oscillations at 8-12 Hz in the naive state, but this shifts to 6-8 Hz with learning in the visual condition, similar to the pattern for DG-DG phase-amplitude coupling. Throughout olfactory learning, PC-DG phase-amplitude coupling is consistent from 6-8 Hz PC oscillatory phase modulating fast DG oscillations.

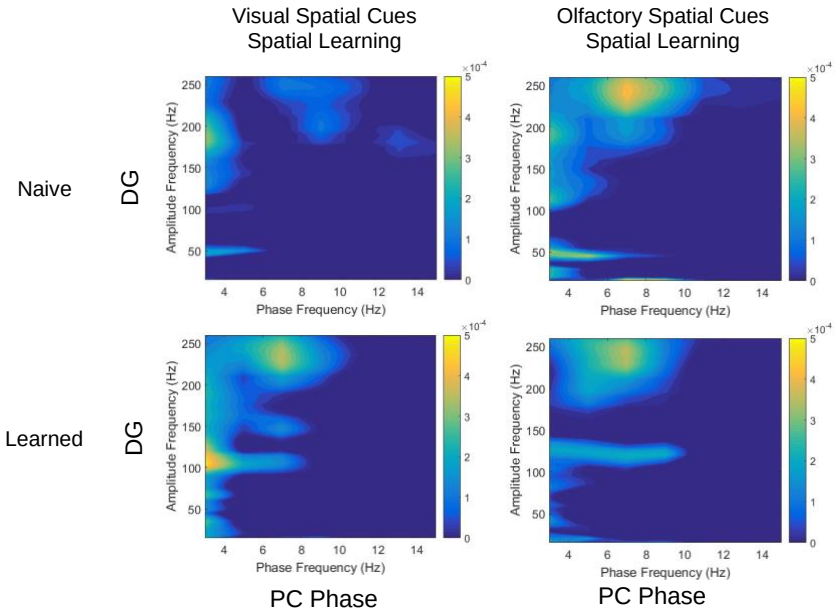

Figure 28. PC phase-amplitude coupling with DG throughout visual and olfactory spatial learning. N=3.

Phase-amplitude coupling among areas that are common to all six rats will now be described, which include OB, PC, CA1, and V1M. Throughout spatial learning with visual spatial cues, OB low frequency activity couples with its own high gamma (~100 Hz) at 4-12 Hz

(Figure 28). With olfactory spatial cues, this coupling only occurs initially in training, but is absent once learning criterion is reached. The opposite relationship occurs for OB coupling to PC high gamma during spatial learning with olfactory spatial cues, where high PC gamma coupling to OB 8-10 Hz phase frequency is present in the naive but not the learned state. Further, this relationship is the opposite during visual spatial cues where OB couples with PC high gamma only once learning criterion is reached (Figure 28). A similar pattern is seen for PC coupling with OB and PC (not shown).

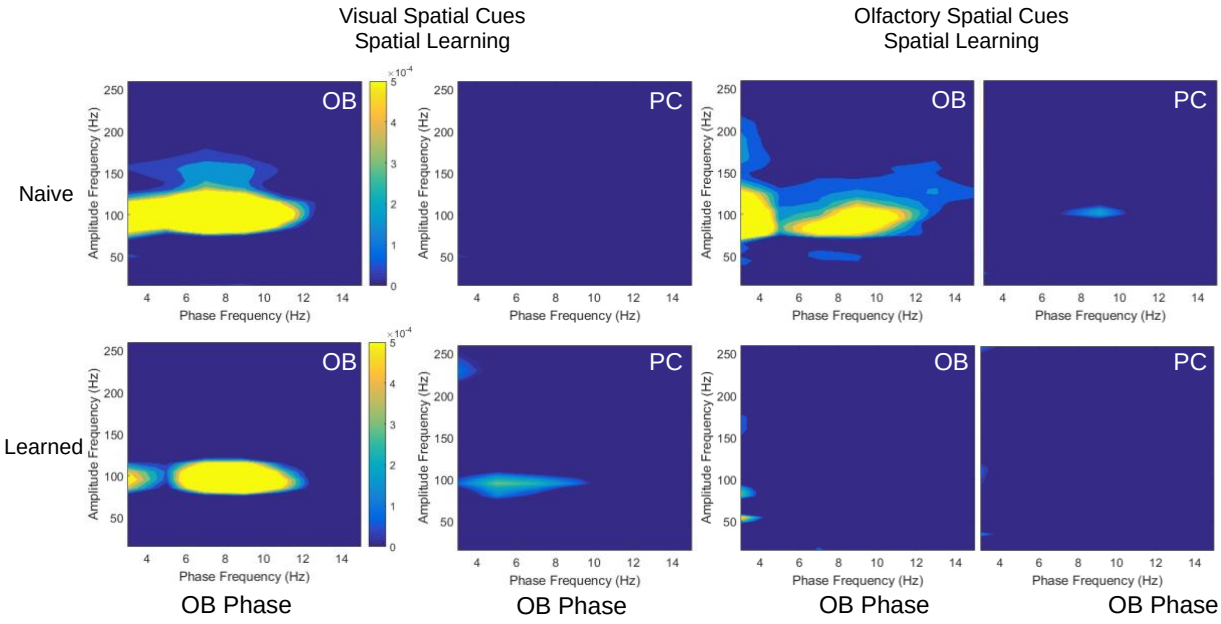

Figure 29. OB phase-amplitude coupling with OB and PC compared during spatial learning with visual versus olfactory spatial cues across learning states. N=6.

There were also some effects of modality of spatial cues during allocentric learning on hippocampal-visual cortex coupling (Figure 29). CA1 theta oscillations at 6-10 Hz couple with V1M low gamma, around 40-50 Hz, initially in training with visual spatial cues, but this coupling is not present once learning criterion is reached. CA1 also showed coupling to its own gamma frequency around 60-70 Hz with the phase of 4-6 Hz oscillations, only early in visual

and olfactory spatial learning as well. There is no CA1-V1M phase-amplitude coupling seen in the naive or learned state of learning with olfactory spatial cues (Figure 29).

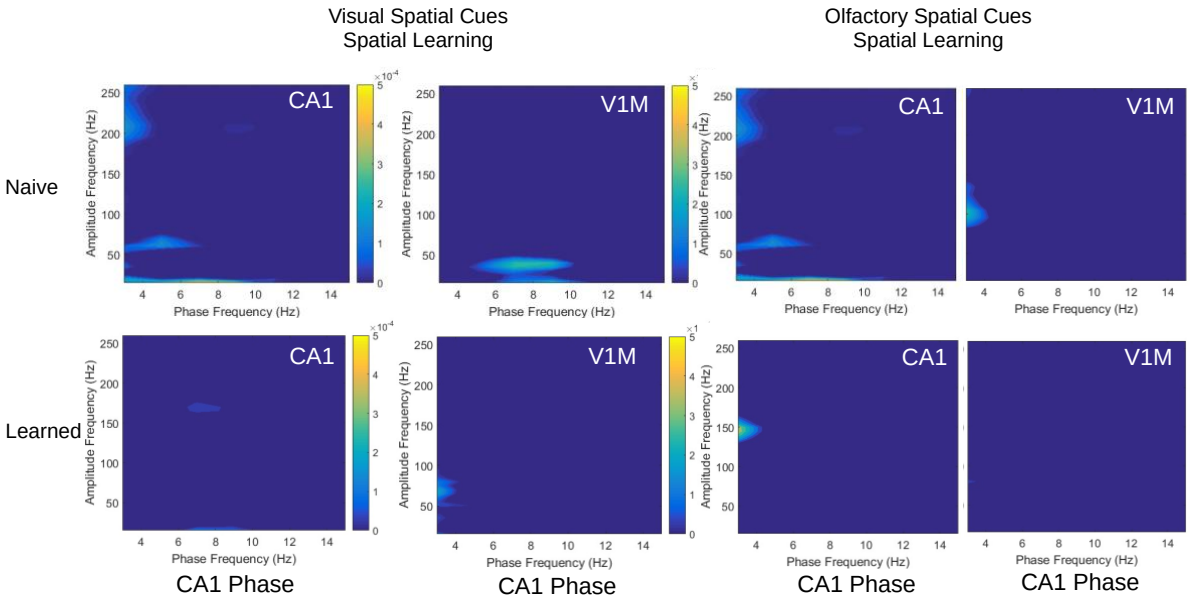

Figure 30. CA1 phase amplitude-coupling with CA1 and V1M during visual and olfactory spatial learning. N=6.

Discussion

Phase-Amplitude Coupling: Foraging

Respiratory oscillations modulate the phase of high frequency gamma oscillations in OB and PC from almost the whole range of respiratory frequencies (4-12 Hz), while respiration modulated CA1 only at 8-12 Hz (Figure 18). This fits with previous findings that the OB LFPs track all respiratory frequencies and phase-amplitude couple with high frequency gamma in OB (Rojas-Líbano et al., 2014), while previous findings suggested that OB and hippocampus match around theta frequency (6-12 Hz) for functionally relevant states for sensorimotor processing (Vanderwolf, 1969; Macrides et al., 1982; Kay, 2005). However, V1M beta oscillations were modulated at 4-12 Hz, suggesting modulation from a wider range of respiratory frequencies than CA1 beta.

High frequency oscillations (>100 Hz) emerged, coupled to the phase of primarily PC and CA1 oscillations at 6-12 Hz, and to some extent DG phase at 6-8 Hz to CA1 fast oscillatory amplitude, during foraging behavior. CA1 showed phase-locked oscillations at 150 Hz to 6-8 Hz PC oscillations (Figure 21). This coupling occurred at a slower frequency than the 8-12 Hz PC oscillations that coupled to CA1 beta, suggesting possibly different pathways supporting these distinct couplings. Sharp wave ripples are extremely synchronous events largely driven by hippocampal circuits that fall within this frequency range (100-250 Hz), and also occur in the piriform cortex with similar behavioral correlates as hippocampal sharp wave ripples in regards to planning and memory consolidation (Manabe et al., 2011; Barnes and Wilson, 2014; Narikiyo et al., 2014; Buzsáki, 2015). PC sharp wave ripples appear to occur separately from hippocampal sharp waves (Manabe et al., 2011; Narikiyo et al., 2014), although some coupling has been described (Buzsáki, 2015). PC modulated the amplitude of DG fast oscillations around 200-250 Hz at phase frequencies of 6-8 Hz, which matched the frequency of PC phase-amplitude coupling with CA1 and V1M fast oscillations at 150 Hz. This could reflect hippocampal and olfactory sharp wave ripples interacting, potentially through entorhinal cortex which is adjacent to PC and hippocampal circuits and a major driver of hippocampal sharp wave ripples (Buzsáki, 2015). However, the high frequency of DG oscillations shown here is within range of pathological ripples which occur above 200 Hz in epileptic rat models and humans (Bragin et al., 1999, 2004; Buzsáki, 2015). However, we saw no signs of seizure activity in the data, and the CA1 oscillations centered at normal sharp wave ripple frequency of 150 Hz argues against this.

While it was expected for respiratory modulation of olfactory areas, it was surprising to see slow V1M oscillations modulate fast frequencies of distal olfactory areas (Figure 23). There was high V1M-OB coherence during foraging at 8-10 Hz (Figure 7; Chapter 3), and OB showed

weak Granger causality to V1M in both foraging conditions at 9-12 Hz (Figure 8), which would suggest the OB should be showing greater modulation of V1M oscillations, unlike the converse which is implied in Figure 23. Respiratory phase, however, strongly modulates both OB and V1M high gamma amplitude, suggesting respiration may help couple olfactory and visual systems. Indeed, respiration also showed Granger causality towards V1M in both foraging conditions at 5-12 Hz (Figure 8). However, this leaves the V1M, and not Resp, phase-amplitude coupling of OB beta oscillations during foraging unexplained. Even PC, a robust beta oscillator (Kay et al., 2009), only modulates OB beta amplitude during olfactory spatial foraging, although it modulates CA1 and V1M at beta frequencies in both foraging conditions (Figure 20). It is likely that other non-recorded areas are involved in linking distal visual and olfactory systems. Beta oscillations can propagate among distributed neural systems, so further analyses of beta coherence, Granger causality, and beta phase amplitude-coupling should help disentangle these interactions.

Phase-Amplitude Coupling: Spatial Learning

Respiratory frequency at 4-12 Hz coupled with OB and PC high gamma throughout spatial learning with either visual or olfactory spatial cues (Figure 24-25), similar to that seen for foraging (Figure 18). Fast DG oscillations around 150 Hz coupled to respiration once learning criterion was reached with visual spatial cues, limited to slower 4-8 Hz respiratory frequency. Similarly, DG oscillations at 6-8 Hz coupled to DG high frequency oscillations around 150 Hz which increased with visual spatial learning (Figure 26). This could be related to previous findings of hippocampal sharp wave ripples (> 100 Hz) entrained to respiration in awake mice (Liu et al., 2017), and suggests a functional relevance of this coupling in spatial learning. There

is also respiratory coupling at 6-8 Hz to PC high frequency oscillations around 150 Hz early in visual spatial learning (Figure 24). Furthermore, PC shows robust 6-8 Hz phase-amplitude coupling with DG high frequency oscillations throughout spatial learning in both conditions (Figure 28), similar to foraging, which lends further support for PC propagating respiratory entrainment of hippocampal sharp-waves in addition to direct modulation from the PC itself. However, this could be entrainment to some other type of fast hippocampal activity so further analysis will be needed here.

Primary sensory and downstream regions showed changes in their interactions throughout spatial learning depending on the modality of spatial cues present. While OB phase-amplitude coupled with its own high gamma throughout learning with visual spatial cues, it only showed coupling with PC at this same frequency once learning was reached (Figure 29). With olfactory spatial cues, OB only coupled to its own high gamma initially in learning, when it also coupled with PC gamma, and both couplings were lost once criterion was reached. This suggests dynamic coupling between OB and PC occurs depending on the modality of spatial cues used for learning a rewarded location. CA1 and V1M show a similar pattern in the visual condition compared to the olfactory condition for OB and PC coupling. CA1 couples to its own gamma oscillations around 6 Hz, and at around 6-8 Hz to V1M low gamma (40-50 Hz), in the naive but not learned state of learning with visual spatial cues (Figure 30). This is another example of a primary sensory area coupling with a downstream area initially in learning but not later, possibly indicative of processes more relevant for initial memory encoding but not needed once learning is accomplished.

Conclusions

During both spatial navigation and learning, respiration modulates olfactory and hippocampal oscillations. A prominent network of beta modulation emerged during navigation between hippocampal, visual, and olfactory systems. Respiratory and PC oscillations at 4-12 Hz showed strong phase-amplitude coupling with hippocampal high frequency oscillations (>100 Hz) especially during spatial learning. Primary sensory areas exhibited dynamic coupling with downstream areas depending on modality of spatial cues and learned state.

Chapter 6: Discussion

Our results demonstrate multiple frequency signatures of interactions between respiratory and brain rhythms across sensory and memory areas during spatial cognition. Dynamic network configurations during different perceptual states have been characterized. Local activity of distal brain regions were to some extent entrained to respiratory and theta rhythms, shown by modulation of fast oscillatory amplitude by the phase of slower respiratory and theta rhythms. Our results support the hypothesis that respiration works dynamically with hippocampal theta (Tort et al., 2018a; Heck et al., 2019) as part of a master clock for global brain connectivity (Kleinfeld et al., 2016) and help to contextualize these coordinated rhythms in cognitive behaviors.

Network Interactions Depend on Behavioral State

The wide range of neural systems recorded here lend insight into dynamics between peripheral and central systems that depend on behavior. Comparisons across spatial cue modalities demonstrate how interactions between sensory and memory systems change depending on what type of sensory information is available and how it is used for behavior. During exploratory foraging behavior, there were minor changes between visual and olfactory conditions shown by directional and phase-amplitude coupling analyses, but in navigation to a trained location, more robust modality differences were present especially with learning.

The olfactory system showed flexibility of interactions between propagating afferent respiratory rhythms and receiving efferent neural oscillatory feedback. Directional analyses using Granger causality showed strong respiratory drive to OB in all behavioral conditions including home cage activity, foraging, and spatial learning, concurrent with varying levels of

interaction with PC. This shows that even though PC is one of the primary receiving cortical areas of olfactory input, and the two structures often couple across multiple frequencies, OB respiratory rhythm is not propagated to PC in all behavioral circumstances. This is supported by Resp-PC and OB-PC coherence peaks at 10 Hz, while Resp-OB coherence peaks at two frequencies, 6-8 Hz and 9-12 Hz (Figure 7). Notably, Resp-PC coherence only rose above home cage activity coherence levels with olfactory spatial cues (Figure 7). Similarly, during spatial learning Resp-PC only showed coherence elevated above home cage activity levels in the naive state of olfactory, and not visual, spatial learning. OB-PC, however, exhibited coherence levels that overlapped with that of home cage activity during spatial learning (Figure 12). It has been shown previously during a difficult olfactory sensorimotor task that OB-PC maintained coupling at sniff frequency (~8 Hz) along with increased OB-hippocampal coherence in relation to accuracy on the task (Kay, 2005). Taken together, this suggests respiratory-OB-PC interactions in relation to exploratory navigation were more consistent with previously reported sensorimotor learning networks than with spatial learning.

Hippocampal and cortical structures also exhibited different frequencies of oscillations and patterns of interactions that depended on behavior. Similar to respiration, hippocampal power exhibited two peaks during foraging (Figure 6), at 6-8 Hz and 9-12 Hz, and one peak during spatial learning (Figure 11), at 8-10 Hz. PC-DG and DG-CA1 coherence, however, showed coherence only at 8 Hz in all behavioral conditions across both experiments. Granger causality shows that DG may drive coherence with PC since there is directional interaction from DG to PC at 5-8 Hz in foraging with visual and olfactory spatial cues (Figure 8). Even though PC and DG were coherent throughout spatial learning, there were only Granger interactions between them during olfactory spatial learning, again at 5-8 Hz (Figure 14). V1M, however,

showed bias towards coupling with hippocampal oscillations of faster frequencies at 9-12 Hz in both exploratory and learned spatial behaviors. Similar to Resp-PC during olfactory spatial learning, V1M-DG exhibited coherence at 10 Hz above home cage levels only in the naive state of visual spatial learning (Figure 12). Moreover, CA1 oscillations at 6-10 Hz phase-amplitude coupled to V1M gamma at 40-50 Hz only in the naive state of visual spatial learning (Figure 30). This suggests that coherence between slower rhythms in the 6-10 Hz range generated by the hippocampus are not only coherent with V1M slow oscillations but also modulate the amplitude of faster oscillations within V1M, specifically during encoding of a spatial memory task.

Concurrent with V1M interactions, CA1 exhibited theta coherence (6-8 Hz) with neocortical areas S1 and mPtA during home cage activity and throughout learning with either spatial cue modality (Figure 14). During home cage activity, this theta network appeared to be driven by CA1, but during spatial learning, the theta oscillation network was no longer apparent between these areas at the level of Granger causality analysis limited to low-frequency interactions (Figure 16). With completion of spatial learning, higher-frequency networks emerged, especially with visual spatial cues (Figure 18). S1 and mPtA went from interacting at theta frequency in the home cage to a dense beta and gamma network with M2. Many of the beta causal interactions were driven by M2 and S1, with moderate causality to PC and mEC. Granger causality interactions at gamma frequency came from mPtA and M2, primarily targeting S1. Future phase-amplitude coupling analyses on these additional neocortical areas will help delineate sources of these interactions occurring at different frequencies. During navigation, phase-amplitude coupling with CA1 and V1M beta oscillations was seen with respect to several areas including Resp, OB, DG, and CA1, so it is possible similar respiratory and theta phase-

amplitude coupling to neocortical oscillations will be seen during spatial learning in complement with directionality results.

The strong Resp-OB and Resp-PC coherence present in foraging was accompanied by phase-amplitude coupling of fast gamma oscillations, around 100 Hz, in OB and PC to respiratory phase at 4-12 Hz. This supports previous findings that OB LFPs not only track the respiratory rhythm but fast gamma amplitude is also strongly modulated by the phase of respiration (Rojas-Líbano et al., 2014). Interestingly, during spatial learning, 4-10 Hz oscillations in OB amplitude coupled with PC after learning was completed with visual spatial cues, but this coupling only occurred in the naive state of olfactory spatial learning (Figure 29). This suggests a role for respiratory coupling of PC high gamma in spatial learning that depends on the modality of spatial cues present. Respiration also coupled with beta oscillations in CA1 at 8-12 Hz, and with V1M at 4-12 Hz, during foraging with both visual and olfactory spatial cues (Figure 18). These findings support recent reports of respiratory coupling with hippocampal beta (Lockmann et al., 2018) and neocortical gamma (Cavelli et al., 2020). Collectively, Chapter 5 demonstrates diverse higher frequency couplings between olfactory, visual, and hippocampal areas to respiratory and theta phase. Further, results support findings from Chapter 3 that network interactions are consistent in the presence of spatial cues of different modalities during foraging.

OB and PC coupled with each other similar to respiration in regards to high gamma during foraging, though PC was limited to phase frequency at 6-12 Hz. Resp and especially PC show strong higher frequency phase-amplitude coupling with hippocampal and visual areas during foraging, at two discrete phase frequencies. At 6-8 Hz, Resp and PC phase coupled with very fast oscillations (~200-250 Hz) in DG, and fast oscillations (~150 Hz) in CA1 and V1M (Figures 18 and 20). This coupling with DG and CA1 fast oscillations was also seen during

spatial learning with either spatial cue modality (Figures 24-25). This could be further evidence of respiratory coupling to hippocampal sharp wave ripples (>100 Hz), previously shown in awake head-fixed mice (Liu et al., 2017). DG phase-amplitude coupling with very fast DG oscillations was very prominent following visual spatial learning (Figure 26), and early in olfactory spatial learning (Figure 27). Notably, slow oscillations in PC also coupled with very fast DG oscillations throughout spatial learning in both modalities (Figure 27). Further analysis is necessary to determine whether these fast hippocampal oscillations (150-250 Hz) are sharp-wave ripples. If so, this would suggest PC may help link olfactory system sharp waves (Manabe et al., 2011; Barnes and Wilson, 2014; Narikiyo et al., 2014) with hippocampal sharp waves which are usually reported to be generated separately (Narikiyo et al., 2014; Buzsáki, 2015). At 9-12 Hz, PC phase coupled with CA1 and V1M beta, similarly to respiratory and OB phase.

Low gamma (40-60 Hz) amplitude in CA1 and V1M were modulated by slower theta rhythms in CA1 during spatial learning. In the naive state of visual spatial learning, CA1 phase at 4-6 Hz couples to its own gamma oscillations around 60 Hz, and V1M low gamma at 40 Hz couples to CA1 phase at 6-8 Hz. These couplings disappear after learning with visual spatial cues is completed (Figure 30). For olfactory spatial learning, only in the naive state between CA1 phase and CA1 low gamma is phase-amplitude coupling present. High and low gamma in CA1 is routed by different pathways, with high gamma phase-locking between CA1 and mEC, and low gamma phase-locking between CA1 and CA3 (Colgin et al., 2009). Different functional roles are theorized for these different pathways, with more precise spatial representation by high gamma from mEC, and a more partial representation for pattern completion by low gamma from CA1 (Brun et al., 2002; Colgin et al., 2009). CA1 theta phase-amplitude coupling with low gamma

oscillations reported here is consistent with this theory, because pattern completion would be expected to be involved in the decision epoch of an allocentric task.

Potential Mediators of Widespread Respiratory and Theta Interactions

Both bands (6-8 Hz and 9-12 Hz) at which we report interactions between LFPs and nasal respiration are within the range of rodent hippocampal theta (Hinman et al., 2011; Tort et al., 2018b) and respiration (Rojas-Líbano et al., 2014), and overlap with human theta (4-8 Hz) and alpha (8-13 Hz) frequencies (Zelano et al., 2016). OB and especially CA1 both appear to drive this faster 9-12 Hz frequency during foraging as shown in the Granger causality results (Figure 8 bottom row). The medial septum is reciprocally connected to olfactory and hippocampal areas including the OB, PC, and DG, and also CA1 via CA3 (Truchet et al., 2002), and is a generator of hippocampal theta (Buzsáki, 2002). Additionally, the medial septum receives projections from the brainstem pontine respiratory group (Cornwall et al., 1990). Recently, a study using a similar open field foraging task showed fast respiratory coupling with CA1 in the 9-12 Hz band, which was shifted to 6-8 Hz with muscimol blockade of the medial septum (Tsanov et al., 2014). This suggests that the faster coupling frequency we saw here only during foraging and not home cage activity may be mediated by the medial septum. While this frequency is consistent with higher frequency theta rhythms supported by the septum (Tsanov et al., 2014), it may also be driven by higher frequency sniffing (Rojas-Líbano et al., 2014). Velocity was low overall (Figure 5) and neither acceleration nor velocity were significantly correlated with Resp-OB or DG-CA1 coherence frequency suggesting that the faster frequencies are not simply due to acceleration or velocity alone (Hinman et al., 2011; Kropff et al., 2021). Viewing the medial septum as a potential mediator of respiratory-brain rhythm interactions may help explain why one study in

humans found that both nasal and oral breathing relate to brain rhythms and behavioral performance (Perl et al., 2019). Those data conflict with several reports suggesting that respiratory coherence is nasal or OB driven (Ito et al., 2014; Yanovsky et al., 2014; Lockmann et al., 2016; Zelano et al., 2016). Orofacial movements in rats and mice are coherent with respiration, and with hippocampal theta in certain behavioral contexts, which are driven by neighboring brainstem areas (Kleinfeld et al., 2014, 2016). This means respiratory and theta oscillations could be coordinated as early as the initial ascending drive for breathing.

The PC showed flexibility in interactions with olfactory and hippocampal systems. Specifically, the PC showed 6-8 Hz coherence with the hippocampus in the home cage when other regions showed no coherence. The PC has extensive reciprocal connections with entorhinal cortex, which is the primary cortical input to the DG (Haberly, 2001). In humans, the PC and HPC show theta coherence specifically during odor discrimination (Jiang et al., 2017). Anatomical data support the PC as a hub for connecting cortical association areas (Bota et al., 2015), which would facilitate widespread coherence between distal brain areas. Our results suggest that the PC is involved dynamically and richly in this network, confirming its anatomical role as a conduit for rhythmic drive across systems in lower respiratory and theta ranges.

Limitations

Some limitations include the presence of olfactory cues in the visual condition (*e.g.*, chocolate sprinkles), although place cells should have been formed based on a visual map with the use of the salient visual spatial cues, and adult rats perform no worse on a spatial task when olfactory cues are removed (Rossier and Schenk, 2003). In the olfactory foraging condition, confound by any visual cues should be minimized by using only red light outside of the rat visual

spectrum, but this does not preclude the presence of other cues from the auditory or somatosensory systems (*e.g.*, sound of ventilation or computer fans that give static spatial information and the presence of any air currents, although these are unlikely within the curtained arena). Another limitation was the lack of interventions on central respiratory areas or the medial septum to parse out whether respiratory coherence is driven primarily by nasal airflow or central pattern generators in the brainstem.

As mentioned in Chapter 4, Granger causality is conditioned on all variables within a dataset for the joint estimations of causality between each pair. It is possible that different networks recorded between the two groups of rats would influence the outcome of Granger causality analyses between each of the pairs, and may help explain some discrepancies between pairs common to the groups. Furthermore, Granger causality analyses depend on multivariate autoregressive models which are constrained by data parameters and determine the amount of time in the past used for error estimates (Barnett and Seth, 2014; Seth et al., 2015). Foraging data was collected over 20 min sessions and was split into 10 s epochs for data cleaning and averaging, while spatial learning data was focused on the 2 s before leaving the center platform of the maze. This led to different model order estimates for the two analyses (Chapter 2) leading to more time (184 ms) being taken into account for optimal fit of models on the foraging data than for spatial learning data (40 ms). A 10 Hz theta cycle is 100 ms so would be fully covered by models in foraging, but less than half a cycle would be present in spatial learning data. This suggests there may have been a bias towards slow frequencies that would have contributed to the absence of higher frequency interactions during foraging and more higher frequency interactions reported during spatial learning. However, slow frequency interactions were still visible in

Granger causality during spatial learning with the low model order just described, arguing against a substantial bias.

Conclusions

Brain rhythms are energetically efficient means for large neuronal populations to coordinate their activity within and across brain regions (Buzsáki, 2006). Respiration maintains homeostasis (Guyenet and Bayliss, 2015). Results presented here demonstrate respiratory and brain rhythms temporally couple at multiple levels during spatial navigation and learning. These results contribute to a growing literature of respiratory-brain rhythm interactions and assist in better understanding how they relate to neurophysiology implicated in learning and memory. Breathing is an ongoing physiological process that has often been considered to be noise or artifact in neural recordings, but it is clearly a signal of coordinated neural processing that must be understood further (Heck et al., 2019). It is easier to grasp why rodents, who rely heavily on sniffing at frequencies that couple directly with brain rhythms, would show respiratory coupling with neural oscillations, but it is harder to explain similar mechanisms of phase-locking in the context of the much slower human respiratory rhythm (~0.2 Hz; Zelano et al., 2016). The role of olfaction in navigation in earlier organisms was primarily for navigation (*i.e.*, chemotaxis), and the olfactory and hippocampal systems evolved in parallel (Jacobs, 2012). Therefore, it is likely that interactions between olfactory and hippocampal systems that were important for survival in these earlier organisms are conserved in humans. Further comparative studies of rodent and human memory will likely unveil evolutionarily conserved mechanisms of coordinated respiratory and brain rhythms.

References

Adrian ED (1942) Olfactory reactions in the brain of the hedgehog. J Physiol 100:459–473.

Adrian ED (1950) The electrical activity of the mammalian olfactory bulb. Electroencephalogr Clin Neurophysiol 2:377–388

Agarwal G, Stevenson IH, Berényi A, Mizuseki K, Buzsáki G, Sommer FT (2014) Spatially distributed local fields in the hippocampus encode rat position. Science 344:626–630

Anderson TM, Garcia AJ, Baertsch NA, Pollak J, Bloom JC, Wei AD, Rai KG, Ramirez JM (2016) A novel excitatory network for the control of breathing. Nature 536:76–80.

Aronoff R, Matyas F, Mateo C, Ciron C, Schneider B, Petersen CCH (2010) Long-range connectivity of mouse primary somatosensory barrel cortex. Eur J Neurosci 31:2221–2233.

Arshamian A, Iravani B, Majid A, Lundström JN (2018) Respiration modulates olfactory memory consolidation in humans. J Neurosci 38:3360–17

Balasubramanian K, Papadourakis V, Liang W, Takahashi K, Best MD, Suminski AJ, Hatsopoulos NG (2020) Propagating Motor Cortical Dynamics Facilitate Movement Initiation. Neuron 106:526-536.e4

Bao X, Gjorgieva E, Shanahan LK, Howard JD, Kahnt T, Gottfried JA (2019) Grid-like Neural Representations Support Olfactory Navigation of a Two-Dimensional Odor Space. Neuron 102:1066-1075.e5

Barnes DC, Wilson DA (2014) Sleep and olfactory cortical plasticity. Front Behav Neurosci 8:1–11.

Barnett L, Seth AK (2014) The MVGC multivariate Granger causality toolbox: A new approach to Granger-causal inference. J Neurosci Methods 223:50–68

Barrie JM, Freeman WJ, Lenhart MD (1996) Spatiotemporal analysis of prepyriform, visual, auditory, and somesthetic surface EEGs in trained rabbits. J Neurophysiol 76:520–539.

Bedrosian TA, Vaughn CA, Weil ZM, Nelson RJ (2013) Behaviour of laboratory mice is altered by light pollution within the housing environment. Anim Welf 22:483–487.

Bedwell SA, Billett EE, Crofts JJ, Tinsley CJ (2014) The topology of connections between rat prefrontal, motor and sensory cortices. Front Syst Neurosci 8:1–10.

Benchenane K, Peyrache A, Khamassi M, Tierney PL, Gioanni Y, Battaglia FP, Wiener SI (2010) Coherent Theta Oscillations and Reorganization of Spike Timing in the Hippocampal- Prefrontal Network upon Learning. Neuron 66:921–936

Berg RW, Kleinfeld D (2003) Rhythmic whisking by rat: Retraction as well as protraction of the vibrissae is under active muscular control. J Neurophysiol 89:104–117.

Berg RW, Whitmer D, Kleinfeld D (2006) Exploratory whisking by rat is not phase locked to the hippocampal theta rhythm. J Neurosci 26:6518–6522.

Beshel J, Kopell N, Kay LM (2007) Olfactory Bulb Gamma Oscillations Are Enhanced with Task Demands. J Neurosci 27:8358–8365

Bhalla U, Bower JM (1997) Multiday recordings from olfactory bulb neurons in awake freely moving rats: Spatial and temporal patterns in odorant responses. J Comput Neurosci 4:221–256.

Bland BH (1986) The physiology and pharmacology of hippocampal formation theta rhythms. Prog Neurobiol 26:1–54

Bland BH, Oddie SD (2001) Theta band oscillation and synchrony in the hippocampal formation and associated structures: the case for its role in sensorimotor integration. Behav Brain Res 127:119–136

Bland BH, Seto MG, Rowntree CI (1983) The relation of mutliple hippocampal theta cell discharge rates to slow wave theta frequency. Physiol Behav 31:111–117.

Bliss TVP, Gardner-Medwin AR (1973) Long-lasting potentiation of synaptic transmission in the dentate area of the unanaesthetized rabbit following stimulation of the perforant path. J Physiol 232:357–374

Boeijinga PH, Lopes da Silva FH (1989) Modulations of EEG activity in the entorhinal cortex and forebrain olfactory areas during odour sampling. Brain Res 478:257–268.

Bokil H, Andrews P, Kulkarni JE, Mehta S, Mitra PP (2010) Chronux: A platform for analyzing neural signals. J Neurosci Methods 192:146–151

Bota M, Sporns O, Swanson LW (2015) Architecture of the cerebral cortical association connectome underlying cognition. Proc Natl Acad Sci 112:E2093-101

Boudreau JC, Freeman WJ (1963) Spectral analysis of electrical activity in the prepyriform cortex of the cat. Exp Neurol 8:423–439.

Bragin A, Engel J, Wilson CL, Fried I, Mathern GW (1999) Hippocampal and entorhinal cortex high-frequency oscillations (100-500 Hz) in human epileptic brain and in kainic acid-treated rats with chronic seizures. Epilepsia 40:127–137.

Bragin A, Wilson CL, Almajano J, Mody I, Engel J (2004) High-frequency oscillations after status epilepticus: Epileptogenesis and seizure genesis. Epilepsia 45:1017–1023.

Bressler SL, Coppola R, Nakamura R (1993) Episodic multiregional cortical coherence at multiple frequencies during visual task performance. Nature 366:153–156.

Brun VH, Otnæss MK, Molden S, Steffenach HA, Witter MP, Moser MB, Moser EI (2002) Place cells and place recognition maintained by direct entorhinal-hippocampal circuitry.

Science (80-) 296:2243–2246.

Buonviso N, Amat C, Litaudon P (2006) Respiratory modulation of olfactory neurons in the rodent brain. Chem Senses 31:145–154.

Burwell RD, Witter MP, Amaral DG (1995) Perirhinal and postrhinal cortices of the rat: a review of the neuroanatomical literature and comparison with findings from the monkey brain. Hippocampus 5:390–408

Buzsáki G (2002) Theta Oscillations in the Hippocampus. Neuron 33:325–340

Buzsáki G (2006) Rhythms of the Brain. New York: Oxford University Press.

Buzsáki G (2015) Hippocampal sharp wave-ripple: A cognitive biomarker for episodic memory and planning. Hippocampus 25:1073–1188.

Buzsáki G, Draguhn A (2004) Neuronal oscillations in cortical networks. Science 304:1926–1929

Buzsáki G, Freeman W (2015) Editorial overview: Brain rhythms and dynamic coordination. Curr Opin Neurobiol 31:5–9.

Buzsaki G, Horvath Z, Urioste R, Hetke J, Wise K (1992) High-Frequency Network Oscillation in the Hippocampus. Science (256-) 5059:1025-1027.

Buzsáki G, Moser EI (2013) Memory, navigation and theta rhythm in the hippocampal-entorhinal system. Nat Neurosci 16:130–138 .

Caplan JB, Madsen JR, Schulze-Bonhage A, Aschenbrenner-Scheibe R, Newman EL, Kahana MJ (2003) Human theta oscillations related to sensorimotor integration and spatial learning. J Neurosci 23:4726–4736.

Cavelli M, Castro-Zaballa S, Gonzalez J, Rojas-Líbano D, Rubido N, Velásquez N, Torterolo P (2020) Nasal respiration entrains neocortical long-range gamma coherence during wakefulness. Eur J Neurosci 51:1463–1477.

Cenquizca LA, Swanson LW (2007) Spatial organization of direct hippocampal field CA1 axonal projections to the rest of the cerebral cortex. Brain Res Rev 56:1–26.

Chaput M (1983) Effects of olfactory peduncle sectioning on the single unit responses of olfactory bulb neurons to odor presentation in awake rabbits. Chem Senses 8:161–177.

Chaput M, Holley A (1979) Spontaneous activity of olfactory bulb neurons in awake rabbits, with some observations on the effects of pentobarbital anaesthesia. J Physiol (Paris) 75:939—948

Chen LL, Lin L-H, Green EJ, Barnes CA, McNaughton BL (1994) Head-direction cells in the rat posterior cortex. Exp Brain Res 101:8–23

Cohen MI (1979) Neurogenesis of respiratory rhythm in the mammal. Physiol Rev 59:1105–1173.

Colgin LL, Denninger T, Fyhn M, Hafting T, Bonnevie T, Jensen O, Moser M-B, Moser EI (2009) Frequency of gamma oscillations routes flow of information in the hippocampus. Nature 462:353–357

Connelly CA, Dobbins EG, Feldman JL (1992) Pre-Botzinger complex in cats: respiratory neuronal discharge patterns. Brain Res 590:337–340

Cornwall J, Cooper JD, Phillipson OT (1990) Afferent and efferent connections of the laterodorsal tegmental nucleus in the rat. Brain Res Bull 25:271–284.

de Olmos J, Hardy H, Heimer L (1978) The afferent connections of the main and the accessory olfactory bulb formations in the rat: An experimental HRP-study. J Comp Neurol 181:213–244.

Dobbins EG, Feldman JL (1994) Brainstem network controlling descending drive to phrenic motoneurons in rat. J Comp Neurol 347:64–86.

Eeckman FH, Freeman WJ (1990) Correlations between unit firing and EEG in the rat olfactory system. Brain Res 528:238–244.

Ellenberger HH, Feldman JL (1994) Origins of excitatory drive within the respiratory network: anatomical localization. Neuroreport 5:1933–1936

Fell J, Axmacher N (2011) The role of phase synchronization in memory processes. Nat Rev Neurosci 12:105–118

Figueres-Oñate M, Gutiérrez Y, López-Mascaraque L (2014) Unraveling Cajal's view of the olfactory system. Front Neuroanat 8:1–12.

Florin E, Gross J, Pfeifer J, Fink GR, Timmermann L (2011) Reliability of multivariate causality measures for neural data. J Neurosci Methods 198:344–358

Fontanini A, Bower JM (2005) Variable coupling between olfactory system activity and respiration in ketamine/xylazine anesthetized rats. J Neurophysiol 93:3573–3581

Fontanini A, Bower JM (2006) Slow-waves in the olfactory system: an olfactory perspective on cortical rhythms. Trends Neurosci 29:429–437.

Forbes WB, Macrides F (1984) Temporal matching of sensory-motor behavior and limbic θ rhythm deteriorates in aging rats. Neurobiol Aging 5:7–17

Fortin NJ, Agster KL, Eichenbaum HB (2002) Critical role of the hippocampus in memory for sequences of events. Nat Neurosci 5:458–462.

Foster JJ et al. (2016) The topography of alpha-band activity tracks the content of spatial

working memory. J Neurophysiol 115:168–177

Frederick DE, Brown A, Brim E, Mehta N, Vujovic M, Kay LM (2016a) Gamma and beta oscillations define a sequence of principal modes present in odor processing. J Neurosci 36:7750–7767.

Frederick DE, Brown A, Brim E, Mehta N, Vujovic M, Kay LM (2016b) Gamma and Beta Oscillations Define a Sequence of Neurocognitive Modes Present in Odor Processing. J Neurosci 36:7750–7767

Frederick DE, Brown A, Tacopina S, Mehta N, Vujovic M, Brim E, Amina T, Fixsen B, Kay LM (2017) Task-Dependent Behavioral Dynamics Make the Case for Temporal Integration in Multiple Strategies during Odor Processing. J Neurosci 37:4416–4426.

Freeman WJ (1968) Effects of surgical isolation and tetanization on prepyriform cortex in cats. J Neurophysiol 31:349–357.

Freeman WJ (2004) Origin, structure, and role of background EEG activity. Part 2. Analytic phase. Clin Neurophysiol 115:2089–2107.

Freeman WJ (2015) Mechanism and significance of global coherence in scalp EEG. Curr Opin Neurobiol 31:199–205

Freeman WJ, Schneider W (1982) Changes in Spatial Patterns of Rabbit Olfactory EEG with Conditioning to Odors. Psychophysiology 19:44–56

Freeman WJ, Skarda CA (1985) Spatial EEG Patterns , Non-linear Dynamics and Perception : the Neo-Sherringtonian View. 10:147–175.

Fries P (2015) Neuron Perspective Rhythms for Cognition: Communication through Coherence.

Gandevia SC, Plassman BL (1988) Responses in human intercostal and truncal muscles to motor cortical and spinal stimulation. Respir Physiol 73:325–337.

Geweke JF (1984) Measures of conditional linear dependence and feedback between time series. J Am Stat Assoc 79:907–915.

Gold PE (2004) Coordination of multiple memory systems. Neurobiol Learn Mem 82:230–242.

Granger CJW (1969) Investigating Causal Relations by Econometric Models and Cross-spectral Methods. Econometrica 3:424-438

Grillner S (2006) Biological Pattern Generation: The Cellular and Computational Logic of Networks in Motion. Neuron 52:751–766.

Grion N, Akrami A, Zuo Y, Stella F, Diamond ME (2016) Coherence between Rat Sensorimotor System and Hippocampus Is Enhanced during Tactile Discrimination. PLoS Biol 14:1–26.

Grosmaitre X, Santarelli LC, Tan J, Luo M, Ma M (2007) Dual functions of mammalian

olfactory sensory neurons as odor detectors and mechanical sensors. Nat Neurosci 10:348–354.

Guyenet PG, Bayliss DA (2015) Neural Control of Breathing and CO2 Homeostasis. Neuron 87:946–961

Haberly LB (2001) Chem. Senses-2001-Haberly-551-76. Chem Senses 26:1–26

Haberly LB, Price JL (1978) Association and commissural fiber systems of the olfactory cortex of the rat II. Systems originating in the olfactory peduncle. J Comp Neurol 181:781–807.

Haggerty DC, Ji D (2015) Activities of visual cortical and hippocampal neurons co-fluctuate in freely moving rats during spatial behavior. Elife 4:1–23.

Heck DH, Kozma R, Kay LM (2019) The rhythm of memory: How breathing shapes memory function. J Neurophysiol 122:563–571.

Heck DH, Mcafee SS, Liu Y, Babajani-feremi A (2016) Cortical rhythms are modulated by respiration. bioRxiv.

Hermer-Vazquez R, Hermer-Vazquez L, Srinivasan S, Chapin JK (2007) Beta- and gamma-frequency coupling between olfactory and motor brain regions prior to skilled, olfactory-driven reaching. Exp Brain Res 180:217–235.

Hinman JR, Penley SC, Long LL, Escabí MA, Chrobak JJ (2011) Septotemporal variation in dynamics of theta: Speed and habituation. J Neurophysiol 105:2675–2686.

Huangfu D, Koshiya N, Guyenet PG (1993) Central respiratory modulation of facial motoneurons in rats. Neurosci Lett 151:224–228.

Huckstepp RTR, Cardoza KP, Henderson LE, Feldman JL (2015) Role of parafacial nuclei in control of breathing in adult rats. J Neurosci 35:1052–1067.

Hurtado JM, Rubchinsky LL, Sigvardt KA (2004) Statistical Method for Detection of Phase-Locking Episodes in Neural Oscillations. J Neurophysiol 91:1883–1898.

Hyman JM, Zilli EA, Paley AM, Hasselmo ME (2005) Medial prefrontal cortex cells show dynamic modulation with the hippocampal theta rhythm dependent on behavior. Hippocampus 15:739–749.

Igarashi KM (2015) Plasticity in oscillatory coupling between hippocampus and cortex. Curr Opin Neurobiol 35:163–168

Igarashi KM, Lu L, Colgin LL, Moser MB, Moser EI (2014) Coordination of entorhinal-hippocampal ensemble activity during associative learning. Nature 510:143–147.

Ito J, Roy S, Liu Y, Cao Y, Fletcher M, Lu L, Boughter JD, Grün S, Heck DH (2014) Whisker barrel cortex delta oscillations and gamma power in the awake mouse are linked to

respiration. Nat Commun 5:1–10.

J.O'Keefe, Recce M (1993) Phase relationship between hippocampal place units and the hippocampal theta rhythm. Hippocampus. 3:317-330

Jacobs LF (2012) From chemotaxis to the cognitive map: The function of olfaction. Proc Natl Acad Sci 109:10693–10700.

Jensen O, Colgin LL (2007) Cross-frequency coupling between neuronal oscillations. Trends Cogn Sci 11:267–269.

Jiang H, Schuele S, Rosenow J, Zelano C, Parvizi J, Tao JX, Wu S, Gottfried JA (2017) Theta Oscillations Rapidly Convey Odor-Specific Content in Human Piriform Cortex. Neuron 94:207-219.e4

Johnson DMG, Illig KR, Behan M, Haberly LB (2000) New features of connectivity in piriform cortex visualized by intracellular injection of pyramidal cells suggest that "primary" olfactory cortex functions like "association" cortex in other sensory systems. J Neurosci 20:6974–6982.

Jones MW, Wilson MA (2005a) Phase precession of medial prefrontal cortical activity relative to the hippocampal theta rhythm. Hippocampus 15:867–873.

Jones MW, Wilson MA (2005b) Theta rhythms coordinate hippocampal-prefrontal interactions in a spatial memory task. PLoS Biol 3:1–13.

Kaplan R, Bush D, Bonnefond M, Bandettini PA, Barnes GR, Doeller CF, Burgess N (2014) Medial prefrontal theta phase coupling during spatial memory retrieval. Hippocampus 24:656–665.

Kay LM (2005) Theta oscillations and sensorimotor performance. Proc Natl Acad Sci U S A 102:3863–3868.

Kay LM, Beshel J (2010) A Beta Oscillation Network in the Rat Olfactory System During a 2-Alternative Choice Odor Discrimination Task. J Neurophysiol 104:829–839.

Kay LM, Beshel J, Brea J, Martin C, Rojas-L??bano D, Kopell N (2009) Olfactory oscillations: the what, how and what for. Trends Neurosci 32:207–214.

Kay LM, Freeman WJ (1998) Bidirectional processing in the olfactory-limbic axis during olfactory behavior. Behav Neurosci 112:541–553

Kay LM, Lancaster LR, Freeman WJ (1996) Reafference and attractors in the olfactory system during odor recognition. Int J Neural Syst 7:489–495

Kay LM, Laurent G (1999) Odor- and context-dependent modulation of mitral cell activity in behaving rats. Nat Neurosci 2:1003–1009

Kepecs A, Uchida N, Mainen ZF (2006) The sniff as a unit of olfactory processing. Chem Senses 31:167–179

Kepecs A, Uchida N, Mainen ZF (2007) Rapid and precise control of sniffing during olfactory discrimination in rats. J Neurophysiol 98:205–213.

Kleinfeld D, Deschênes M, Ulanovsky N (2016) Whisking, Sniffing, and the Hippocampal θ-Rhythm: A Tale of Two Oscillators. PLOS Biol 14:e1002385

Kleinfeld D, Deschênes M, Wang F, Moore JD (2014) More than a rhythm of life: breathing as a binder of orofacial sensation. Nat Neurosci 17:647–651

Komisaruk BR (1970) Synchrony between limbic system theta activity and rhythmical behavior in rats. J Comp Physiol Psychol 70:482–492.

Kramis R, Vanderwolf CH, Bland BH (1975) Two types of hippocampal rhythmical slow activity in both the rabbit and the rat: Relations to behavior and effects of atropine, diethyl ether, urethane, and pentobarbital. Exp Neurol 49:58–85.

Kropff E, Carmichael JE, Moser EI, Moser M-B (2021) Frequency of theta rhythm is controlled by acceleration, but not speed, in running rats. Neuron 109:1029-1039.e8

Kunicki C, C. Moioli R, Pais-Vieira M, Salles Cunha Peres A, Morya E, A. L. Nicolelis M (2019) Frequency-specific coupling in fronto-parieto-occipital cortical circuits underlie active tactile discrimination. Sci Rep 9:1–14.

Lefèvre L, Courtiol E, Garcia S, Thévenet M, Messaoudi B, Buonviso N (2016) Significance of sniffing pattern during the acquisition of an olfactory discrimination task. Behav Brain Res 312:341–354

Litaudon P, Garcia S, Buonviso N (2008) Strong coupling between pyramidal cell activity and network oscillations in the olfactory cortex. Neuroscience 156:781–787.

Liu Y, McAfee SS, Heck DH (2017) Hippocampal sharp-wave ripples in awake mice are entrained by respiration. Sci Rep 7:1–9

Lockmann ALV, Laplagne DA, Tort ABL (2018) Olfactory bulb drives respiration-coupled beta oscillations in the rat hippocampus. Eur J Neurosci 48:2663–2673.

Lockmann AL V, Laplagne DA, Leão RN, Tort ABL (2016) A Respiration-Coupled Rhythm in the Rat Hippocampus Independent of Theta and Slow Oscillations. J Neurosci 36:5338–5352

Lubenov E V., Siapas AG (2009) Hippocampal theta oscillations are travelling waves. Nature 459:534–539

Luskin MB, Price JL (1983) The topographic organization of associational fibers of the olfactory system in the rat, including centrifugal fibers to the olfactory bulb. J Comp Neurol 216:264–

291.

Macrides F (1975) Temporal relationships between hippocampal slow waves and exploratory sniffing in hamsters. Behav Biol 14:295–308.

Macrides F, Chorover SL (1972) Olfactory Bulb Units: Activity Correlated with Inhalation Cycles and Odor Quality. Science (80-) 175:84–87

Macrides F, Eichenbaum HB, Forbes WB (1982) Temporal Relationship Between Sniffing and the Limbic Theta Rhythm During Odor Discrimination Reversal Learning. J Neurosci ence 2:1705–1717.

Mamad O, McNamara HM, Reilly RB, Tsanov M (2015) Medial septum regulates the hippocampal spatial representation. Front Behav Neurosci 9:1–16.

Manabe H, Kusumoto-Yoshida I, Ota M, Mori K (2011) Olfactory cortex generates synchronized top-down inputs to the olfactory bulb during slow-wave sleep. J Neurosci 31:8123–8133.

Marder E, Calabrese RL (1996) Principles of rhythmic motor pattern generation. Physiol Rev 76:687–717.

Martin C, Beshel J, Kay LM (2007) An Olfacto-Hippocampal Network Is Dynamically Involved in Odor-Discrimination Learning. J Neuro-physiol 98:2196–2205.

Martin C, Gervais R, Hugues E, Messaoudi B, Ravel N (2004) Learning Modulation of Odor-Induced Oscillatory Responses in the Rat Olfactory Bulb: A Correlate of Odor Recognition? J Neurosci 24:389–397.

Masaoka Y, Izumizaki M, Homma I (2014) Where is the rhythm generator for emotional breathing? Progress in Brain Research 209:367-377

Maskill D, Murphy K, Mier A, Owen M, Guz A (1991) Motor cortical representation of the diaphragm in man. J Physiol 443:105–121.

McNaughton BL, Barnes CA, O'Keefe J (1983) The contributions of position, direction, and velocity to single unit activity in the hippocampus of freely-moving rats. Exp Brain Res 52:41–49.

Miller MW, Vogt BA (1984) Direct connections of rat visual cortex with sensory, motor, and association cortices. J Comp Neurol 226:184–202.

Mitra PP, Bokil H (2008) Observed Brain Dynamics. New York: Oxford University Press.

Moberly AH, Schreck M, Bhattarai JP, Zweifel LS, Luo W, Ma M (2018) Olfactory inputs modulate respiration-related rhythmic activity in the prefrontal cortex and freezing behavior. Nat Commun 9, 1528

Monod B, Mouly AM, Vigouroux M, Holley A (1989) An investigation of some temporal aspects of olfactory coding with the model of multi-site electrical stimulation of the olfactory bulb in the rat. Behav Brain Res 33:51–63.

Montgomery SM, Buzsáki G (2007) Gamma oscillations dynamically couple hippocampal CA3 and CA1 regions during memory task performance. Proc Natl Acad Sci U S A 104:14495–14500.

Moore JD, Deschênes M, Furuta T, Huber D, Smear MC, Demers M, Kleinfeld D (2013) Hierarchy of orofacial rhythms revealed through whisking and breathing. Nature 497:205–210.

Morris RGM, Anderson E, Lynch GS, Baudry M (1986) Selective impairment of learning and blockade of long-term potentiation by an N-methyl-D-aspartate receptor antagonist, AP5. Nature 319:774–776.

Mozell MM (1958) Electrophysiology of the olfactory bulb. J Neurophysiol 21:183–196

Narikiyo K, Manabe H, Mori K (2014) Sharp wave-associated synchronized inputs from the piriform cortex activate olfactory tubercle neurons during slow-wave sleep. J Neurophysiol 111:72–81.

Newman EL, Gillet SN, Climer JR, Hasselmo ME (2013) Cholinergic Blockade Reduces Theta-Gamma Phase Amplitude Coupling and Speed Modulation of Theta Frequency Consistent with Behavioral Effects on Encoding. J Neurosci 33:19635–19646

Newman LA, Scavuzzo CJ, Gold PE, Korol DL (2017) Training-induced elevations in extracellular lactate in hippocampus and striatum: Dissociations by cognitive strategy and type of reward. Neurobiol Learn Mem 137:142–153

Nguyen Chi V, Muller C, Wolfenstetter T, Yanovsky Y, Draguhn A, Tort ABL, Branka k J (2016) Hippocampal Respiration-Driven Rhythm Distinct from Theta Oscillations in Awake Mice. J Neurosci 36:162–177 A

Nitz DA (2006) Tracking route progression in the posterior parietal cortex. Neuron 49:747–756.

Nitz DA (2012) Spaces within spaces: Rat parietal cortex neurons register position across three reference frames. Nat Neurosci 15:1365–1367.

Nusser Z, Kay LM, Laurent G, Homanics GE, Mody I (2001) Disruption of GABA(A) receptors on GABAergic interneurons leads to increased oscillatory power in the olfactory bulb network. J Neurophysiol 86:2823–2833

O'Keefe J, Dostrovsky J (1971) The hippocampus as a spatial map. Preliminary evidence from unit activity in the freely-moving rat. Brain Res 34:171–175

O'Keefe J, Nadel L (1978) The Hippocampus as a Cognitive Map, 1978th ed. Oxford University Press.

Olsen GM, Ohara S, Iijima T, Witter MP (2017) Parahippocampal and retrosplenial connections of rat posterior parietal cortex. Hippocampus 27:335–358.

Onoda N, Mori K (1980) Depth distribution of temporal firing patterns in olfactory bulb related to air-intake cycles. J Neurophysiol 44:29–39.

Orem J, Trotter R (1994) Behavioral Control of Breathing. Physiology 9:228–232

Pager J (1985) Respiration and olfactory bulb unit activity in the unrestrained rat. Statements and reappraisals. Behav Brain Res 16:81–94.

Pagliardini S, Janczewski WA, Tan W, Dickson CT, Deisseroth K, Feldman JL (2011) Active expiration induced by excitation of ventral medulla in adult anesthetized rats. J Neurosci 31:2895–2905.

Pais-Vieira M, Lebedev MA, Wiest MC, Nicolelis MAL (2013) Simultaneous top-down modulation of the primary somatosensory cortex and thalamic nuclei during active tactile discrimination. J Neurosci 33:4076–4093.

Pan WX, McNaughton N (2004) The supramammillary area: Its organization, functions and relationship to the hippocampus. Prog Neurobiol 74:127–166.

Parker PRL, Brown MA, Smear MC, Niell CM (2020) Movement-Related Signals in Sensory Areas: Roles in Natural Behavior. Trends Neurosci 43:581–595

Perl O, Ravia A, Rubinson M, Eisen A, Soroka T, Mor N, Secundo L, Sobel N (2019) Human non-olfactory cognition phase-locked with inhalation. Nat Hum Behav 3:501–512

Potter H, Chorover SL (1976) Response plasticity in hamster olfactory bulb: peripheral and central processes. Brain Res 116:417–429.

Ranade S, Hangya B, Kepecs A (2013) Multiple Modes of Phase Locking between Sniffing and Whisking during Active Exploration. J Neurosci 33:8250–8256 A

Ravel N, Caille D, Pager J (1987) A centrifugal respiratory modulation of olfactory bulb unit activity: a study on acute rat preparation. Exp Brain Res 65:623–628.

Ravel N, Pager J (1990) Respiratory patterning of the rat olfactory bulb unit activity: Nasal versus tracheal breathing. Neurosci Lett 115:213–218

Rennaker RL, Chen CFF, Ruyle AM, Sloan AM, Wilson DA (2007) Spatial and temporal distribution of odorant-evoked activity in the piriform cortex. J Neurosci 27:1534–1542.

Rojas-Líbano D, Frederick DE, Egaña JI, Kay LM (2014) The olfactory bulb theta rhythm follows all frequencies of diaphragmatic respiration in the freely behaving rat. Front Behav Neurosci 8:214

Rojas-Líbano D, Kay LM (2008) Olfactory system gamma oscillations: The physiological

dissection of a cognitive neural system. Cogn Neurodyn 2:179–194.

Rojas-Líbano D, Wimmer Del Solar J, Aguilar-Rivera M, Montefusco-Siegmund R, Pedro X, Maldonado E (2018) Local cortical activity of distant brain areas can phase-lock to the olfactory bulb's respiratory rhythm in the freely behaving rat. J Neurophysiol 120:960–972

Rossier J, Schenk F (2003) Olfactory and/or visual cues for spatial navigation through ontogeny: olfactory cues enable the use of visual cues. Behav Neurosci 117:412–425

Sabolek HR, Penley SC, Hinman JR, Bunce JG, Etan J, Escabi M, Chrobak JJ, Sabolek HR, Penley SC, Hinman JR, Bunce JG, Markus EJ, Escabi M, Chrobak JJ (2013) Theta and Gamma Coherence Along the Septotemporal Axis of the Hippocampus Theta and Gamma Coherence Along the Septotemporal Axis of the Hippocampus. 1192–1200.

Santiago AC, Shammah-Lagnado SJ (2004) Efferent, Connections of the Nucleus of the Lateral Olfactory Tract in the Rat. J Comp Neurol 471:314–332.

Save E, Nerad L, Poucet B (2000) Contribution of multiple sensory information to place field stability in hippocampal place cells. Hippocampus 10:64–76.

Selverston AI, Ayers J (2006) Oscillations and oscillatory behavior in small neural circuits. Biol Cybern 95:537–554.

Seth AK, Barrett AB, Barnett L (2015) Granger causality analysis in neuroscience and neuroimaging. J Neurosci 35:3293–3297

Shipley MT, Adamek GD (1984) The connections of the mouse olfactory bulb: A study using orthograde and retrograde transport of wheat germ agglutinin conjugated to horseradish peroxidase. Brain Res Bull 12:669–688.

Siapas AG, Wilson MA (1998) Coordinated interactions between hippocampal ripples and cortical spindles during slow-wave sleep. Neuron 21:1123–1128.

Silson EH, Steel A, Kidder A, Gilmore AW, Baker CI (2019) Distinct subdivisions of human medial parietal cortex support recollection of people and places. Elife 8:554915

Simons DJ (1978) Response properties of vibrissa units in rat SI somatosensory neocortex. J Neurophysiol 41:798–820.

Skaggs WE, McNaughton BL, Wilson MA, Barnes CA (1996) Theta phase precession in hippocampal neuronal populations and the compression of temporal sequences. Hippocampus 6:149–172.

Skelin I, Kilianski S, McNaughton BL (2018) Hippocampal coupling with cortical and subcortical structures in the context of memory consolidation. Neurobiol Learn Mem 160:21-31

Smith JC, Abdala APL, Koizumi H, Rybak IA, Paton JFR (2007) Spatial and functional

architecture of the mammalian brain stem respiratory network: A hierarchy of three oscillatory mechanisms. J Neurophysiol 98:3370–3387.

Smith JC, Ellenberger HH, Ballanyi K, Richter DW, Feldman JL (1991) Pre-Bötzinger complex: A brainstem region that may generate respiratory rhythm in mammals. Science (80-) 254:726–729

Solari N, Hangya B (2018) Cholinergic modulation of spatial learning, memory and navigation. Eur J Neurosci 48:2199–2230.

Squire LR (1992) Memory and the Hippocampuss: A Synthesis From Findings With Rats, Monkeys, and Humans. Psychol Rev 99:195–231.

Squire LR, Stark CEL, Clark RE (2004) The medial temporal lobe. Annu Rev Neurosci 27:279–306.

Stopfer M, Bhagavan S, Smith BH, Laurent G (1997) Impaired odour discrimination on desynchronization of odour-encoding neural assemblies. Nature 390:70–74

Swanson LW (1981) A direct projection from Ammon's horn to prefrontal cortex in the rat. Brain Res 217:150–154.

Tan W, Janczewski WA, Yang P, Shao XM, Callaway EM, Feldman JL (2008) Silencing preBötzinger Complex somatostatin-expressing neurons induces persistent apnea in awake rat. Nat Neurosci 11:538–540.

Thomson DJ (1982) Spectrum estimation and harmonic analysis. Proc IEEE 70:1055–1096

Tort ABL, Brankačk J, Draguhn A (2018a) Respiration-Entrained Brain Rhythms Are Global but Often Overlooked. Trends Neurosci 41:186–197.

Tort ABL, Komorowski R, Eichenbaum H, Kopell N (2010) Measuring phase-amplitude coupling between neuronal oscillations of different frequencies. J Neurophysiol 104:1195–1210

Tort ABL, Kramer MA, Thorn C, Gibson DJ, Kubota Y, Graybiel AM, Kopell NJ (2008) Dynamic cross-frequency couplings of local field potential oscillations in rat striatum and hippocampus during performance of a T-maze task. Proc Natl Acad Sci 105:20517–20522

Tort ABL, Ponsel S, Jessberger J, Yanovsky Y, Brankačk J, Draguhn A (2018b) Parallel detection of theta and respiration-coupled oscillations throughout the mouse brain. Sci Rep 8

Travers JB, Dinardo LA, Karimnamazi H (1997) Motor and premotor mechanisms of licking. Neurosci Biobehav Rev 21:631–647.

Travlos GS, Wilson R, Murrell JA, Chignell CF, Boorman GA (2001) The Effect of Short Intermittent Light Exposures on the Melatonin Circadian Rhythm and NMU-Induced

Breast Cancer in Female F344 / N Rats. Toxicol Pathol 29:126–136.

Truchet B, Chaillan FA, Soumireu-Mourat B, Roman FS (2002) Learning and memory of cue-reward association meaning by modifications of synaptic efficacy in dentate gyrus and piriform cortex. Hippocampus 12:600–608.

Tsanov M, Chah E, Reilly R, O'Mara SM (2014) Respiratory cycle entrainment of septal neurons mediates the fast coupling of sniffing rate and hippocampal theta rhythm. Eur J Neurosci 39:957–974.

Uchida N, Mainen ZF (2003) Speed and accuracy of olfactory discrimination in the rat. Nat Neurosci. 11:1224-1229

Ueki S, Domino EF (1961) Some evidence for a mechanical receptor in olfactory function. J Neurophysiol 24:12–25

Van Groen T, Wyss JM (1990) Extrinsic projections from area CA1 of the rat hippocampus: Olfactory, cortical, subcortical, and bilateral hippocampal formation projections. J Comp Neurol 302:515–528.

Vanderwolf CH (1969) Hippocampal electrical activity and voluntary movement in the rat. Electroencephalogr Clin Neurophysiol 26:407–418.

Vanderwolf CH (1971) Limbic-diencephalic mechanisms of voluntary movement. Psychol Rev 78:83–113.

Vanderwolf CH (1992) Hippocampal activity, olfaction, and sniffing: an olfactory input to the dentate gyrus. Brain Res 2:197-208

Verhagen J V., Wesson DW, Netoff TI, White JA, Wachowiak M (2007) Sniffing controls an adaptive filter of sensory input to the olfactory bulb. Nat Neurosci 10:631–639.

Von Stein A, Sarnthein J (2000) Different frequencies for different scales of cortical integration: From local gamma to long range alpha/theta synchronization. Int J Psychophysiol 38:301–313.

Wachowiak M (2011) All in a Sniff: Olfaction as a Model for Active Sensing. Neuron 71:962–973

Walsh RR (1956) Single Cell Spike Activity in the Olfactory Bulb. Am J Physiol Content 186:255–257

Welker WI (1964) Analysis of Sniffing of the Albino Rat. Behaviour 22:223–244

Wesson DW, Carey RM, Verhagen J V., Wachowiak M (2008) Rapid encoding and perception of novel odors in the rat. PLoS Biol 6:717–729.

Wesson DW, Verhagen J V., Wachowiak M (2009) Why sniff fast? The relationship between

sniff frequency, odor discrimination, and receptor neuron activation in the rat. J Neurophysiol 101:1089–1102.

Whitlock JR, Pfuhl G, Dagslott N, Moser MB, Moser EI (2012) Functional Split between Parietal and Entorhinal Cortices in the Rat. Neuron 73:789–802

Wilber AA, Skelin I, Wu W, McNaughton BL (2017) Laminar Organization of Encoding and Memory Reactivation in the Parietal Cortex. Neuron 95:1406-1419.e5

Wilson MA, Mcnaughton BL (1993) Dynamics of the Hippocampal Ensemble Code for Space. Science (80-) 261:1055–1058.

Witter MP (1993) Organization of the entorhinal—hippocampal system: A review of current anatomical data. Hippocampus 3:33–44.

Yanovsky Y, Ciatipis M, Draguhn A, Tort AB, Brankack J (2014) Slow oscillations in the mouse hippocampus entrained by nasal respiration. J Neurosci 34:5949–5964

Zelano C, Jiang H, Zhou G, Arora N, Schuele S, Rosenow J, Gottfried JA (2016) Nasal Respiration Entrains Human Limbic Oscillations and Modulates Cognitive Function. J Neurosci 36:12448–12467

Zhang S, Manahan-Vaughan D (2015) Spatial olfactory learning contributes to place field formation in the hippocampus. Cereb Cortex 25:423–432.